SYSTEMS APPLICATIONS OF VERTICAL CAVITY MULTI QUANTUM WELL OPTOELECTRONIC MODULATORS

A DISSERTATION

SUBMITTED TO THE DEPARTMENT OF ELECTRICAL ENGINEEERING

AND THE COMMITTEE ON GRADUATE STUDIES

OF STANFORD UNIVERSITY

IN PARTIAL FULFILLMENT OF THE REQUIREMENTS

FOR THE DEGREE OF

DOCTOR OF PHILOSOPHY

Jeffry S. Powell

September 1997

I certify that I have read this dissertation and that in my opinion it is fully adequate, in scope and quality, as a dissertation for the degree of Doctor of Philosophy.

_____

James S. Harris, Principal Adviser

I certify that I have read this dissertation and that in my opinion it is fully adequate, in scope and quality, as a dissertation for the degree of Doctor of Philosophy.

_____

Martin Morf

I certify that I have read this dissertation and that in my opinion it is fully adequate, in scope and quality, as a dissertation for the degree of Doctor of Philosophy.

_____

Fouad Tobagi

Approved for the University Committee on Graduate Studies

_____

Abstract

A large portion of the 'optical computing' research over the last 10 years has been centered around vertical cavity optoelectronic modulators grown by molecular beam epitaxy. These devices have several characteristics which make them desirable from a systems standpoint, including low power dissipation, high speed, large contrast ratio, high bandwidth, the ability to fabricate dense arrays, integration with GaAs and silicon VLSI, and a wide range of wavelengths of operation (for WDM). This thesis examines several systems applications of these devices, both those already realized and potential future applications.

First, early experiments using a configuration of two of these devices known as a symmetric self electro-optic effect device (S-SEED) to perform threshold logic (a type of pattern logic) are discussed and compared with similar devices for Boolean logic. Next, an application of these modulators to optical neural networks is briefly discussed, where the modulators are used simply as output devices and are integrated with MESFET circuitry and GaAs photodetectors.

The main part of this thesis discusses a reflection/transmission modulator (or X-modulator) developed here at Stanford which turns out to be a very powerful device in terms of optical computation, routing, and interconnection. The device is essentially a 3 input, 3 output conservative and reversible switch, an optoelectronic implementation of a Fredkin gate. The use of these devices for optical logic is exhibited and an implementation of a full adder using only 5 devices is shown. Using arrays of these modulators, various reconfigurable switching, routing, and interconnection networks are constructed, including crossbar switches and field programmable gate arrays. Ongoing research with these devices is focussed on improving their characteristics and making them more flexible for use in systems applications. In particular, reduced operating voltages are obtained using

graded buffer layer techniques, methods for optically controlling the devices are examined, and gain layers are incorporated into these structures to compensate for the losses involved in cascading the devices.

Finally, a new technology offered by AT&T at a workshop given last summer which involves smart pixels based on quantum well modulators and detectors flip chip bonded on to silicon VLSI chips is described. This technology has already demonstrated 1000's of optical inputs and outputs on a single chip and thus achieving aggregate data rates approaching 1 Tb/s. This technology has been used here to implement 2x2 switches (similar to the X-gate above) and a 4x4 optical crossbar switch for comparison with similar structures implemented using X-modulators.

Acknowledgments

One of the things I enjoyed most about my experience at Stanford was the freedom to explore an area of solid state devices from a more systems oriented point of view.

Much of the work in this thesis would have been impossible without the valuable input and constant flow of ideas from my secondary advisor, Professor Martin Morf. Martin continues to interact with me and others in the Harris group to better integrate systems and device research. I would also like to thank Professor Fouad Tobagi for serving as my orals committee chairman and being my third reader and Professor Joseph Goodman for serving on my orals committee.

Nothing would get done in the Harris group without the cooperation of and assistance from the other students in the group. When you have been at Stanford for six years, there are far too many names to point out individually. However, I would particularly like to thank John Trezza for his friendship and willingness to share his immense modulator knowledge. Daxin Liu has also provided me with valuable information related to my thesis topic. Susan Lord taught me how to use the MBE machines without causing too many problems. Mike Larson, Herman Chui, Guoying Ding, Chris Coldren, Ken Bacher, Chris Ebert, Freddy Sugihwo, and many others kept the equipment in the lab up and running most of the time without which the Harris group would come to a grinding halt. Finally, I would like to thank Bardia Pezeshki, who pioneered much of the modulator work at Stanford and helped me to focus on a subject while I was a beginning graduate student wavering between topics.

Sharleen Beckwith kept the Harris group in line, out of jail, and for the most part nonexplosive by making sure safety regulations were obeyed. Gail Chun Creech, Susie Burns, and Lu Miao helped me in many ways by dealing with the paperwork and bureaucracy necessary to escape from Stanford University with my sanity intact.

I would like to thank Professor Demetri Psaltis at CalTech for his input on the neural network portion of this thesis and Takashi Doi, a visiting scholar from Mitsubishi Heavy Industries in Japan, for his help with the threshold logic experiments. Michael Godfrey allowed me to use his computer lab for the design of my hybrid SEED chip and Dana How helped me verify that the design would actually work and prevented me from wiring power to ground and destroying the whole chip.

No one could survive the rigors of graduate school without the support of friends and family. I would like to thank anyone who has played volleyball with me in the last six years for making my Stanford experience more enjoyable. I would especially like to thank my roommates Arjun Prabhu and Matt Husman (also John Trezza) for their friendship, time, and humor. Many other friends from Stanford and from my church were also important sources of support. To list a few names, Pavan Heard, Maria Doyle, Janese Bechtol, Ann Dillner, Robin Seydel, Jeffrey Oldham, Ken and Becky Dutch, Bob Olmstead...and many more. Finally, I would like to thank my parents William and Iolene Powell and my siblings Willy and Jennifer for not bothering me about finishing my PhD and my wife Miriam for bothering me about finishing my PhD. I realize that being married to a PhD student can be very trying at times and greatly appreciate the continued love and support of my wife, who deserves her own chapter of acknowledgments. I am certain that I have missed many names that should be included here. Next time I write a thesis I will have a more exhaustive list, I promise!

Table of Contents

List of Figures

Chapter 1--Introduction

1.0 Overview

A large portion of the 'optical computing' research over the last 10 years has been centered around vertical cavity optoelectronic modulators grown by molecular beam epitaxy. These devices have several characteristics which make them desirable from a systems standpoint, including low power dissipation, high speed, large contrast ratio, high bandwidth, the ability to fabricate dense arrays, integration with GaAs and silicon VLSI, and a wide range of wavelengths of operation (for WDM). This thesis examines several systems applications of these devices, both those already realized and potential future applications.

First, early experiments using a configuration of two of these devices known as a symmetric self electro-optic effect device (S-SEED) to perform threshold logic (a type of pattern logic) are discussed and compared with similar devices for Boolean logic. Next, an application of these modulators to optical neural networks is briefly discussed, where the modulators are used simply as output devices and are integrated with MESFET circuitry and GaAs photodetectors.

The main part of this thesis discusses a reflection/transmission modulator (or X-modulator) developed here at Stanford which turns out to be a very powerful device in terms of optical computation, routing, and interconnection. The device is essentially a 3 input, 3 output conservative and reversible switch, an optoelectronic implementation of a Fredkin gate. The use of these devices for optical logic is exhibited and an implementation of a full adder using only 5 devices is shown. Using arrays of these modulators, various reconfigurable switching, routing, and interconnection networks are constructed, including crossbar switches and field programmable gate arrays. Ongoing research with these

devices is focussed on improving their characteristics and making them more flexible for use in systems applications. In particular, reduced operating voltages are obtained using graded buffer layer techniques, methods for optically controlling the devices are examined, and gain layers are incorporated into these structures to compensate for the losses involved in cascading the devices.

Finally, a new technology offered by AT&T at a workshop given last summer which involves smart pixels based on quantum well modulators and detectors flip chip bonded on to silicon VLSI chips is described. This technology has already demonstrated 1000's of optical inputs and outputs on a single chip and thus achieving aggregate data rates approaching 1 Tb/s. This technology has been used here to implement 2x2 switches (similar to the X-gate above) and a 4x4 optical crossbar switch for comparison with similar structures implemented using X-modulators.

1.1 Motivations

The title of this work is Systems Applications of Multi Quantum Well Vertical Cavity Optoelectronic Modulators which hints at the two-fold nature of its purpose. This purpose involves investigating both device physics and systems level aspects of quantum well modulators. In the past, modulators have been studied extensively as individual switching elements, but not always keeping systems concepts in mind. Most of the work has been focused on single element switches which operate in a mode where light is either reflected or absorbed. Over the last several years the design, simulation, and growth capabilities for modulators have been vastly improved, allowing for much more flexibility in obtaining devices with a specific set of optimized parameters. Some of the specific devices of interest include: GaAs/AlGaAs modulators optimized for modulation ratio and insertion loss,[1] large reflectivity modulators using InGaAs,[2] large reflectivity change normally off modulators,[3] arrays of modulators for beam steering using both amplitude [4,5]

and optical phase modulators,[6] high contrast modulators,[7] low voltage, low chirp modulators,[8] zero chirp modulators,[9] high contrast zero phase change modulators,[10] phase flip modulators,[11] modulators using coupled quantum wells,[12] and reflection transmission modulators (X-modulator).[13] Designing optoelectronic switches for specific systems applications requires a knowledge of the design tradeoffs inherent in the device design. This knowledge is crucial if system specifications are to be met. The emphasis of this thesis is therefore on an approach which involves applying this knowledge to several specific systems applications.

1.2 Why Optical Computing?

Researchers have long been interested in optical computing, which has changed in meaning over time from dreams of a purely optical computer to a marriage of electronic and optic components (smart pixels) to simply hybridization of optical devices with electronics solely for the purpose of interconnection. In this work, we will investigate this spectrum of so-called 'optical computing', from modulators which perform Boolean logic, threshold logic, and conservative invertible logic to large arrays of modulators hybridized to silicon VLSI electronics for interconnections. Along the way we will highlight the relevant device parameters necessary for the applications discussed.

As electronic circuits become smaller and denser, many problems arise, primarily in the areas of power dissipation and interconnection. Clock and signal skew results from delay variations in separate clock and signal paths. Power dissipation from line drivers may be high because of the capacitive loading effects of electrical lines. Thermal management becomes more difficult with increased power dissipation and higher interconnection density. Sensitivity to electromagnetic interference (EMI) is present. Interconnect reliability is critical in many applications, and many system failures may be traced to I/O problems.

1.3 Optics vs. Electronics

Using optical or optoelectronic solutions for computing and interconnection has several advantages as well as limitations. The inherent parallelism of large arrays of optical devices results in higher interconnection densities with lower power dissipation (and thus fewer heat removal problems). This parallelism also allows for better signal and clock distribution, and thus less skew due to the constant delay achievable. Optical beams can cross each other with little or no crosstalk. Optical beams also have less sensitivity to EMI. Optical solutions also take advantage of the third dimension, freeing up more chip area for processing, rather than communication. Because of the high switching speeds of modulators, much higher data bandwidth is obtainable. Modulators can also more easily be integrated with fiber optics for communications purposes.

The main limitations of current optoelectronic technology involve mainly alignment and packaging issues. Optoelectronic solutions also remain more expensive than electronic ones. Fabrication issues, especially with respect to integration of electrical components with with optical ones are currently under investigation by many researchers.

1.4 Wavelength Division Multiplexing

Modulators are not only useful in computational and routing systems, but also for wavelength division multiplexing (WDM) applications. In our laboratory we have designed and experimentally verified exciton systems which provide absorptive modulation at a wide range of wavelengths. When growing wafers using molecular beam epitaxy, the substrate is rotated, which results in a radial thickness uniformity of about 2% across the wafer, which may be exploited to produce a one dimensional array of devices operating at different wavelengths on one wafer. This same array of devices can be used with a broadband source to demultiplex wavelengths. A clocked array of devices can also be used

for serial/parallel and parallel/serial conversions. Because our devices are vertical cavity devices, there is also an angular dependence to the wavelength of operation of the devices which may also be used to obtain multiple wavelengths on one wafer. Using angles other than the optimum angle (usually normal incidence) does result in a degradation of the contrast ratio however. Devices with either small optical bandwidth (for wavelength selectivity) or larger bandwidth (for many wavelengths with one device) can be designed.

1.5 Other Applications

Modulators prove to be useful in many other applications other than interconnections and computing. Researchers have demonstrated systems using modulators for beamsteering,[14] mode locking of lasers,[15] analog to digital converters,[16] addressing holographic memories,[17] optical neural networks,[18] and optical correlation.[19] The recent growth of smart pixel research[20] may very well result in many other new systems applications as yet undiscovered.

Chapter 2--Quantum Well Modulator Background

2.1 Introduction

This chapter provides the basic background necessary for understanding the physics of the devices that are the focus of this thesis as well as a discussion on how their parameters are relevant to systems concepts. This includes optical bandwidth, speed, contrast ratio, and insertion loss. A brief description will also be given of the InGaAs/AlGaAs materials system used to form the devices and the molecular beam epitaxy growth technique employed to produce the desired structures. The design methodology used by the Harris group at Stanford will also be described. This approach incorporates real data into simulations and includes in-situ reflectivity measurements to obtain device characteristics closely matching those desired. The Kramers Kronig relation will also be explained, which is useful for designing phase modulators, for it transforms differences in two absorption data sets (as a function of frequency) into changes in refractive index data.

2.2 Modulator Structure

Figure 2-1 depicts a typical vertical cavity multi quantum well (MQW) optoelectronic modulator structure as grown by molecular beam epitaxy (MBE) on a GaAs substrate. As shown Figure 2-1, the modulator consists of two components: a multi quantum well region absorber is sandwiched between two quarter wave mirror stacks of reflectivities R_f and R_b. These stacks form a Fabry-Perot cavity in a direction perpendicular to the substrate. The mirror stacks are doped p and n-type so that a reverse bias may be applied across the intrinsic region of the structure. This bias allows us to modulate the aborption of the quantum well region using an effect known as the quantum confined Stark effect (similar to the normal Stark shift in bulk material). The wells can provide large amounts of absorption and can be used to obtain large changes in absorption. The specific

design of the optical cavity can transform the absorptive behavior of the quantum wells into changes in reflection and transmission amplitude and/or phase. The simulation techniques discussed later in this chapter optimize the Fabry-Perot cavity for a particular set of desired characteristics. This section will describe these two components of the modulator device, first the quantum well absorptive material, and then the Fabry-Perot cavity.

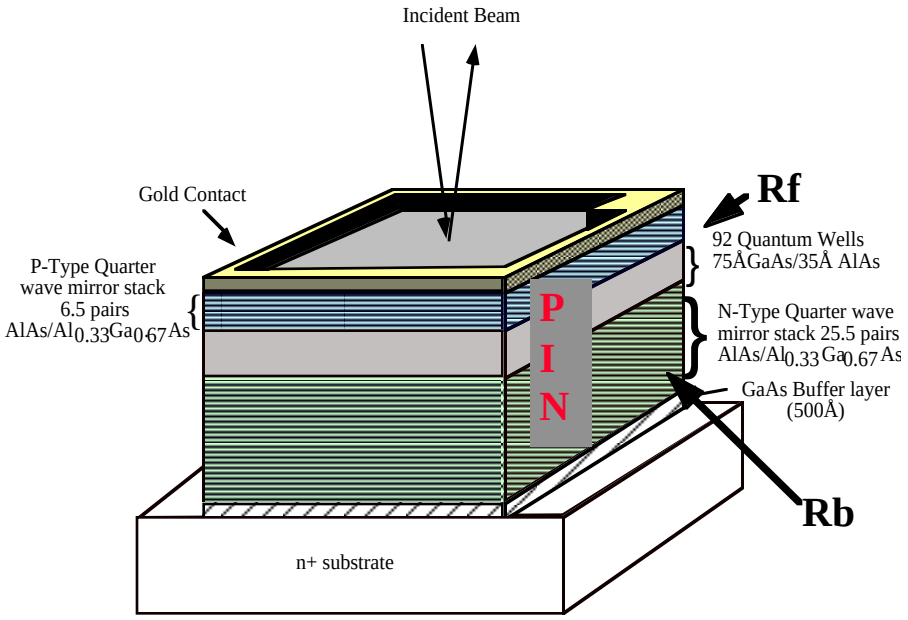

Figure 2-1: Typical vertical cavity quantum well modulator structure as grown by MBE

2.2.1 Quantum Well Absorptive Region

A quantum well is a thin region, typically <150 Å, of narrower bandgap material such as $In_{0.26}Ga_{0.74}As$ sandwiched between two barrier regions of larger bandgap material such as $Al_{0.33}Ga_{0.67}As$ (Figure 2-2). Because of the small size of this potential well region, the allowed energy levels for electrons (or holes for the valence band) confined within it become quantized[1]. The probability amplitude of the envelope of the wavefunctions of the electrons and holes is approximately sinusoidal within the well and exponentially decaying into the barriers. The absorption of a two dimensional semiconductor such as this quantum well region is given by[2]:

$$\alpha(\omega) \sim \sum_{i,j} \left|I_{hj}^{ei}\right|^2 \left|d_{cv}\right|^2 \rho_r^{2D} \cdot H(\hbar\omega - E_{hj}^{ei})$$

where the first term in the summation is the overlap integral of the electron and hole wavefunctions, $\left|d_{cv}\right|^2$ is the interband dipole matrix element, ρ_r^{2D} is the two dimensional density of states and $H(\hbar\omega - E_{hj}^{ei})$ is the Heaviside step function with $E_{hj}^{ei} = E_g + E_{ei} - E_{hj}$ being the energy term for given discrete electron and hole energy levels E_{ei} and E_{hj} along with the bandgap E_g.

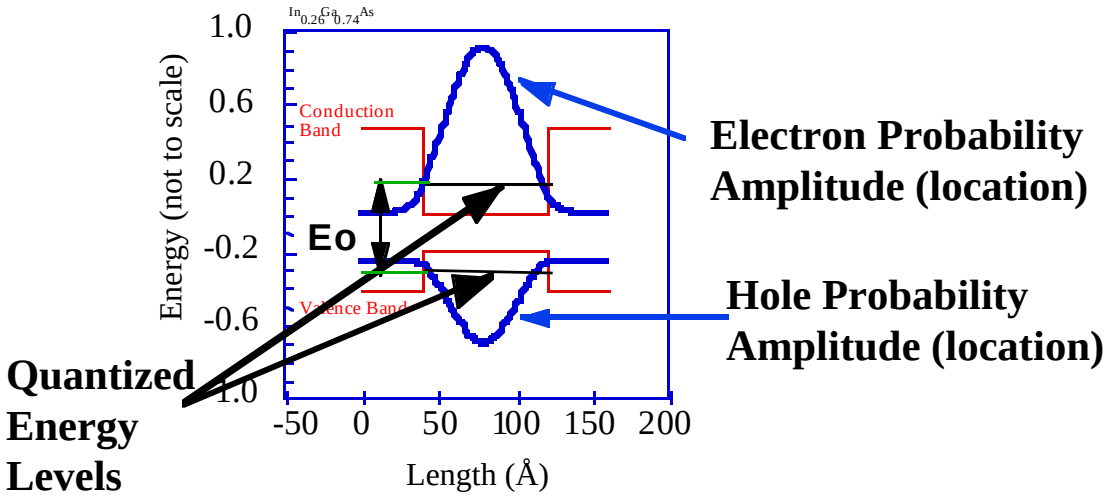

Figure 2-2: Single quantum well band structure, energy levels, and wavefunctions

If we now consider Coulombic effects between electrons and holes, additional resonances due to exciton absorption are observed in the absorption spectra. When a photon is absorbed by a semiconductor an electron is promoted to the conduction band and a hole remains in the valence band. The electron and hole interact with each other to form the a bound state similar to a hydrogen atom called an exciton. These excitons are present in bulk material but are short-lived because the bound electron-hole pair is quickly ionized by the large population of thermal phonons and other scattering mechanisms. When the carriers are confined within a quantum well however, their lifetime is longer and the resonance is enhanced. The two carriers orbit around each other much like an electron and

proton in the hydrogen atom. This interaction produces a set of strong, discrete absorption peaks just below the band gap. The strong exciton absorption peaks can be utilized in many devices as will be discussed later. Mathematically, we can write the exciton wavefunction as a wave packet constructed of linear combinations of electron and hole Bloch functions and use these in the Schrodinger equation with the Coulomb potential function. The resulting absorption spectrum for a 2-D semiconductor, for example a quantum well of dimensions smaller than the Bohr radius, the absorption spectrum is given by[3]:

$$\alpha(\omega) = | d_{cv} |^2 \sum_{i,j,n} | < \zeta_{ei}(z) | \zeta_{hj}(z) > |^2 | \phi_n^{xy}(r_{xy} = 0) |^2 \, \delta(\hbar\omega - E_n^{2D}),$$

where $| < \zeta_{ei}(z) | \zeta_{hj}(z) > |^2$ is the overlap integral of the electron and hole wavefunctions in the z direction, $| \phi_n^{xy}(r_{xy} = 0) |^2$ is the transverse probability that the electron and hole occupy the same unit cell, and

$$E_n^{2D} = E_g + E_{ei} - E_{hj} - \frac{E_B}{(n - \frac{1}{2})^2}.$$

E_B/n^2 is the n^{th} exciton binding energy, where E_B is the Rydberg energy. For our purposes this value can range from 10 to 100 meV. Figure 2-3 below[4] shows the absorption for a quantum well structure with and without exciton effects. Note that we still observe the staircase absorption spectrum, but now each step acquires its own set of excitonic resonances. The overall result of excitons in quantum wells is an enhancement of the two dimensional oscillator strength and binding energies which allow for exciton absorption resonances to be observed at room temperature. This is the fundamental result which allows one to use quantum well structures for various types of electroabsorption devices.

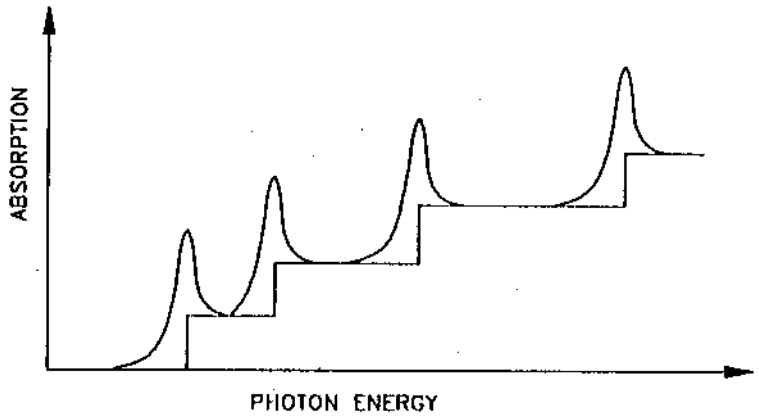

Figure 2-3: Quantum well absorption spectrum, with excitonic resonances[4]

2.2.2 Quantum Confined Stark Effect

The most common physical effect used to modulate the electro-absorption of quantum well material is known as the quantum confined Stark effect (QCSE)[5] which shows up as a red shift of the electro-absorption when an electric field is applied across a quantum well or wells. The effect can be understood with the aid of Figure 2-4. Recalling the quantum well band structure of Figure 2-2, we note that an electric field merely tilts the bands. If Schrodinger's equation is re-solved for this new system, it turns out that the new optical transition energy is lower than in the zero field case. This is the result of a combination of four effects. First, the electrons and holes move to opposite sides of the wells in order to go to the region of lowest potential energy. This actually increases the transition energy because the well is effectively narrowed. Second, the band tilting shifts the confined energy levels approximately quadratically with voltage. This turns out to be the dominant effect and the new transition energy is lower. Third, in addition to this lowering of the transition energy, the overlap integral of the electron and hole wavefunctions decreases because of their spatial separation and thus the peak value of the excitonic absorption is quenched. Fourth and last, the wavefunctions also interact more with the interfacial roughness at the barrier edge and the peak is thus broadened. Figure 2-5 depicts three of these effects as measured experimentally in an InGaAs quantum well at a variety of applied electric fields[6]. In this case, the peak is shifted by almost 300 Å and is

reduced from 18,000 cm^{-1} to 6000 cm^{-1}. The full width half maximum value of the peak is also increased.

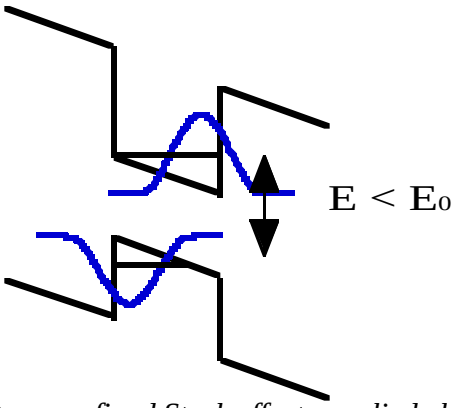

Figure 2-4: Quantum confined Stark effect--applied electric field red shifts the energy levels and spatially separates the carriers

There are other methods of modulating the absorption properties of quantum well regions, some of which will be discussed in later chapters. The QCSE, however has proven itself to be the most useful. Note that in Figure 2-5 there are two possible wavelengths where absorption modulation is of interest. At wavelength I, the absorption is reduced from 18,000 cm^{-1} to approximately 5000 cm^{-1}, while at wavelength II, the absorption is increased from near 0 to 6000 cm^{-1}. These two regions of operation will be utilized to create normally off and normally on devices. In both cases the absolute value of the change in absorption (α_{max}–α_{min}) is comparable, but at wavelength II, the ratio $\alpha_{max}/\alpha_{min}$ is much larger, because of the large residual absorption at wavelength I. This difference allows for very large contrast ratio devices to be designed and fabricated successfully in normally on devices.

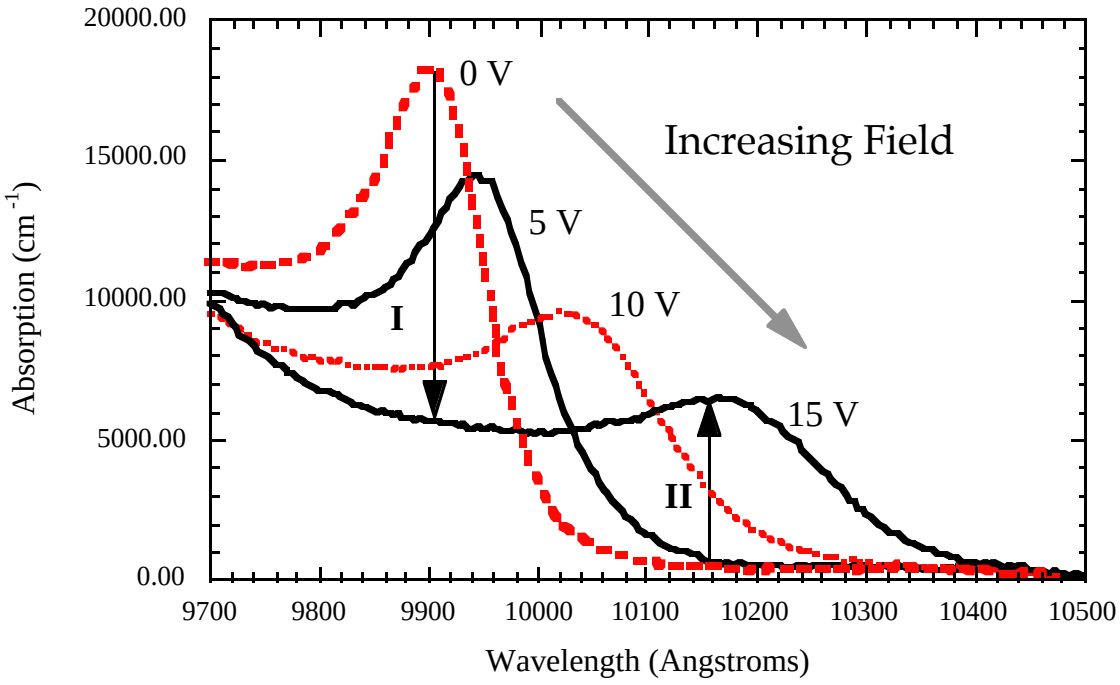

Figure 2-5: Experimentally measured quantum confined Stark effect in $In_{0.2}Ga_{0.8}As/Al_{0.33}Ga_{0.67}As$ quantum wells[6]

2.2.3 Kramers Kronig Relation

The Kramers-Kronig relation[7] is an integral transformation for linear causal systems that is generally used to relate the real and complex parts of a material's optical susceptibility, as given by the relation relating the polarization of a material and the electric field applied:

$$P(\omega) = \chi(\omega)E(\omega) \qquad P(\omega) = (\chi'(\omega) + i\chi''(\omega))E(\omega)$$

The Kramers-Kronig relationship between $\chi'(\omega)$ and $\chi''(\omega)$ is given by:

$$\chi'(\omega) = \frac{2}{\pi} \Pr \int_0^\infty d\omega' \frac{\omega' \chi''(\omega')}{\omega'^2 - \omega^2} \qquad \chi''(\omega) = \frac{-2\omega}{\pi} \Pr \int_0^\infty d\omega' \frac{\chi'(\omega')}{\omega'^2 - \omega^2}$$

Pr in the transformation indicates that the principal value of the integral should be taken (i.e. omit the point where $\omega = \omega'$). The complex dielectric constant $\varepsilon=\varepsilon' + i\varepsilon''$ is directly

related to the complex susceptibility and from ε one can derive the index of refraction and the absorption of the material. Thus, for the purposes of this work, a more useful version of the above transformation can be derived, which turns out to relate changes in refractive index to changes in absorption, under the approximation that the real part of the dielectric constant ε' is much less than the imaginary part ε'' in semiconductor materials[8].

$$\Delta n(\lambda_0) = \frac{c}{\pi} \Pr \int_0^\infty d\lambda \frac{\Delta\alpha(\lambda)}{1 - (\lambda / \lambda_0)^2}$$

The important point to note about the above relation is that the denominator is antisymmetric about λ_0, which means that if $\Delta\alpha$ is a symmetric function about the same point (for example, if it has a local maximum that is large and broad enough), the integral will be zero, resulting in zero refractive index change. This aspect of the relation will become useful in Chapter 7 where coupled quantum wells are used to obtain a modulator with zero phase change over a 5 volt voltage swing.

2.2.4 Fabry Perot Cavities

This section describes the optical resonant cavities into which the active quantum well material is placed. By placing the wells in such cavities, light passes through the absorptive many times instead of a single time. A simple Fabry-Perot cavity consists of a cavity region containing absorbing or gain material surrounded by two reflective mirrors as shown in Figure 2-6. The mirror layers are physically realized in our modulators by alternating quarter wave layers of materials with differing refractive indices. For a simple interface between materials of refractive index n_1 and n_2, the reflection and transmission are given by:

$$r = \frac{n_1 - n_2}{n_1 + n_2} \text{ and } t = \frac{2\sqrt{n_1 n_2}}{n_1 + n_2}$$

A simple extension of the analysis necessary to obtain the above formulas can be used to obtain the reflectivity of a quarter wave stack consisting of p layers on a substrate with refractive index, n_{sub}, which is given by:

$$R = \left[\frac{1 - (n_2/n_1)^{2p}(n_2^{\,2}/n_{sub})}{1 + (n_2/n_1)^{2p}(n_2^{\,2}/n_{sub})}\right]$$

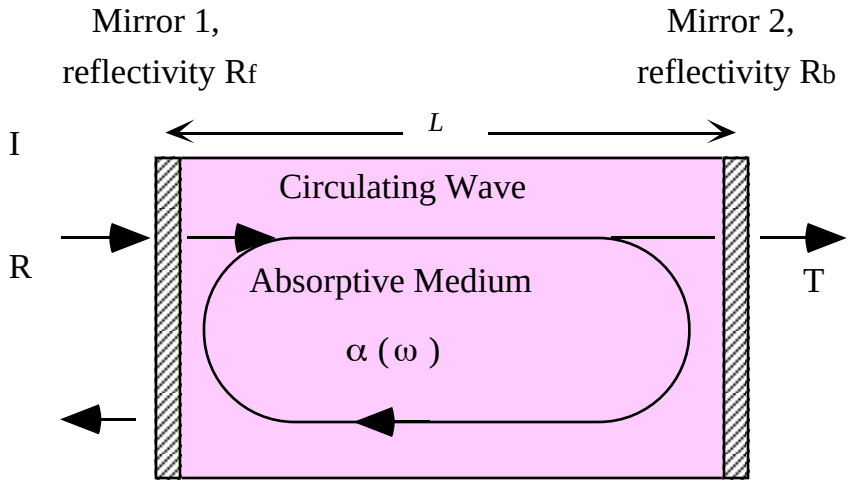

Figure 2-6: Schematic of general Fabry Perot cavity, with incident, reflected, transmitted, and circulating optical signals

The 1's in the equation may be replaced by the refractive index of the incident medium, usually air, where n=1. Typical values in this equation show that very high reflectivies, on the order of 99.9%, are obtainable using 20 or more layers. Examining Figure 2-6 in more detail, we can write a set of simultaneous equations describing the electric fields of the incident, reflected, and circulating light:

$$E_{refl} = r_f E_{inc} + jt_f r_b e^{(2j\beta L - 2\alpha_e L)} E_{circ}$$

$$E_{circ} = jt_f E_{inc} + r_f r_b e^{(2j\beta L - 2\alpha_e L)} E_{circ}$$

where r and t represent the electric field reflectivity and transmissivity of the front and back mirrors. $\beta=n\omega/c$ and α_e represent the phase and absorption properties of the cavity region and both functions of frequency ω or wavelength λ. The cavity is of length L. The imaginary j's represent a 90 degree phase shift associated with the transmission through the mirror. Defining a back mirror effective reflection coefficient, $r_b' = r_b e^{-2\alpha_e L}$, and eliminating E_{circ} from the equations, the ratio of the reflected field to the incident field is obtained as:

$$\frac{E_{refl}}{E_{inc}} = \frac{r_f - r_b' e^{2j\beta L}}{1 - r_f r_b' e^{2j\beta L}}$$

A more useful ratio, that of the field intensities, which is a measurable quantity, is given by:

$$\frac{R}{I} = \frac{I_{refl}}{I_{inc}} = \frac{r_f^{\,2} + r_b'^{\,2} - 2r_f r_b' \cos(2j\beta L)}{1 + r_f^{\,2} r_b'^{\,2} - 2r_f r_b' \cos(2j\beta L)}$$

A similar analysis produces an expression for the ratio of the transmitted intensity to the incident intensity:

$$\frac{T}{I} = \frac{I_{trans}}{I_{inc}} = \frac{T_f T_b e^{-\alpha L}}{1 + R_f R_b e^{-2\alpha L} - 2r_b r_f e^{-\alpha L} \cos(2\beta L)} \ ,$$

where R and T now represent the intensity reflection and transmission coefficients and are related by R + T = 1 for a single mirror. For the entire cavity, some of the light is absorbed by the quantum wells. In order to build up a resonant field in the cavity, the cavity length L should be equal to an integral multiple of $\lambda/2$, or half the wavelength for which the mirror layers have been designed. At these half integral wavelengths or modes of the cavity,

$\cos(2j\beta L)=1$ and the reflectivity drops to a minimum value of R_{min}. Between these modes at some point, $\cos(2j\beta L)= -1$ and the reflectivity reaches a maximum value R_{max}. These two values are given by:

$$R_{min} = \left[\frac{r_b' - r_f}{1 - r_b' r_f}\right]^2 \quad \text{and} \quad R_{max} = \left[\frac{r_b' + r_f}{1 + r_b' r_f}\right]^2.$$

More will be said about the interaction between the absorptive media and Fabry-Perot cavity in a later section which will discuss parameters of interest of these devices from a systems point of view.

2.3 Device Modeling and In-situ Measurements

At Stanford University, we have developed good computer modeling techniques for all aspects of quantum well optoelectronic switching. By investigating both the quantum electronic nature of the active materials and the optical properties of the cavities into which they are placed, accurate predictions of device performance can be made. Furthermore, the extensive fabrication facilities at Stanford enable us to physically realize devices, and test them to verify our theoretical predictions. This capability, combined with the ability to incorporate empirical results into our models, permits our simulations to be continuously refined, allowing the programs to become increasingly accurate in predicting device behavior. In this section, our design methodology and simulation tools will be described.

A consistent, reproducible approach to optoelectronic device design and development requires simulation and experimental device feedback into simulation programs. Our design capabilities have allowed us to investigate quantum wells utilizing the $In_xGa_yAl_{1-x-y}As$ material system. Band offsets and effective masses can be obtained for materials containing any combination of the group III elements. Eigenfunctions and

eigenenergies (including coulomb interactions) for the exciton states associated with a quantum well system are defined. The quantum well region can consist of any combination of semiconductor quantum wells and barriers, each with user defined thicknesses. The eigenfunctions and eigenenergies are found using the transmission method similar to that described in this section for optical cavities[9]. The available design software also allows user defined voltages to be applied to the structure, allowing analysis of wavelength shifts of absorption. While investigating multiple, single quantum wells, excitonic absorptive modulation at a variety of wavelengths, including 632 nm (HeNe wavelength)[10], 1300nm[11], and 1550nm[12] (the fiber optic communications wavelengths), have been designed and experimentally verified. Changes in absorption between 5000 cm^{-1} and 10,000 cm^{-1} have been readily achieved. Furthermore, because we can simulate the structures at a variety of voltages, we can determine from discrepancies between simulation and experiment the relative quality of experimentally grown crystals containing interfaces between highly strained layers.

The above described simulation is sufficient for designing transmissive-absorptive modulators. For other types of device design, however, resonant cavity effects are crucial for accurate prediction of device response. To address these issues, our group has developed a complex device simulation program which accounts for the optical properties of all epitaxial layers. By including absorption and refraction as a function of wavelength, we can accurately predict device response at a cavity resonance. At a resonance wavelength, photons make many effective passes through the cavity layers and thus the active material, and accurate knowledge of the optical properties of these layers is crucial. A detailed analysis of the complex absorption/dispersion of excitons is particularly important. Analytical models of exciton absorptive behavior are insufficient for predicting how experimentally developed devices behave, particularly under bias. To alleviate this problem we have extended our simulation tools to operate in a mixed analytic-empirical mode. Optically passive elements of our device structure models use complex optical

constants as obtained from the literature[13]. The active quantum well regions are modeled by incorporating experimentally derived absorption data as a function of wavelength and at a variety of voltages. Dispersive data is then obtained by performing a Kramers-Kronig transformation (described in Section 2.2.3) on the experimental absorption data. While a theoretical model of quantum wells would allow us to predict energy level shifting and absorption maxima quenching via the quantum confined Stark-effect, our mixed analytic-empirical approach allows us to account accurately for experimental conditions. For example, quantum well absorptive broadening due to imperfect crystal interfaces or quenching of absorptive resonances due to large incident light intensities or temperature related effects on performance are easily incorporated. Because the exciton data is experimentally derived, it provides the high accuracy required for good modeling of device behavior at Fabry-Perot cavity resonances as a function of voltage. Figure 2-7 shows data from the first of the devices developed and grown in our group at Stanford using these simulation tools[14].

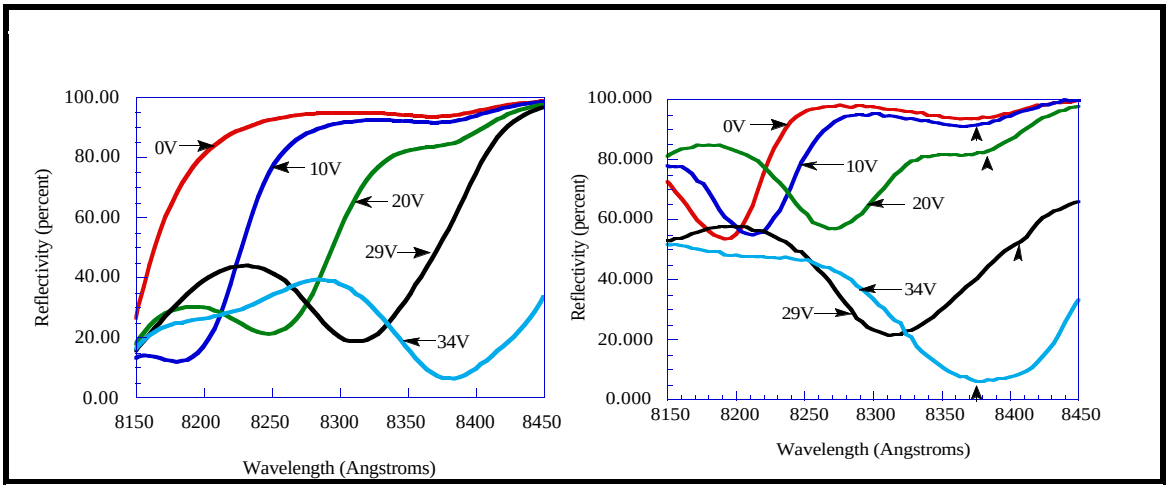

Figure 2-7: Theoretical Prediction and Experimental Data of Initial Reflection Modulator [14]

The simulation even on this first pass attempt was extremely good at predicting the experimental results of the device operation at the Fabry-Perot wavelength (denoted by the vertical arrows in the experimental plot). The device of the data shown is one designed to operate before the matching condition (where increases in absorption cause decreases in device reflectivity). It was designed to give a large change in reflectivity (here 90%) which was achieved in the experimental device. The simulation program is designed to accept optical data from a number of sources, so that simulation of different material systems or quantum well schemes can be incorporated merely by including a file which containes optical absorption and refraction data as a function of wavelength. Such flexibility is essential when designing devices which can operate at a variety of wavelengths and may contain a variety of materials. While the data above show device response for normally incident light, the program can predict the device behavior when either TE or TM polarized light impinges on the device at any angle. Furthermore, optical waves can be calculated and displayed and, for waveguides, waveguide modes can be determined. What follows here is a description of the transfer matrix method used in these simulations.

The thin film model used by our programs is described in many optics texts, such as MacLeod[15]. Each layer in the structure is represented by a complex matrix that relates the admittance vector $\mathbf{Y}$ (given by $\vec{\mathbf{H}} = \mathbf{Y}(\vec{\mathbf{r}} \mathrm{x} \vec{\mathbf{E}})$) at its front surface to the admittance vector at the back. For a layered structure of materials, we may simply multiply a matrix per layer by the incident admittance and use the admittance at the surface to obtain the reflectivity or transmittivity of the structure. Thus, we may write:

$$\begin{bmatrix} B \\ C \end{bmatrix} = \prod_{j=1}^{n} \begin{Bmatrix} \cos(\delta_j) & \sin(\delta_j)/\eta_j \\ i\eta_j \sin(\delta_j) & \cos(\delta_j) \end{Bmatrix} \begin{bmatrix} 1 \\ \eta_s \end{bmatrix}$$

where $\delta_j = \frac{2\pi n}{\lambda} d\cos(\theta)$, $Y = \frac{C}{B}$, and the reflectivity of the structure can be calculated using the relation:

$$R = \left| \frac{\eta_{inc} - Y}{\eta_{inc} + Y} \right|^2$$

For normal incidence, η_{inc} can be replaced by the refractive index n. Figure 2-8 depicts the typical zero bias reflectivity spectrum of a modulator simulated using this method.

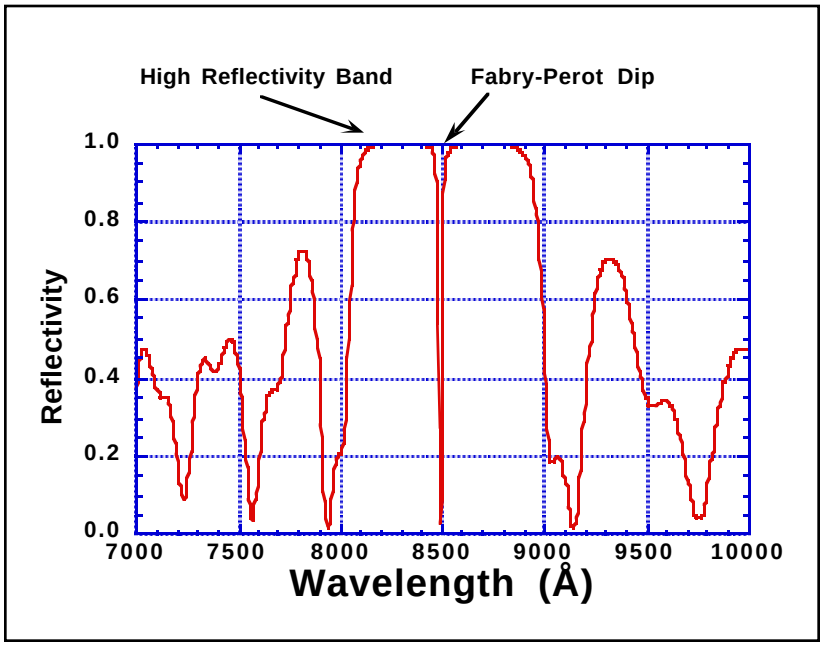

Figure 2-8: Zero bias reflectivity spectrum of a GaAs/$Al_{0.33}Ga_{0.67}As$ modulator

The width of the central high reflectivity band can be calculated as:

$$\delta_W = \frac{4\lambda_0}{\pi} \sin^{-1}\left(\frac{n_2 - n_1}{n_2 + n_1} \right)$$

To closely match the reflectivity spectra of our grown structures to the designed characteristics, a multi-step growth methodology is used. First, a quantum well only structure is grown to determine where the peak exciton wavelength lies for the current growth parameters and well/barrier thicknesses. This wavelength is determined by removing the wafer from the growth chamber, allowing it to cool to room temperature, and while still under vacuum, measuring its reflectivity through a port window in the MBE

system. Next, several periods of the back mirror are grown and the wafer is again removed from the growth chamber and its reflectivity is measured. This in-situ method of monitoring growth and making corrections was pioneered by the Harris group at Stanford and assures close matching of parameters to the designed goal, while having minimal side-effects on the quality of the structures grown[16].

2.4 Design Tradeoffs and Systems Parameters of Interest

Designing proper optoelectronic switches for a given system application requires a knowledge of the design tradeoffs inherent in the device design. A good knowledge of the parameter space is thus crucial if system specifications are to be met with 'standardized' optoelectronic components. It is also possible to utilize our simulation techniques to develop simpler analytic models which can predict device responses at Fabry-Perot resonant wavelengths.

Individual optoelectronic switches can be characterized with a number of parameters. The more important parameters are: modulation ratio (MR), change in reflectivity (ΔR) (related to insertion loss), operating voltage, reflected phase, chirp, optical bandwidth (OB), and speed. Furthermore, when devices are combined, additional parameters, such as crosstalk and fanout, become important. Contrast ratio and change in reflectivity are determined by the properties of the cavity and how well the Fabry-Perot mode is matched to the exciton resonance. Operating voltage is determined by the physical length of the cavity and the peak value of the excitonic absorption when employing the QCSE. The optical bandwidth of a modulator depends upon the thickness of the cavity as well as upon the indices of refraction used in the mirror stacks and the front mirror reflectivity. The switching speed of a device depends on the method by which it is switched. For voltage controlled modulators, device capacitance is the limiting factor, whereas for optically controlled devices, exciton lifetimes determine the speed. Our group's investigation to date has involved the tradeoffs of the individual device parameter

space utilizing analytic techniques around single wavelengths[17,18]. For example, when working with X-modulators (whose operation is described in Chapter 5):

> For a fixed voltage, as modulation ratio increases, ΔR increases and OB decreases.
> For a fixed ΔR, as voltage increases, OB increases and MR decreases.
> For a fixed MR, as voltage increases, OB increases and ΔR decreases.

Different system needs require optimization of different parameters. For example, phase switches want to have ΔR=0 while optical logic switches want ΔR to be maximized to increase noise margins. Temperature insensitive switching requires a large OB while fiber optic communications requires many closely spaced channels with little inter-channel interference. The latter requires a small OB. Low voltage operation is almost always preferred and is compatible with high frequency operation; however, if gigahertz operation is not required, a higher voltage could be used to enhance other characteristics. Figure 2-9 shows a typical result of a parameter space plot for an X-modulator (see Chapter 5).

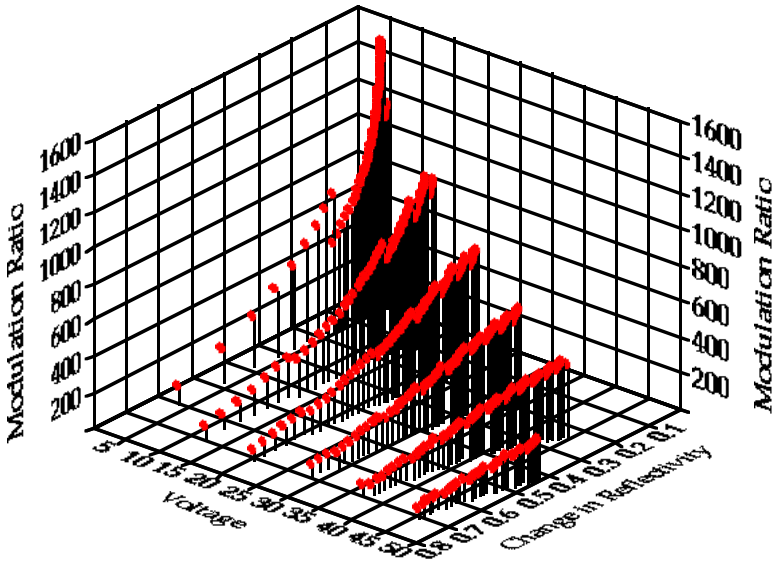

Figure 2-9: Modulation Ratio and Change in Reflectivity vs. Voltage for X-modulators

Because of these device level design tradeoffs, system level requirements are necessary to find the optimum device for a particular application. If optimization of only

one parameter is required, then with the given state of device fabrication technology, devices simultaneously optimized for changes in reflectivity of over 95%, modulation ratios of over 1500, and frequencies over 50 GHz should be achievable.

Speed and power dissipation are two final aspects of MQW modulator devices of interest to systems designers. The microscopic electroabsorption mechanisms (such as the QCSE) have been tested down to a 200 fsec timescale, so that the speed of modulation and detection tends to be limited by circuit parameters,and not by the basic device physics. Within reverse biased p-i-n MQW regions however, there are some speed limitations, such as the carrier emission from the quantum wells[19] and the carrier transport from the wells to the electrodes[20]. Total power dissipation in MQW modulators has several components. First, there is the charging and discharging of the device capacitance. This capacitance tends to be quite small (100 fF or less) so that for a 5 Volt swing, the energy required is around 1 picojoule. Absorbed optical energy must also be dissipated. MQW diodes have nearly unity quantum efficiency, so for a typical input power of 100 μW, all of the power is absorbed. Finally, the photocurrent generated by absorption must be resistively dissipated. For the optical input power above, about 70-80 μA of current is generated. For typical operating voltages and device resistances, around 500-600 μWatts must be dissipated. Therefore the total power that must be dissipated by a modulator is less than 1 mW.

2.5 Molecular Beam Epitaxy Growth

The devices created for this work were grown using a growth technique known as molecular beam epitaxy (MBE). This technique enables well controlled atomic layer by layer crystal growth of many semiconductors, metals, insulators, and superconductors. Many references are available on topics relevant to MBE growth[21,22], so only a brief description of the method will be given.

The new devices described in this thesis were grown on 2 inch GaAs substrates using a Varian GEN II commercial system. A simplified schematic of the growth chamber of an MBE system is shown in Figure 2-10. This chamber is maintained at ultra high vacuum around 10^{-10} Torr, so that a given element experiences no collisions between the source itself and the wafer. The substrate is placed on a rotating substrate heater. The rotation results in more uniform growth thicknesses across the wafer 's surface. Source materials are heated by their crucibles and the temperature of the source controls its flux rate into the growth chamber. Material from a given source will be deposited on the wafer only when the shutter blocking its entry into the chamber is open. Thus, using the elements available in our system (arsenic, gallium, aluminum, indium, beryllium, and silicon) we may grow any material within the InGaAs/AlGaAs materials system. Silicon is used as the n-type dopant and beryllium as the p-type dopant. In the figure, the shutters for silicon, aluminum, gallium, and arsenic are open, so that n-type AlGaAs will be deposited on the wafer in this configuration. The particular composition and doping of the material grown depends upon the fluxes of the individual materials, which also determines the growth rate. An overpressure of the group V element of 10 to 15 is normally required to obtain quality crystalline growth, in this case arsenic. The temperature of the substrate heater is another variable which must be controlled and its particular value depends upon the type of material grown. For example, AlGaAs is usually grown above 650˚ C and InGaAs is grown below 550˚ C.

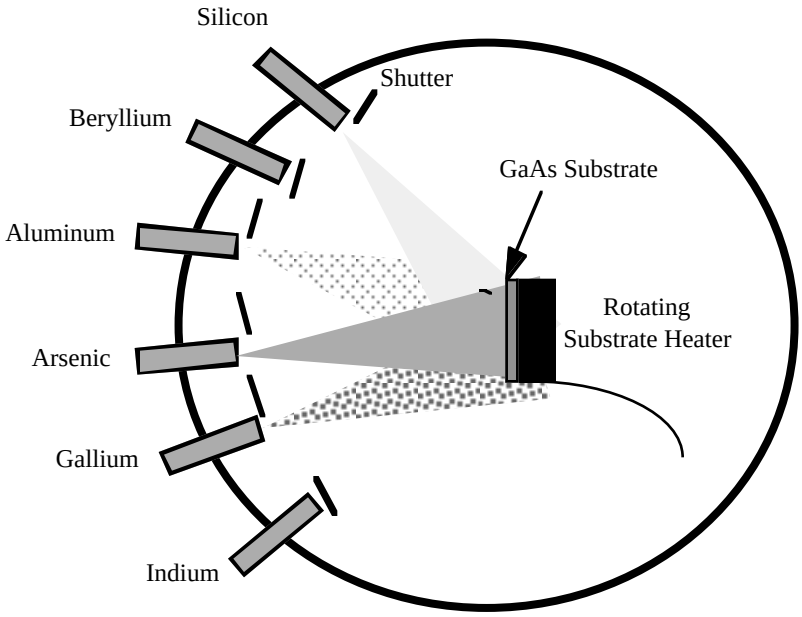

Figure 2-10: Simplified Schematic of MBE growth chamber with shutters opened to grow n-type AlGaAs

Chapter 3--Threshold Logic with SEEDs

3.0 Introduction

Much of the research effort in this thesis is focused on a particular type of quantum well modulator device known as a self electrooptic effect device (SEED)[1]. This chapter will describe both the SEED and S-SEED (symmetric SEED)[2] configurations, summarize how Boolean logic may be implemented with these devices, describe an alternative type of logic known as threshold logic, demonstrate threshold logic using SEEDs, and give a simple transient analysis of an S-SEED device to estimate its switching speed.

3.1 SEEDs

In order to understand the operation of the SEED, a knowledge of the quantum confined Stark effect and the photocurrent behavior of the p-i-n MQW diode is needed. The QCSE has been previously described in Section 2.2.2. At the large reverse bias voltages necessary for the QCSE, the diode also functions as a photodetector. Optical detection in the diode consists of absorption of the incident photons followed by recombination of some of the photoexcited electron-hole pairs and tunneling of the other electrons and holes through the barrier regions to the contacts to generate a photocurrent. At low bias, recombination dominates and little current is generated. At higher bias, tunneling dominates and the photocurrent follows the absorption spectrum of the MQW region. As the field increases however, the QCSE is also taking place, which reduces or increases the absorption at the wavelength of interest (typically one operates with decreasing absorption, i.e. region I in Figure 2-5). As the absorption decreases, so does the number of photons generated, thus yielding a negative differential resistance region (NDR) of the photocurrent-voltage curve. This NDR can be exploited to obtain bistable devices.

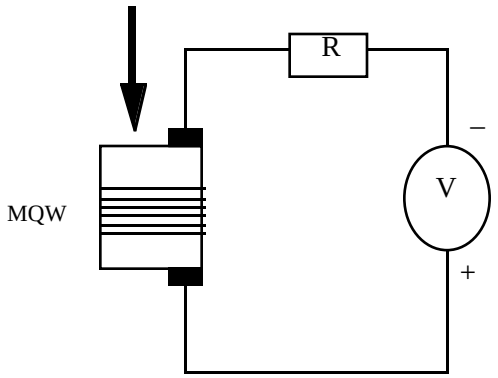

Figure 3-1: Standard SEED configuration (resistor load)

The first SEED devices[1] used the configuration shown in Figure 3-1, where a MQW diode is placed in series with a resistive load. The diode functions as both a modulator and a detector in this case. Initially there is no light shining on the device, in which case there is no photocurrent and practically all of the bias voltage falls across the MQW region of the device. As light is shining on the device, photocurrent is generated (with nearly unity quantum efficiency) which yields an increased voltage drop across the resistor, thus reducing the voltage applied to the MQW region. As we know from the QCSE discussion, this reduced voltage means increased absorption and increased photocurrent as positive feedback. Above some value of input optical power, this process switches the device into a highly absorbing, low voltage state. If the input power is decreased, at some much lower power, the device will switch back into its initial high resistance state. Because of the NDR of the photocurrent, a load line analysis can easily show that the device exhibits a hysteresis loop in its bistability. The main problem with this configuration is that it provides no gain and is thus not very useful for systems requiring cascaded devices or fanout. In Section 5.5.3 a structure will be discussed which may incorporate a gain layer into these devices.

3.2 Symmetric SEEDs

The next step in the development of SEEDs was to replace the load resistor with another MQW diode, yielding a device called a symmetric SEED (or S-SEED)[2]. The device can be understood just as the normal SEED configuration where now the load SEED can be viewed as a resistor whose resistance is set by the optical input power. Figure 3-2 shows a load line analysis of the S-SEED. The power on the upper device in the inset is held constant as the power on the other device is increased. Points where the curves for the two devices intersect are solutions. In the case where there is more than one point of intersection, the device will switch to the other point if it is a point of stable equilibrium, which is determined by the slopes of the two curves at that point.

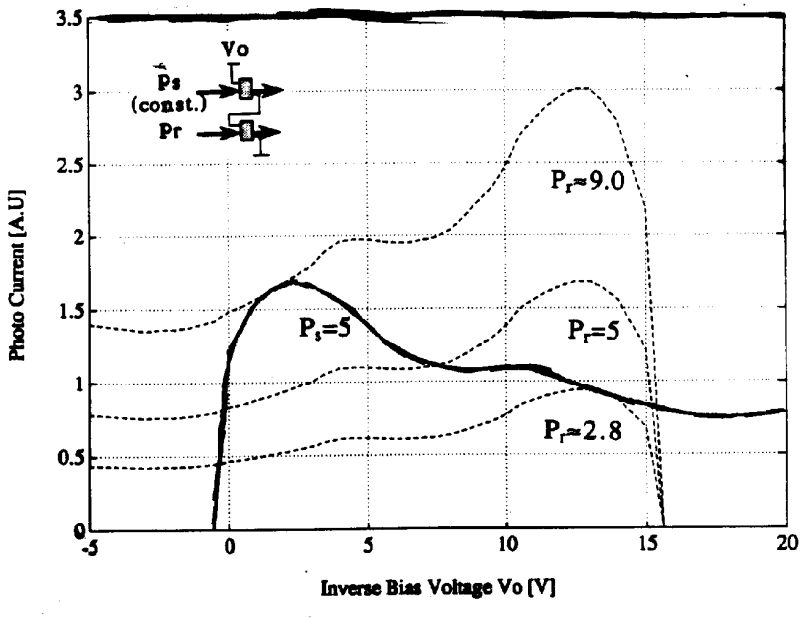

Figure 3-2: Load line analysis of S-SEED

The S-SEED has two optical inputs P_{in1} and P_{in2} and two optical outputs P_{out1} and P_{out2}. If P_{in1} and P_{in2} are kept equal, the S-SEED will maintain its current state. If both signals are reduced by the same amount, the state will still be maintained. Switching of the device occurs only when the photocurrent in one diode starts to exceed that of the other.

Therefore the switching is controlled by the ratio of the optical input powers and not their absolute values. If the two inputs are reduced to some small value, and then one is increased slightly, the device will switch, at which point the input powers can be set equal and increased many times to read out the state of the device. This affords an effective time-sequential gain whereby a small input signal can control a larger output signal. This two phased clock technique also has the advantage of isolating the output signals from the input, since they impinge upon the devices at different times. Switching energies in S-SEEDs can be as low as a few picojoules, and for higher switching energies, switching times have been measured to be as low as a few hundred picoseconds.

3.3 Boolean Logic with S-SEEDs

The S-SEEDs described in the previous section can be used to perform optical logic given their bistable characteristics. This logic is accomplished by presetting the device in one of the two states, then clocking in the input as described above, and finally using more powerful beams of equal intensity to read out the output, essentially a three phase clocked logic. The logic operation performed by the gate depends on its preset state. An important aspect of S-SEED logic is that it is implemented in a dual rail format, i.e. using two beams instead of one. Therefore, if the beams are attenuated equally by the devices or other elements of the system, the logic level is preserved, thus alleviating the need for high contrast ratio devices. This type of two beam logic is also important for implementing receivers using MQW modulators (or other devices), for it allows for increased sensitivity[3].

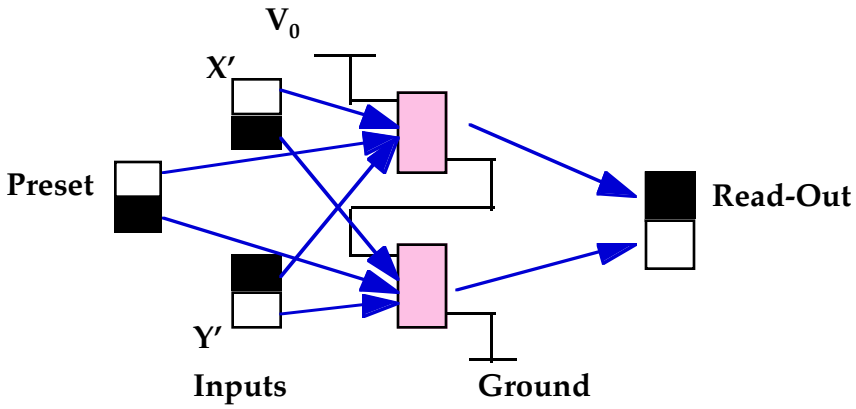

Figure 3-3: S-SEED implementation of a NAND operation, using three phase clock of preset, input, read-out

Figure 3-3 illustrates the three phase logic operation of an S-SEED which is preset to be a NAND gate. Figure 3-4 illustrates how the preset state determines whether the gate is a NAND or a NOR gate. AND and OR gates may also be implemented using S-SEEDs if normally-on devices are used instead of the normally-off devices shown here.

INPUT		OUTPUT		
X′	Y′	0	1	PRESET
0	0	1	1	
0	1	1	0	
1	0	1	0	
1	1	0	0	
		NAND	NOR	

Figure 3-4: Truth table of S-SEED as a NAND or NOR gate, depending on the preset value

Using several of these NAND and NOR gates, one can simply construct a full adder circuit, as demonstrated in Figure 3-5. An electronic logic full adder is typically implemented with on the order of 25-40 transistors, depending upon the exact implementation[4]. Note that this implementation requires 13 S-SEEDs, or 26 total MQW

devices, for comparison with the threshold logic implementation described later in this chapter and with the X-modulator implementation of Chapter 5.

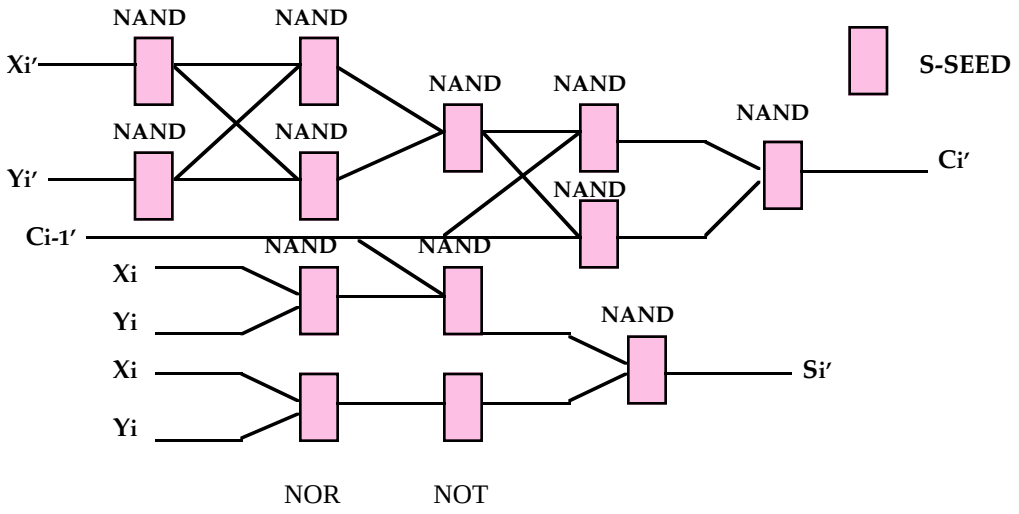

Figure 3-5: Full adder circuit constructed with Boolean logic SEEDs

Several programs were written in Mathematica and Matlab to predict the bistable characteristics of S-SEEDs constructed with devices grown at Stanford. The input to the programs consisted of the device reflectivity and responsivity as a function of voltage, upon which a simulated load line analysis was performed using the responsivity data and the P_{out} vs. P_{in} curves calculated from the stable points using the reflectivity data. Figure 3-6 illustrates this process.

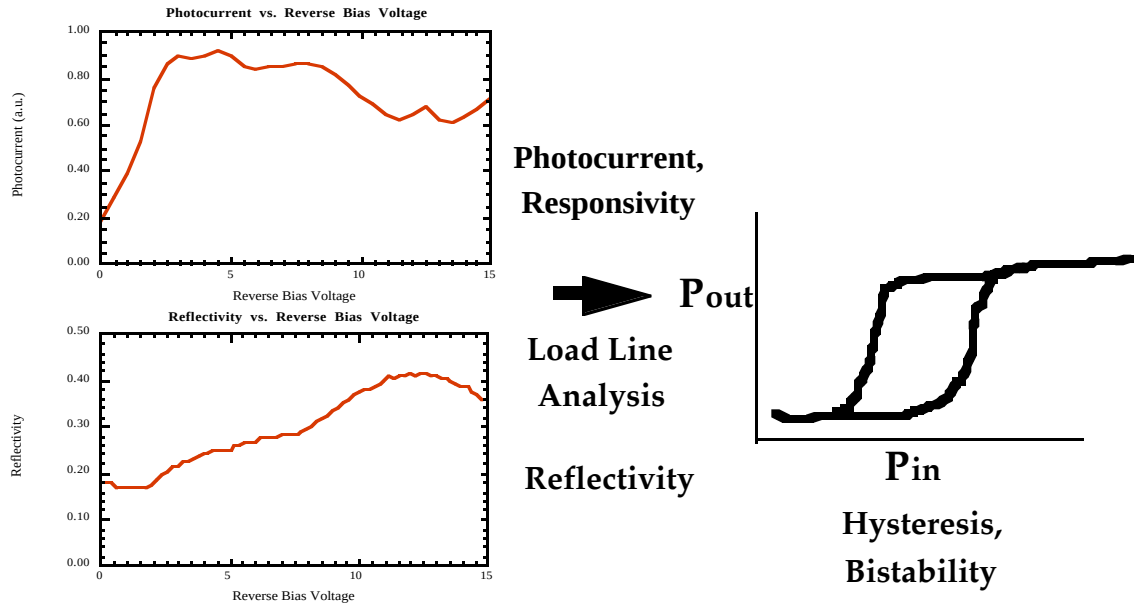

Figure 3-6: Conceptual illustration of simulation performed to calculate bistability loops for S-SEEDs given real device responsivity and reflectivity

The results of these caculations are shown in Figure 3-7. Note that the acronym REAM in the Figure is simply another name for a MQW modulator and stands for reflective electro-absorption modulator. The four graphs in each part of Figure 3-7 represent, going clockwise starting at the upper left: 1) load line analysis, using experimental responsivity data, 2) reflectivities of the devices at the stable points calculated in 1 as a function of input power, 3) the resultant output powers, and 4) the experimental reflectivity data used in the calculations. The calculations were performed for several values of reverse bias voltage V_0, however we show only the results for 8 and 14 volts here. 8 volts was the minimum voltage for which a bistability loop of any significant width is observed. Near 14 volts was the voltage at which the maximum bistability loop width occurred. Wider loops indicate better noise tolerance in bistable systems.

8 volts

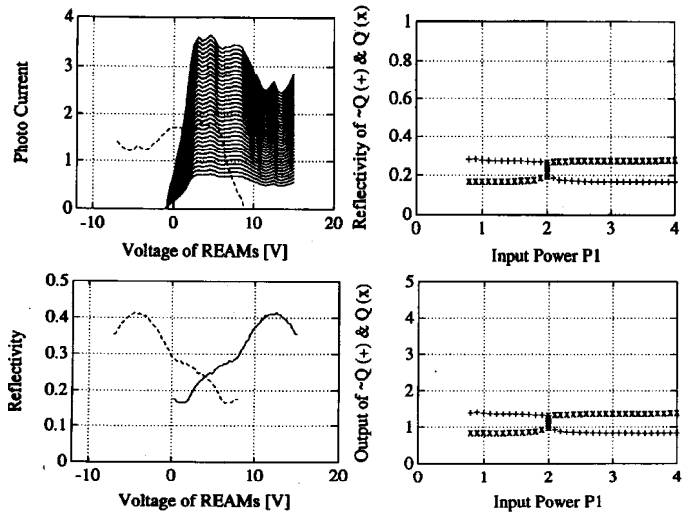

(a)

14 Volts

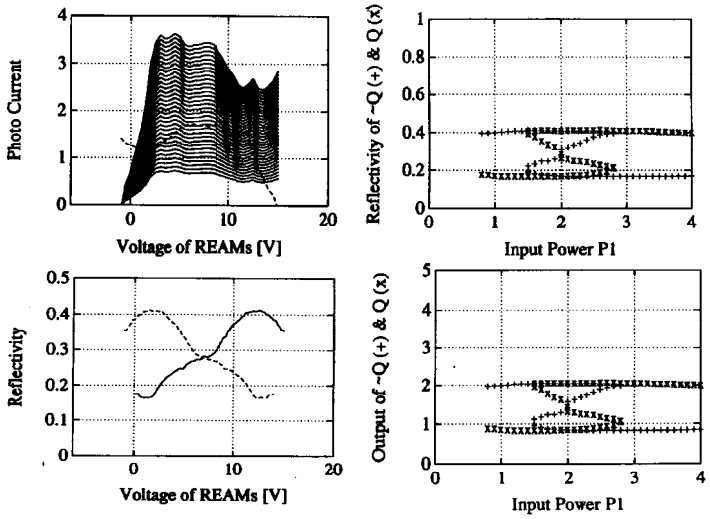

(b)

Figure 3-7: Results of S-SEED bistability simulations at (a) 8 volts and (b) 14 volts reverse bias.

In order to verify the results of our simulations, two of the modulators grown in our lab were arranged in an S-SEED configuration and the appropriate input output data taken with a chart recorder (results shown in Figure 3-8). The simulations were able to accurately predict the onset of bistability as well as the width of the bistable region as a

function of reverse bias. The left edge of the graph is 1 mW and the right is 3 mW. Figure 3-9 shows data taken from the two individual devices switching simultaneously and shows that the device characteristics are not completely symmetric.

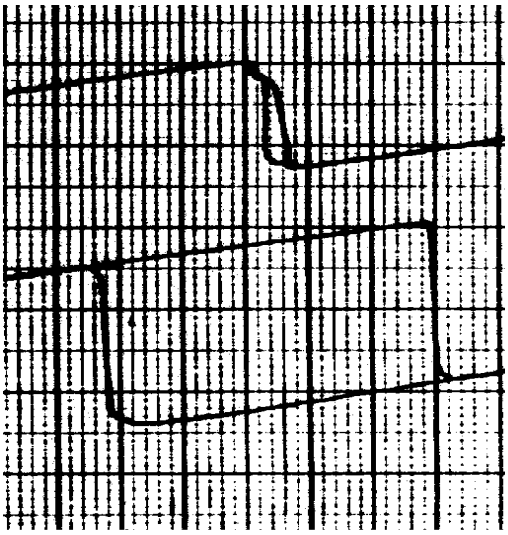

Figure 3-8: Experimentally measured bistability of S-SEED at 8 (top) and 14 (bottom) volts

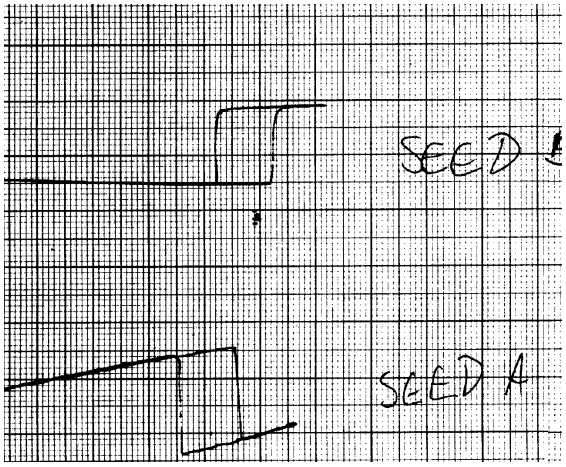

Figure 3-9: Experimental verification of switching of both devices in the S-SEED. Note the asymmetry in switching point

3.4 Threshold Logic with SEEDs

Consider the same S-SEEDs from above and assume that many inputs may impinge upon the devices at once. This setup realizes a thresholding element. A thresholding element is a device with a single bi-valued output and a number of possibly multi-valued

inputs. Each input has a gain, i.e. it is multiplied by a real number referred to as a weight. The output of the device is defined as 'zero' unless the sum of the weighted inputs exceeds some threshold, u, in which case it is defined as 'one'. More formally, $S = \sum_{i=1}^{n} a_i x_i$. If S>u, then the output y='one'; else, y='zero'. Threshold logic is a richer form of logic than Boolean logic, and a considerable amount of research has been carried out on synthesis and decomposition using threshold elements[5].

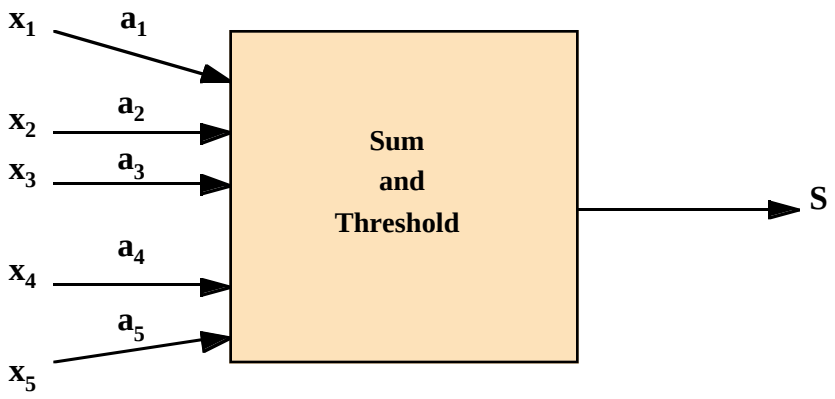

Figure 3-10: Single thresholding element

As an example of how threshold logic may reduce the complexity of a given circuit, let us return to the full adder of the previous section. Figure 3-11 depicts an S-SEED with a contrast ratio of 2 implementing a single thresholding element where all of the input weights are 1. Using this single element, construct a full adder as shown in Figure 3-12. Note that this implementation requires only 10 active modulators (2 per block) compared with the 26 required by the earlier Boolean implementaion. To verify that this design is correct, Figure 3-13 depicts a simulation of the outputs C_i and S_i for all possible input combinations, thus verifying the truth table for this circuit.

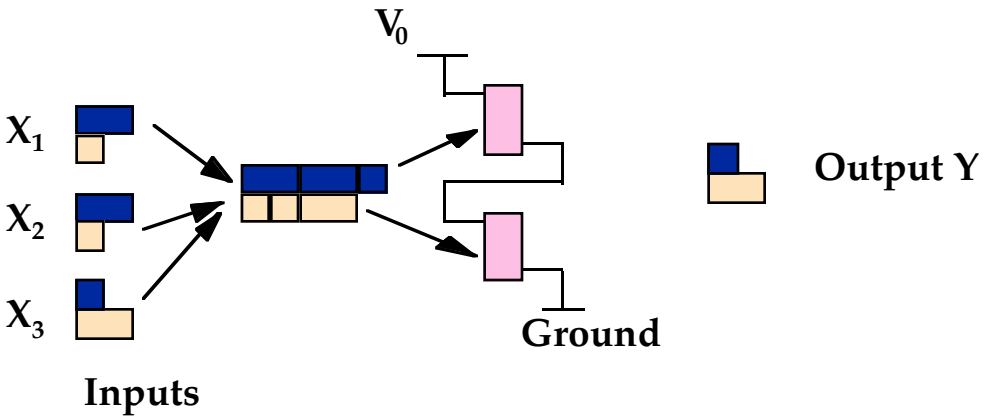

Figure 3-11: S-SEED implementing a single threshold element

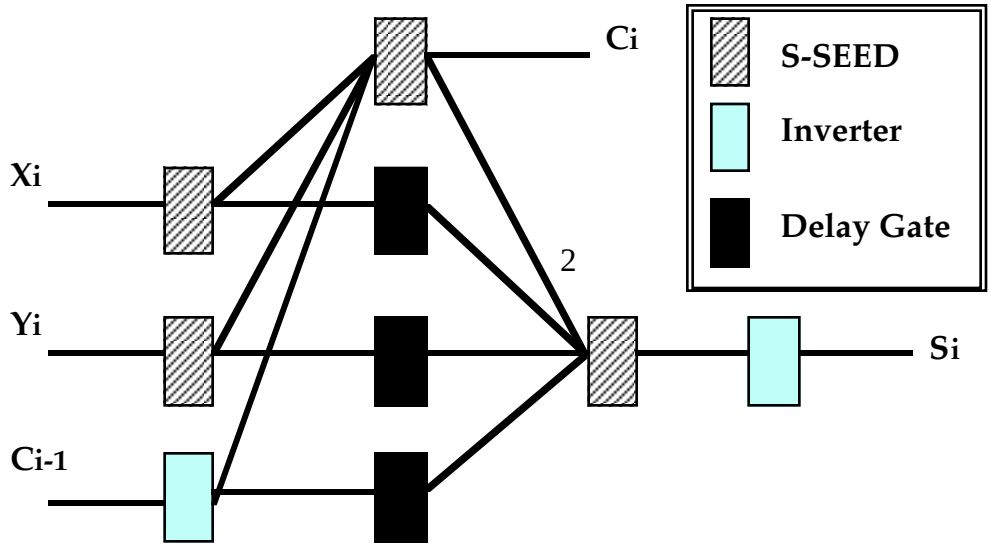

Figure 3-12: Full adder constructed with threshold logic SEEDs

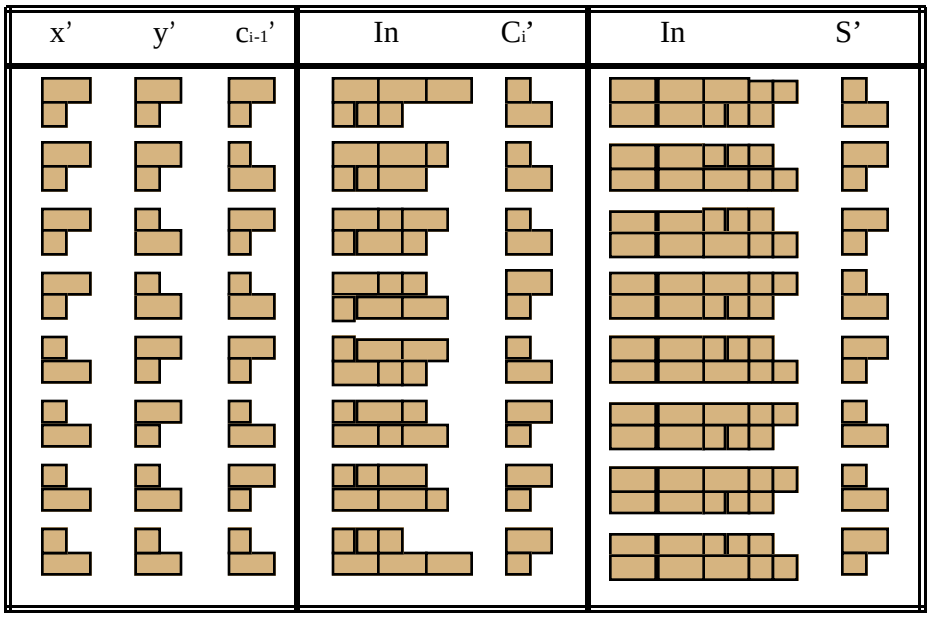

Figure 3-13: Simulated table of full adder with threshold logic, contrast ratio=2:1

3.5 Transient Analysis

To estimate the switching speed of our S-SEEDs, we used a simple circuit model of the devices as shown in Figure 3-14[6]. In this model, we replace each device by a capacitance in parallel with a current source which puts out current according to $i=S_1P_1$, with S being the responsitivity of the device and P being the optical power incident upon it. We can represent this model by the following set of differential equations:

$$v_1 + v_2 = v_0 \qquad (1)$$

$$\frac{dv_1}{dt} = \frac{i - S_1(v_1)P_1(t)}{C_1} \qquad (2)$$

$$\frac{dv_2}{dt} = \frac{i - S_2(v_2)P_2(t)}{C_2} \qquad (3)$$

From (1), and V_0 constant follows $\frac{dv_1}{dt} + \frac{dv_2}{dt} = 0$ and combined with (2) and (3) produces:

$$\frac{dv_1}{dt} + \frac{dv_2}{dt} = \frac{i - S_1(v_1)P_1(t)}{C_1} + \frac{i - S_2(v_2)P_2(t)}{C_2} = 0.$$

Solving this for the current, we see that $i = \frac{C_2 S_1(v_1)P_1(t) + C_1 S_2(v_2)P_2(t)}{C_1 + C_2}$ and combined with (2) and (3) produces:

$$\frac{dv_1}{dt} = \frac{S_2(v_0 - v_1)P_2(t) - S_1(v_1)P_1(t)}{C_1 + C_2} \qquad (4)$$

$$\frac{dv_2}{dt} = \frac{S_1(v_0 - v_2)P_1(t) - S_2(v_2)P_2(t)}{C_1 + C_2} \qquad (5)$$

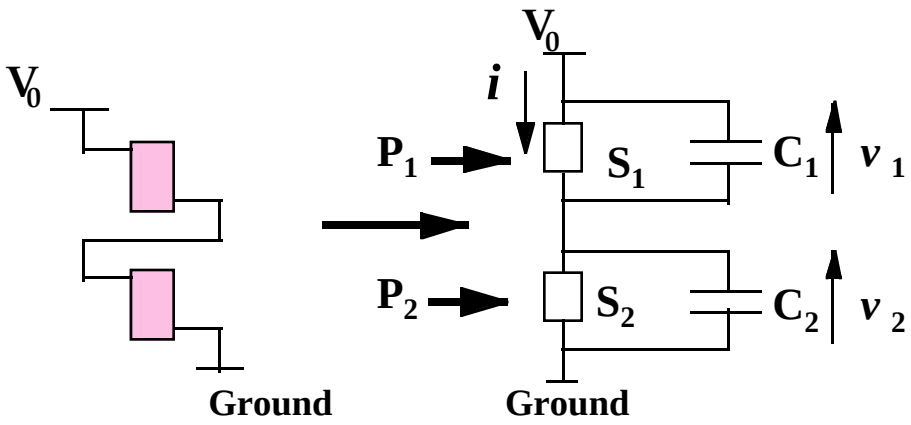

Figure 3-14: Circuit model used for transient analysis of S-SEEDs

These equations were used for the transient simulations. First, experimental reflectivity and responsivity data were obtained for S-SEED devices from the literature. These curves were then fitted with n^{th} order polynomials using a least squares method. Using a Runge-Kutta method implemented in Matlab $v_1(t)$ and $v_2(t)$ were calculated under the following assumptions: 1) V_0 the bias voltage is held constant, 2) C_1 and C_2 the capacitances are constant during the switching, 3) the transient is determined by the time it takes to charge the capacitance of each p-i-n diode with the photocurrent generated by the diodes, 4) the input, P_1, is a step function ($P_1(t)=P_1^0 + \Delta P/2\ (1 + t/|t|)$), and 5) P_2 is constant. Simulations were done for a variety of values of P's and C's, with V_0=10 volts.

Results for two particular sets of values are shown in Figures 3-15(a) and (b). Both figures show the responsivity data used for these devices as well as voltage versus time and the corresponding reflectivity vs. time. Figure 3-15(a) uses parameters of P_1=0.34 mW, P_2=0.22 mW, and C_1=C_2=20 pF. Figure 3-15(b) uses P_1=4.3 mW, P_2=3.2 mW and C_1=C_2=15 pF. In both sets of data, ΔP was varied between 0.05 and 1.0 mW and it was determined that the devices switch faster for larger ΔP. In accordance with assumption 3 above, we find that providing more power to the devices generates more current, which switches them faster. In addition, devices with lower capacitances switch faster, as would be expected. For a device with a capacitance of 20 pF switching times varied between 40 picoseconds and 2 nanoseconds for reasonable values of P_1. The devices grown in our laboratory typically are larger in area so that they are more easily optically probed, and thus have larger capacitances and switch slower. Our experimentally measured switching times were on the order of 20 μsec (Figure 3-16), which is larger than the values simulated because of other stray capacitances in the measurement set-up and packaging of the devices. Repeating the simulations with larger value of capacitance (from the pads and the probes) results in a value close to that measured experimentally. Other more complex models of SEED devices have also been studied which involve more complex circuit models and better experimental measurements and thus typically provide more accurate results[7]. In general, however, the device switching speed remains constrained by the driving electronics.

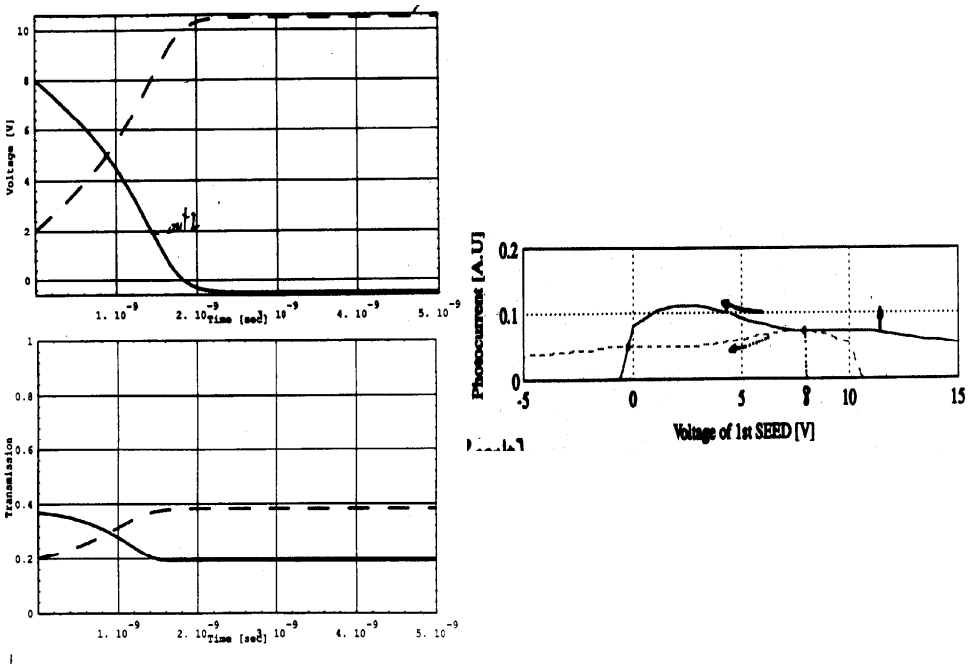

Figure 3-15 (a): Results of transient analysis calculations showing rise and fall times of the two devices switching simultaneously

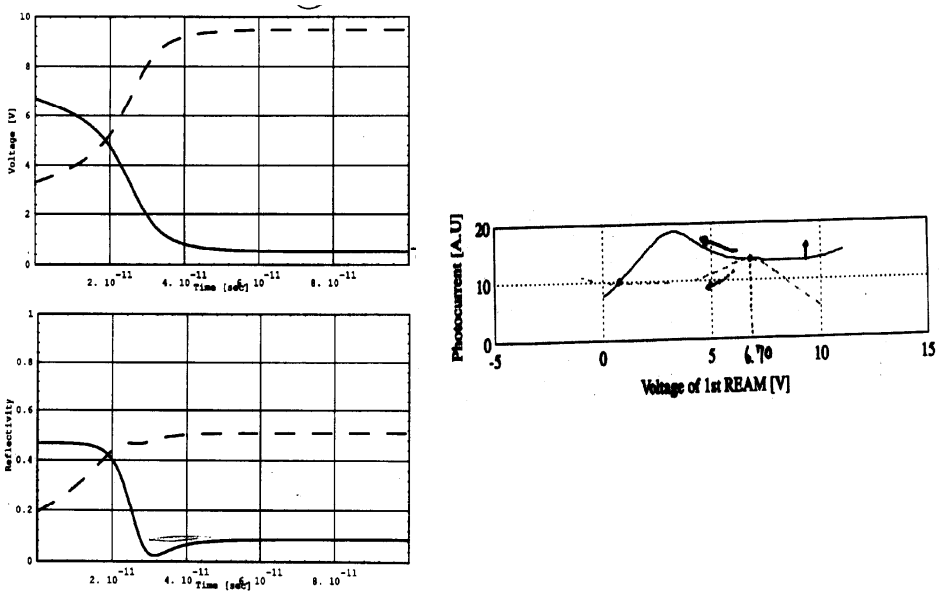

Figure 3-15 (b): Results of transient analysis calculations showing rise and fall times of the two devices switching simultaneously

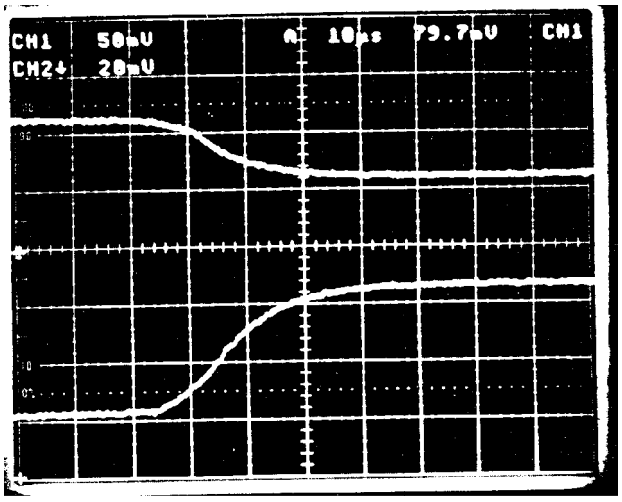

(a)

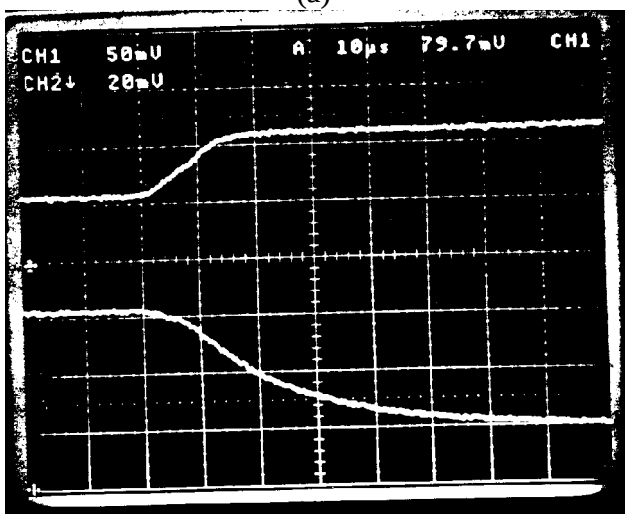

(b)

Figure 3-16: Experimental switching of S-SEED devices vs. time: The two curves represent the two devices, (a) modulator 1 switching to absorbing state, (b) modulator 1 switching to reflecting state

3.6 Conclusions

In this chapter, we have described a configuration of MQW modulator devices known as a self electro-optic effect device or SEED and an extension of this device called a symmetric SEED. These devices can perform Boolean logic as well as a more powerful type of logic known as threshold logic. Computer simulations were performed to accurately predict the bistability loops of the devices and their transient time behavior.

Small devices should be able to switch in on the order of 2 nanoseconds, but device switching speed is typically limited by the driving electronics, not by the devices themselves. The ability of these devices to perform threshold logic was confirmed. The two parameters of importance for this application are contrast ratio and responsivity. The devices also need to be closely matched in terms of these parameters to obtain symmetric switching. These devices can also be integrated with GaAs circuitry and silicon CMOS (see Chapter 6). This chapter has only scratched the surface of the wide variety of applications for which SEEDs have been demonstrated useful, including neural networks[8] (Chapter 4), optical clock recovery[9], chip-to-chip optical interconnections[10], and even an electro-optical computer[11].

Chapter 4--Optoelectronic Neural Networks

4.1 Introduction

Neural networks have a wide variety of potential applications, including associative memory, pattern recognition, and error correction.[1,2,3] Standard electronics often runs into an interconnection bottleneck when trying to implement a neural network. Optical realizations of these networks appear to be ideally suited for such architectures which require massively parallel interconnections between successive layers of neurons. The threshold logic elements from the previous chapter are reminiscent of the basic element in many neural network implementations, the McCulloch-Pitts neuron[4] shown in Figure 4-1, which was motivated by biological models of human neuron cells[5]. In the most common networks, many of these neurons are connected together in a layered structure such as that of Figure 4-2, with the added feature that each element has adjustable weights multiplying the inputs and performs an adjustable sigmoid shaped thresholding, instead of a hard thresholding as is performed by the SEED devices. The smooth sigmoid threshold can be implemented by integrating modulators with GaAs MESFET circuitry. By adjusting the weights in this network depending on the value of the output of the network for a given input, the network can learn a task, such as recognizing a face.

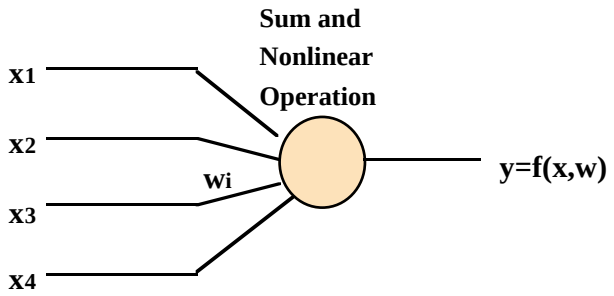

Figure 4-1: The McCulloch-Pitts Neuron

Learning by a neural network is accomplished by any one of several algorithms, including back-propagation and steepest descent methods.[6] Psaltis at Caltech has actually implemented a real time face recognition network using arrays of modulators integrated with transistors.[7] The work of this chapter is based on discussions with the CalTech group on how modulators can be used in implementing arrays of single neuron elements.[8]

In optical neural network implementations, optoelectronic neuron circuits can be arranged in 2-D arrays and can be interconnected optically via the third dimension.[9,10,11] The optical interconnections can be realized with holograms or spatial light modulators and each neural plane can consist of many (1,000 to 10,000) neuron circuits. Each neuron performs a simple function, such as the sigmoidal threshold function of Figure 4-3, on to the next neural plane. In order to build large 2-D neural planes each node in the network has to dissipate very little power (less than 0.1 mW), be able to detect low optical input signals (10-100 nW), and produce a large optical output signal (1-10 μW).

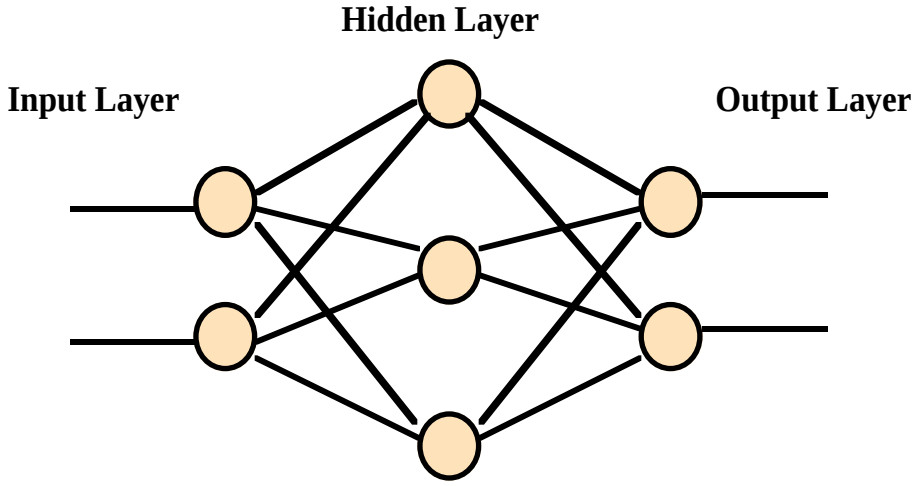

Figure 4-2: Multi-layered feedforward neural network architecture

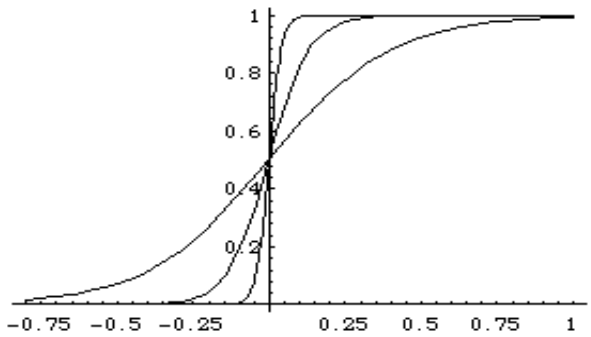

Figure 4-3: Typical single neuron threshold function, $1 / (1 + \exp(-\lambda x))$ for $\lambda=5,15,50$

4.2 Output Device Implementation Considerations

Although neural networks can be constructed of SEED-like devices,[12] it is sometimes advantageous to combine several optical input and output devices together with electronic circuitry, so that each portion of the neuron element is optimized for its own particular function. When selecting output devices (e.g. modulators or LED's), there are three major considerations to take into account: interconnection loss, density of neurons (related to power dissipation), and speed.

4.2.1 Interconnection Loss

The interconnection loss of a neuron is determined by a number of factors including the number of connections per neuron, type of interconnection medium, and the type of light source used. In order to connect the output of a single neuron to multiple other elements, some optical gain must be provided, so that the signals are not lost when propagating through several layers of the system. The number of connections per neuron may affect the choice of interconnection medium between holographic interconnects and spatial light modulators as well as the choice of light source. Choices of light source include on chip laser diodes and LED's and off-chip lasers combined with modulators and employed as the output devices. Coherent sources are typically better for two reasons. First, common holographic interconnections made using photorefractive mateials are more

efficiently read and written with coherent light, and second, incoherent sources radiate light into a large solid angle and thus only a portion of the output light is captured by the next neuron. Given a coherent source, one can select laser diodes or modulators as output devices. This choice is determined by other considerations described in the next sections.

4.2.2 Density of Neurons

If a large density of neuron elements per area is required, the power dissipation of a single neuron becomes a limiting factor. For a maxium dissipation of 10 W/cm^2 using LED's with small currents, a density of about 100,000 elements/cm^2 can be achieved. For LED's, however, higher density means slower operation which becomes a problem if speed is a consideration. Because of interconnection loss considerations, we must choose between laser diodes and modulators. The choice between these is clear if neuron density is a consideration. Modulators operate with reverse bias, so that the currents flowing through them are small, and they thus can be fabricated in dense arrays. Array uniformity in terms of operating wavelength and contrast ratio may be the only limiting factor using modulators as output devices.

4.2.3 Speed

Many networks do most learning or training off-line before use, so that learning speed is not a problem, while others must learn during operation and must be faster. If high speed operation is desired, modulators again should be chosen as the output devices because of their potentially very high switching speeds as described in Chapter 2. In addition, because the charging time of the devices is the speed limitation, scaling down the devices will reduce their capacitances, allowing for a higher density of neurons, which may also be desirable.

4.3 An Optoelectronic Neuron

MESFET based GaAs optoelectronic circuits enable low power consuming and highly complex circuits. To detect the incoming optical signal, instead of using p-i-n modulators as detectors which have relatively low responsivity (1 A/W), a better choice is GaAs photoconductors which have much higher responsivities (> 500 A/W for 100 nW optical input). These detectors are easy to fabricate and integrate with MESFET circuitry for complex thresholding functions because they have the same epitaxial structure as a GaAs MESFET and thus can be grown on the same wafer. As discussed previously, multiple quantum well modulators can be used to convert the electrical output signal back to an optical output signal.

Figure 4-4 shows the circuit diagram for a simple sigmoidal threshold function. The two optical inputs control the gate voltage on an enhancement mode MESFET. Input P_2 can be either the threshold against which P_1 is compared or it can be the summation of the negative inputs if bipolar weights are implemented. The drain voltage on the MESFET controls the voltage across the MQW. Figure 4-5 illustrates how the same epitaxial structure may be used to realize all three devices represented in the circuit.

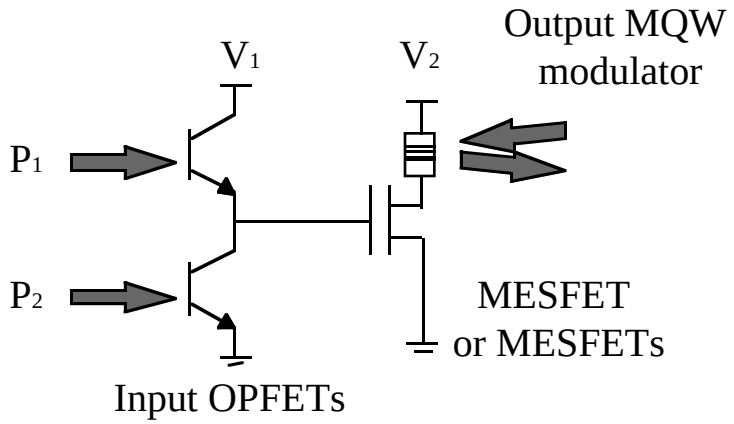

Figure 4-4: Schematic circuit diagram of optoelectronic neuron with optical FETs as inputs and MQW modulator as output

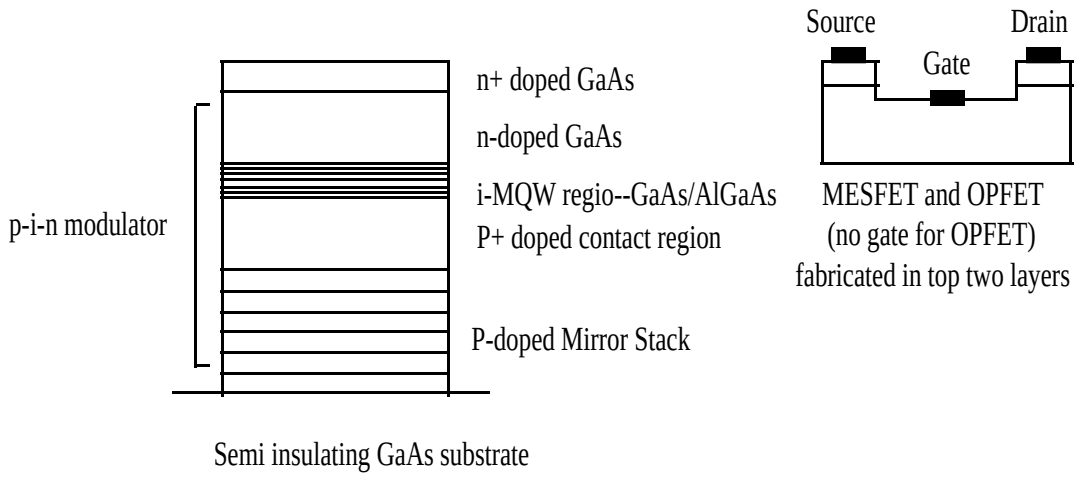

Figure 4-5 Epitaxial structure for p-i-n modulators, MESFETs, and OPFETs

4.4 Conclusions

The main advantages of modulators as output devices over direct sources, such as light emitting diodes and semiconductor laser diodes, stem from the fact that the light source for the output signal is generated off-chip so that there is not a direct trade-off between optical gain and the power consumption of the circuit. Modulators are also preferred due to their use of coherent light sources and potential high speed operation. While it was originally intended to grow the structure of Figure 4-5 for use in the CalTech group's neural network[13], devices with similar structures were made available through an AT&T workshop offering a FET-SEED technology which had already proven successful[14]. The chip obtained from this workshop was used by the CalTech group instead. Several studies were performed of the benefits of this technology for neural network applications[15,16] as well as in many other systems[17,18]. These applications would benefit immensely from the use of modulators grown at Stanford in place of those grown by AT&T. This benefit would result because of the fact that our devices can be optimized for a particular set of desirable parameters (as described in Chapter 2), whereas the AT&T devices which do not reside in Fabry-Perot cavities are not as flexible in their designs.

Chapter 5--X-Modulators

5.0 Introduction

To perform extremely efficient optical switching, routing, and logic, photonic switches and gates should ideally be conservative (preserving optical input power) and reversible (inputs and outputs can be interchanged). Such a device forms a natural and complete primitive for decomposing logic functions. The transmission reflection modulators we have developed[1] (hereafter known as X-modulators) when used as an X-gate (inputs on both sides of the device), or as a single device controllable exchange function—an exchange bypass or 2x2 switch (see Figure 5-1).

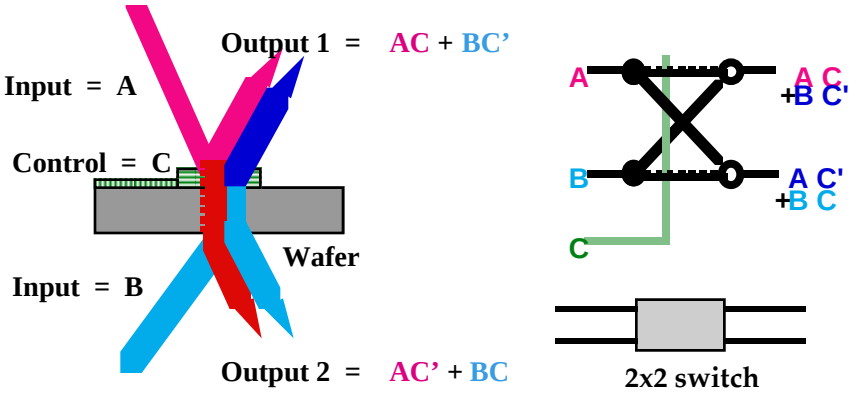

Figure 5-1: Conceptual representations of the X-modulator

The X-gate's current implementation is electro-optical, with one electrical control and two optical data inputs. It is the logical implementation of a Fredkin gate (3-input, 3-output conservative, reversible gate).[2,3] Logic that is conservative and reversible can have very low power dissipation, in that it conserves the number of 1's in the input and output. The reversibility of the gate increases its architectural functionality. These devices are essentially controllable optical routing elements, mirrors, or beamsplitters. In one state beams incident from opposite sides of the device are reflected and in the other state they are transmitted or cross each other. Using arrays of these devices, various switching networks can be constructed, including crossbar switches and other regular or irregular 2-D or 3-D

architectures. This chapter will describe the basics of conservative invertible logic, discuss the X-modulator device design, describe several potential systems applications of the device including optical logic and interconnection, and finally describe some refinements to the initial device design that make it more amenable to systems applications, including voltage reduction, optical control, and incorporated gain layers for fan-out and level restoration.

5.1 Conservative Invertible Logic

Conservative and invertible (CI) logic is defined as follows — an n-input n-output Boolean function *f* is said to be conservative and invertible if it satisfies the following conditions:

- B^n –> B^n is bijective, where B={0,1}
- For any input vector x, w(x)=w(f(x)) where
  $w[x]=w[(x_1,x_2,...x_n)]=\Sigma^n_{i=1}x_i$.

The first condition represents the invertibility of the function. There is a unique mapping between the inputs and the outputs and vice versa, so that the inputs may be determined given the outputs. The second condition describes the conservative aspect of the function. What it implies is that the number of 1's in the output is the same as that of the input. More generally, the function w() represents a metric on the inputs that is preserved to the outputs. Figure 5-2 shows the truth table for one such 3 input-3 output CI function, namely the X-gate whose optoelectronic realization is the focus of this chapter.

Input a b c	Output d e f
0 0 0	0 0 0
0 0 1	0 0 1
0 1 0	0 1 0
0 1 1	1 0 1
1 0 0	1 0 0
1 0 1	0 1 1
1 1 0	1 1 0
1 1 1	1 1 1

d=ac′+ bc

e=ac + bc′

f=c

Figure 5-2: Truth table of X-gate

By counting arguments, one can compute that there are a total of only 36 possible 3-input 3-output CI functions. These functions fall into six equivalent classes with respect to permuations of the output. The six representative functions of these classes are the X (x input conditionally switches y and z), Y (y controls), Z (z controls), R (right rotation), L (left rotation), and I (identity) gates. Furthermore, there are only three equivalent classes with respect to input and output permutation. The representative gates are X (for Y and Z), R (with L), and I. The X-gate and the R-gate are also individually logically complete, meaning that any Boolean function may be realized by some combination of several X-gates or several R-gates. In addition to this fact, they are universal in that using some cascade connections of X-gates with wire permutations can realize any 3-3 CI function. Figure 5-3 demonstrates how several common Boolean functions may be realized using X-gates and also includes the logic functions for X- and R-gates. Note that all of these functions can also be defined using threshold (majority) functions, i.e. the inputs can be switched to the outputs between two permutations depending on if the majority of the inputs are on.

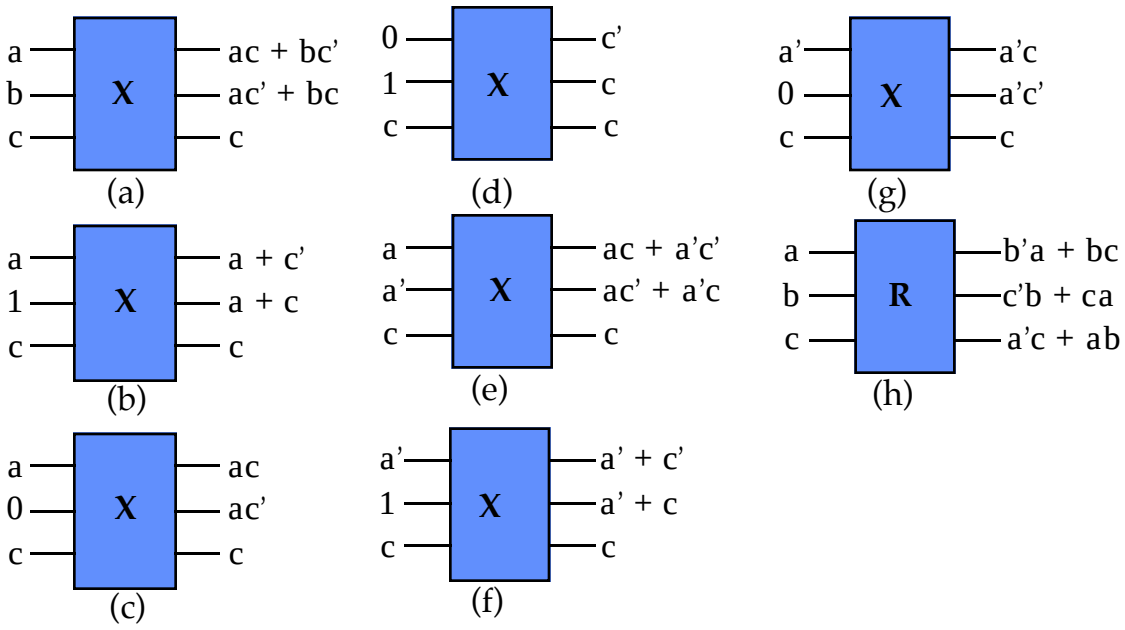

Figure 5-3: Common Boolean functions using X-gates (a-g) and the R-gate(h): a) X-gate, b) OR gate, c) AND gate, d) NOT gate or fanout, e) XOR gate, f) NOR gate, g) NAND gate, h) R-gate.

An important aspect of CI logic readily apparent from this figure is that it is often necessary to insert additional constants or sources at the input of a gate or function and that there are frequently extra signals at the output which may or may not be useful for further computation. As an example of this, note that part d of the figure implements both a 1-2 fanout of the signal and generates its inverse. Figure 5-4 demonstrates how X-gates can be used to construct Y, Z, L, or R-gates. Note that for the Y and Z gates, a simple permutation of inputs is sufficient, whereas for the R and L gates, two X-gates are required. It is also possible to realize logic functions using R-gates, as well as constructing X,Y,Z, and L-gates with R-gates. In this case it is interesting to note that it takes 4 R-gates to realize an X-gate (only two were required for the reverse mapping). Figure 5-5 shows how an X-gate may be realized using R-gates.

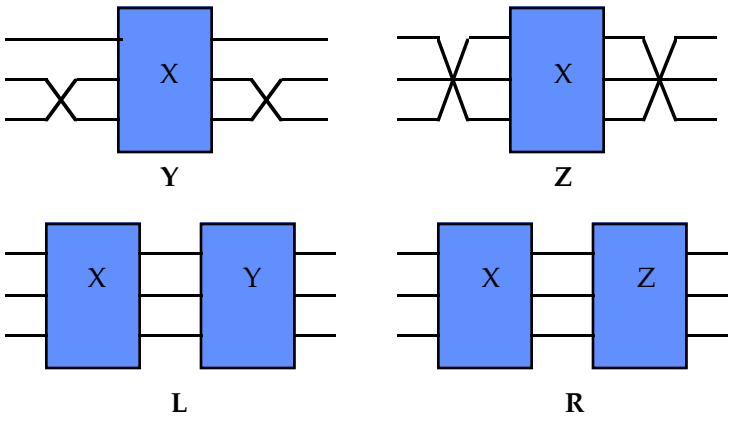

Figure 5-4: Universality of X-gate, demonstrating its use in constructing other 3-3 CI functions (Y, Z, L, and R-gates).

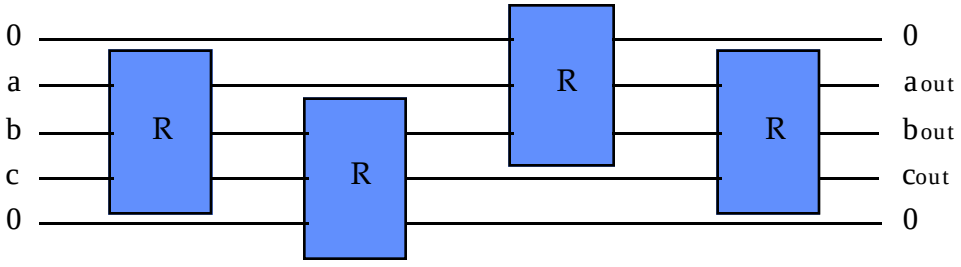

Figure 5-5: Construction of X-gate using 4 R-gates.

Because these X-gate type switches can perform logic functions, it is quite natural to construct a full adder from them, as we have done for Boolean logic and threshold logic with SEEDs. This full adder is shown in Figure 5-7. A program has been written in Mathematica to synthesize logic functions using X-gates[4]. While I have shown how typical Boolean functions may be implemented using X-gates, a direct mapping of combinational logic onto X-gate logic is typically not the most efficient design in terms of number of devices.

Input			Output		
a	b	c	d	e	f
0	0	0	0	0	0
0	0	1	0	0	1
0	1	0	0	1	0
0	1	1	1	0	1
1	0	0	1	0	0
1	0	1	1	1	0
1	1	0	0	1	1
1	1	1	1	1	1

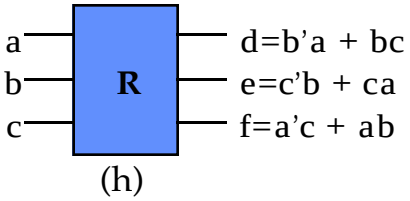

Figure 5-6: Truth table of R-gate.

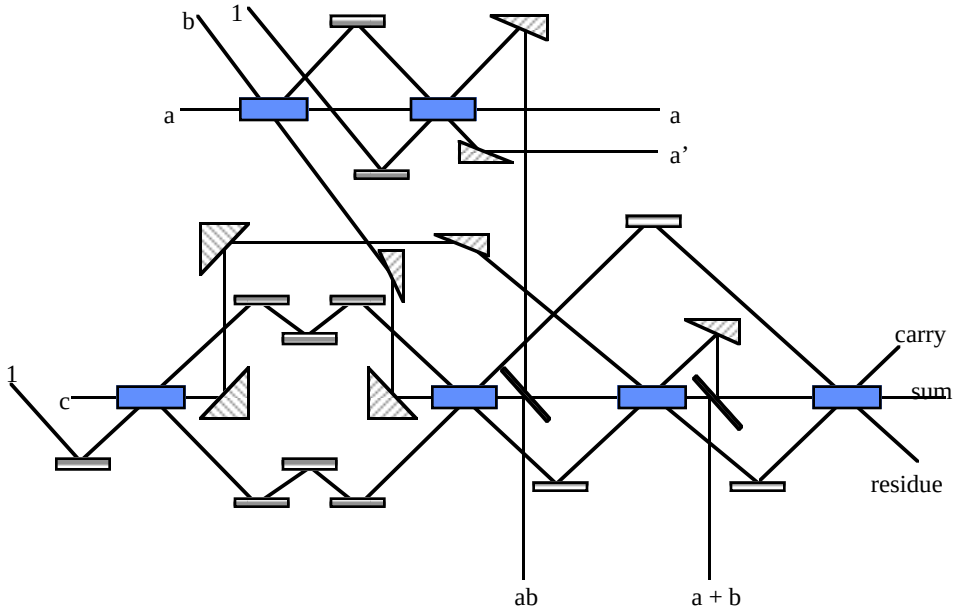

Figure 5-7: Optical implementation of a full adder using CI X-gates

5.2 Previous Optical Implementations

There have been several optical implementations of Fredkin gates prior to the quantum well modulator based gate as described by Shamir et. al.[5]: the polarization switching gate, acoustooptic gate, photorefractive gate, and waveguide or coupler switch. In a polarization switching gate, two orthogonal polarizations of light impinge upon an electrooptic modulator which rotates polarizations by 90 degrees when active. The control signal for this modulator may be either an electrical signal or an optical signal converted to an electrical one by a photodetector. Both beams share the same physical path and can be separated by a polarizing beam splitter if necessary. In an acoustooptic gate, two laser beams are incident upon an acoustooptic deflector at the Bragg angle. If the acoustic control signal is present each beam is deflected into the other channel.

Photorefractive gates are based on four-wave mixing so that two control (or pump) beams when present will phase conjugate the two input signals thus switching the outputs. Perhaps the most promising of these four implementations is the modulated waveguide or fiber coupler which may be either electrically controlled or use an orthogonally polarized control signal to activate the coupling region (consisting of a nonlinear or electrooptic material) between the two inputs.[6,7]

5.3 Device Design and Theory

The device can be thought of as a front mirror with electric field reflectivity r_f and an effective back mirror with reflectivity $r_b e^{-\alpha L}$, where α is the quantum well exciton absorption and L is the optical cavity thickness. The device is designed to contain nearly matched front and effective back mirrors at zero applied field, so that the value of R and T will be nearly equal. With no bias on the structure, the quantum well absorption peak is at

a shorter wavelength than the cavity resonance so that the absorption at resonance is low. From simple cavity theory, the device's intensity reflectivity and transmittivity are given by:

$$R = \left[\frac{r_b\, e^{-\alpha L} - r_f}{1 - r_f r_b\, e^{-\alpha L}} \right]^2 \qquad T = \frac{\left(1 - r_f^2\right)\left(1 - r_b^2\right) e^{-\alpha L}}{\left(1 - r_f r_b e^{-\alpha L}\right)^2}$$

As the front and back mirror reflectivities become equal, R becomes zero and T nears unity (for small α). Larger minimum values of α decrease the maximum transmission. Application of an electric field red shifts the lowest energy exciton absorption towards the Fabry-Perot wavelength via the quantum confined Stark effect (QCSE), thus increasing the absorption at that wavelength. Consequently, this increases the device reflectivity R and decreases T. These operating conditions are illustrated in Figure 5-8.

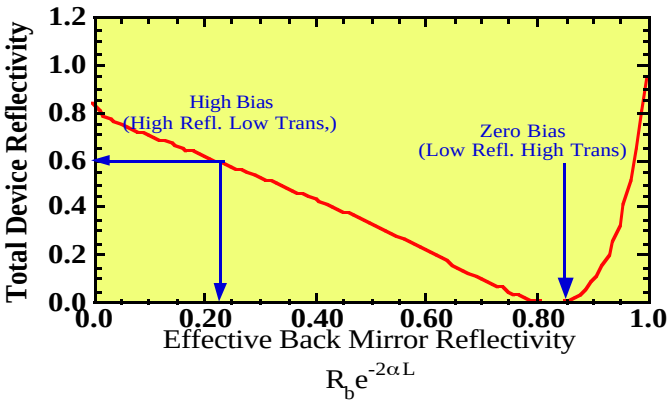

Figure 5-8: Operating conditions for the X-modulator

The structure of the X-modulator consists of a slightly asymmetric Fabry-Perot cavity containing top and bottom mirrors of 10 and 12.5 periods of GaAs/AlAs quarter wave stacks surrounding an undoped cavity of 48, 75 Å $In_{0.2}Ga_{0.8}As$ quantum wells. The bottom of the wafer was antireflection coated with a 1/2 wave layer of SiN_x to remove any effects of the semi-insulating substrate on transmission properties. This structure is shown

in Figure 5-9. Even though the front and back mirrors differ in their number of periods, their reflective properties are similar, for the top mirror also includes the semiconductor/air interface. This particular device was designed to have equal reflectivities from both sides of the device as well as having equal values of reflection and transmission. In-situ measurements and corrections were made at three points during the growth. The first correction was made after half of the bottom mirror was grown. The second was made just after the growth of the cavity region to place the cavity mode at the center of the wafer about 200 Å from the zero bias exciton absorption. The third correction was made just before the complete structure was grown, to ensure that the zero bias response was correct and that no additonal growth was required. The wavelength at which the exciton and cavity mode occurs is 9740 Å, where the GaAs substrate is transparent, allowing light to pass through the device from either side. Additionally, at zero bias, the front and back mirror reflectivies are nearly equal, so that the device characteristics should be the same from the front side and back side of the wafer.

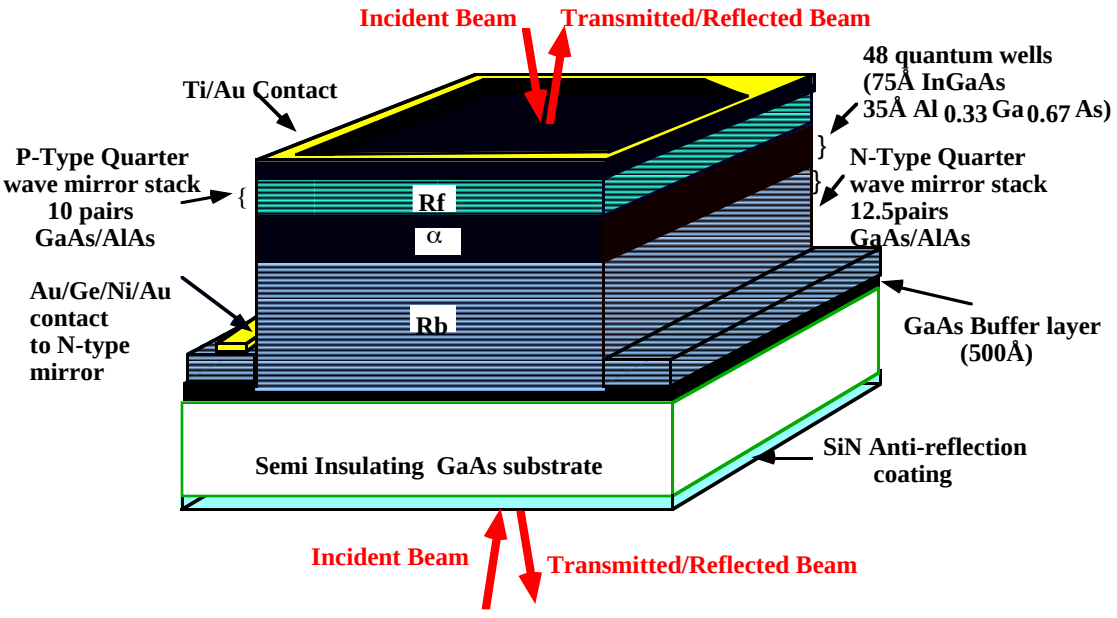

Figure 5-9: Device structure of the X-Modulator

Using our thin films computer simulations, we can calculate and predict modulation ratio (MR), optical bandwidth (OB), and change in reflectivity (DR) (related to insertion loss) for our devices and study the tradeoffs between them. See Reference 8[8] and Chapter 2 for a further discussion of the device parameter space and design tradeoffs.

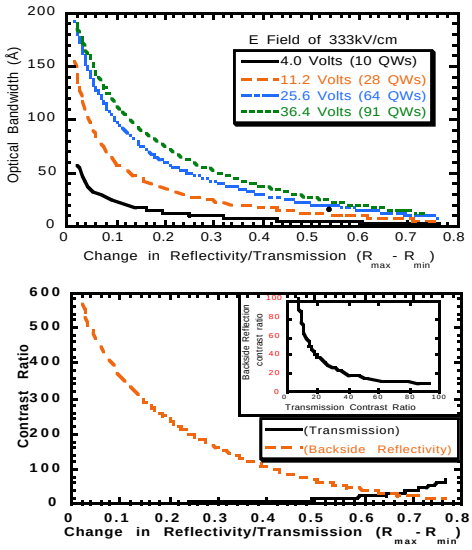

Figure 5-10: Parameter space for X-modulator: Optical bandwidth and contrast ratio vs. change in reflectivity.

Figure 5-10 illustrates some of the parameters of interest for an X-modulator. To summarize the results shown there:

- For fixed voltage, as MR increases, DR increases and OB decreases.
- For fixed DR, as voltage increases, OB increases and MR decreases.
- For fixed MR, as voltage increases, OB increases and DR decreases.

We can control the front and back mirror reflectivities, cavity length, distance in wavelength between the zero bias exciton peak and the Fabry-Perot wavelength, and maximum and minimum absorption to tune a given device for a desired application. Figure 5-11 shows the theoretical and experimental reflectivity and transmission spectra for our device which is shown to switch between 60% and 6% reflectivity and transmission in both states.

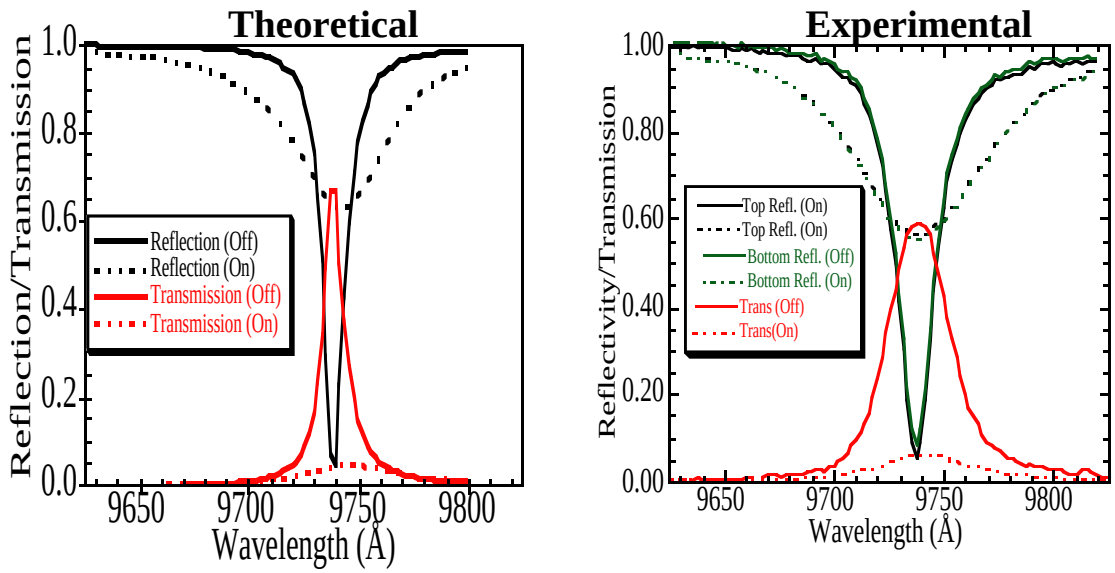

Figure 5-11: Theoretical and experimental curves for reflection and transmission of the X-modulator. "On" indicates response with 40 Volts applied.

Devices which are not symmetric from the front and back sides of the wafer may also be designed, and can result in higher contrast ratios. The contrast ratio of the symmetric device is 10, whereas the contrast ratio of the device simulated in Figure 5-12 is around 80. At the end of this chapter an arrangement of devices is shown which can symmetrize these characteristics, as well as enhance the contrast ratio even further.

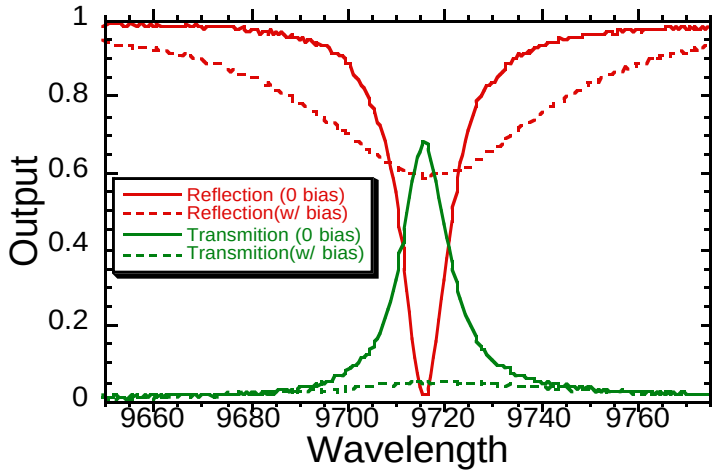

Figure 5-12: Simulated characteristic for asymmetric X-modulator with higher contrast ratio

In order to investigate device stacking, it is necessary to investigate device response at various angles of incidence and for TE versus TM polarized light. Incident angle must be accounted for when designing devices, however, angle can be used advantageously to increase device yield in MBE grown wafers which typically display a radial growth nonuniformity. Figure 5-13 shows the zero bias reflectivity spectra for the X-modulator, which was designed for optimal performance at normal incidence (0˚). As can be seen from these simulations, for incident angles larger than 25°, the zero bias reflectivity becomes strongly angular dependent. This effect occurs because the Fabry-Perot mode, initially at 9840 Å, shifts as the light sees a different effective optical distance, but the exciton absorption does not shift in the same manner. Thus, the contrast ratio is degraded and we see a split in the TE and TM characteristics Such dependencies will in turn affect multiple device characteristics, such as crosstalk and insertion loss. In addition, we show how the use of a larger cavity can offset angular dependencies. The wider cavity device is designed to be matched to the 9840 Å device with an incident angle of 25˚. When designing structures for operation at non-normal incidence, the value of the exciton absorption at a given wavelength could be affected if TE polarized light is not used. This is the result of differences in the amount of absorption of TE and TM polarized light by the heavy hole and light hole excitons. Heavy hole TM absorption is essentially zero while light hole absorption is enhanced for light travelling in the plane of the quantum well material.

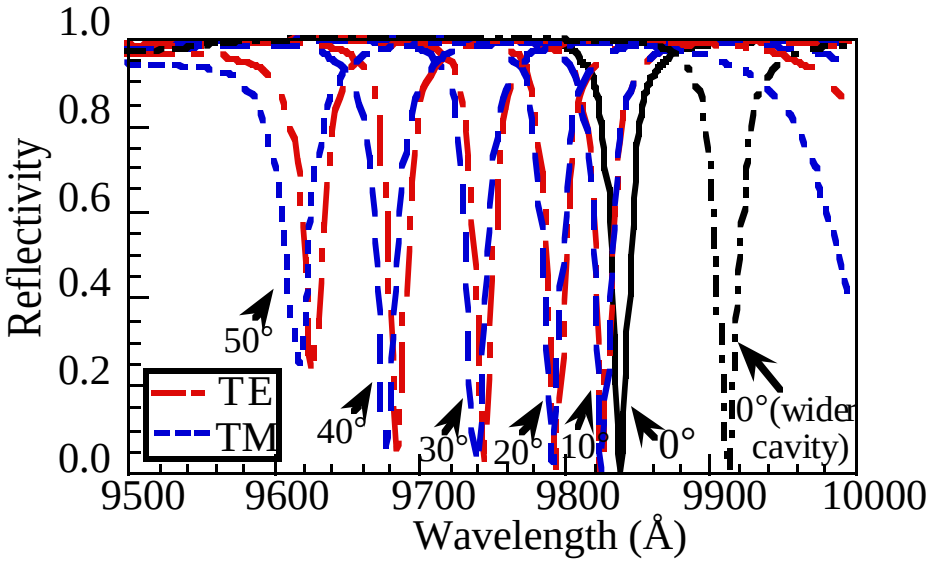

Figure 5-13: Simulation of zero bias reflectivity of X-modulator at various angles using TE and TM polarized light, demonstrating the degradation of the contrast ratio and the TE-TM split. The reflectivity of a wider cavity optimized for 25˚ is also shown.

5.4 Systems Applications

In this section, we will describe some of the possible systems applications of the X- and R-gates. As previously stated, X- and R-gates are useful for computation, coding, switching, and routing. To begin with, we have demonstrated the logic and routing functionality of the X-gate by stacking two devices in series and verifying the expected output functions as shown in Figure 5-14[9]. Because large optical output is available in both states, an incident optical signal at A or B could be routed to any of the three optical outputs, depending on the state of the electrical inputs, D and E. We theoretically predicted and experimentally verified the logic performance of two stacked 200 μm x 200 μm square X-modulators. Light incident at 21˚ off normal incidence was used, which imparted a 50Å blue shift to the Fabry-Perot resonant wavelength. For these measurements, only input A was an 'on' optical signal, making the outputs D, D'E, and DE' for outputs 1, 2, and 3 respectively. Output 1 represents the single device reflectivity response as shown previously in this chapter. Figure 5-14 shows the logic high and some of the various logic

low levels at the FP wavelength for outputs 2 and 3, given the various combinations of the electrical inputs.

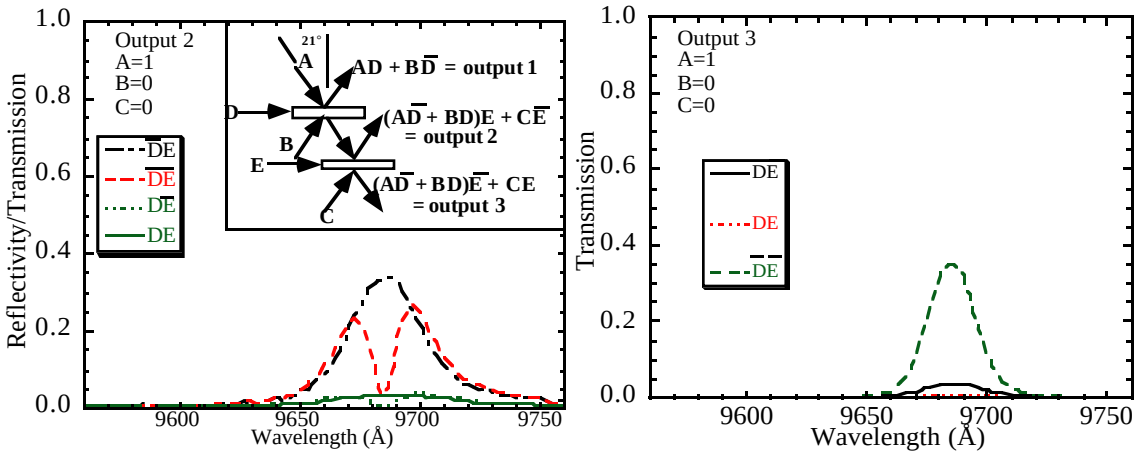

Figure 5-14: Measured signal versus wavelength for output 2 and output 3 (shown schematically in inset) of a dual stacked X-modulator system. Output 1 is similar to the plots shown in Figure 1 with the appropriate wavelength shift.

A single X-gate with an electrical control signal performs a simple 2x2 exchange operation. This operation is useful for sorting and routing networks. Using regular arrays of these devices as shown in Figure 5-15, we can easily construct a 4x4 (or in general, an NxN) optical crossbar switch, permuting the 4 optical inputs to the 4 optical outputs in a conservative manner (number of 1's is preserved). Crossbar design issues include reconfiguration time, signal bandwidth, total data throughput, and data word size. Optical crossbars, such as the one shown here, should outperform electronic versions in all of these areas. The reconfiguration time for the network shown should be around 0.1 nsec, the signal bandwidth is large because the data path is all optical, and the data throughput can be large because many lines can be switched in parallel, as can the data word size.

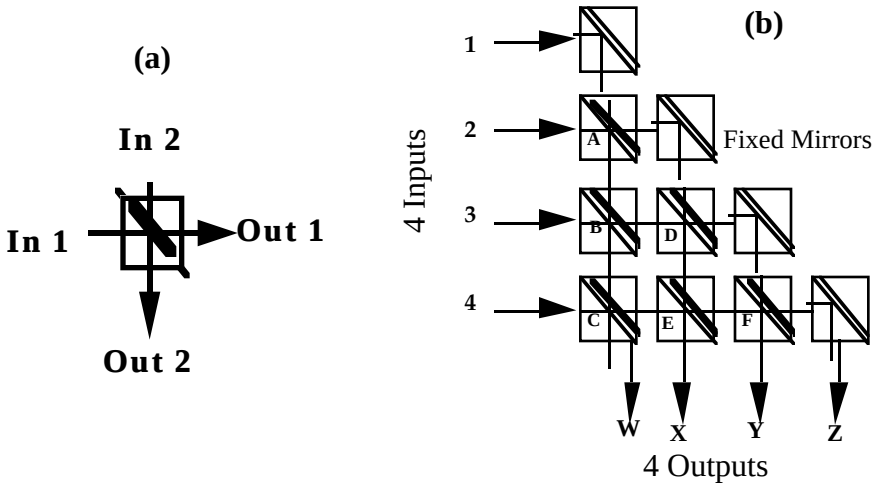

Figure 5-15: (a) Schematic representation of X-gate, (b) 4x4 optical crossbar using 6 X-gates in a regular triangular array.

For simplicity, we will first examine the 4x4 crossbar switch shown in Figure 5-15. The minimal implementation of the 4x4 crossbar requires only 5 X-gates and is shown in Figure 5-16, along with a schematic representation of how this switch might be realized using stacked devices. This implementation of the crossbar may also be flattened onto a single wafer layer with a few mirrors placed around the structure (a multibounce type architecture) as shown in Figure 5-17.

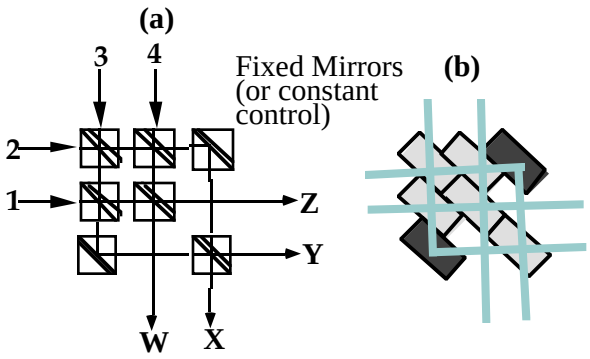

Figure 5-16: Minimal realization of 4x4 crossbar with 5 X-gates

Figure 5-18 depicts the worst signal to noise ratio for any of the output channels over all of the possible voltage switching configurations given optimally symmetric individual X-modulators with the given changes in reflectivity/transmission ($R_{on} - R_{off} =$

$T_{on} - T_{off}$) and contrast ratio ($T_{on}/T_{off} = R_{on}/R_{off}$) for both the 5 and 6 element realizations. It is also possible to use asymmetric device structures (where $T_{max} \neq R_{max}$) and vary other device parameters to adapt optimal X-modulator device structures to specific

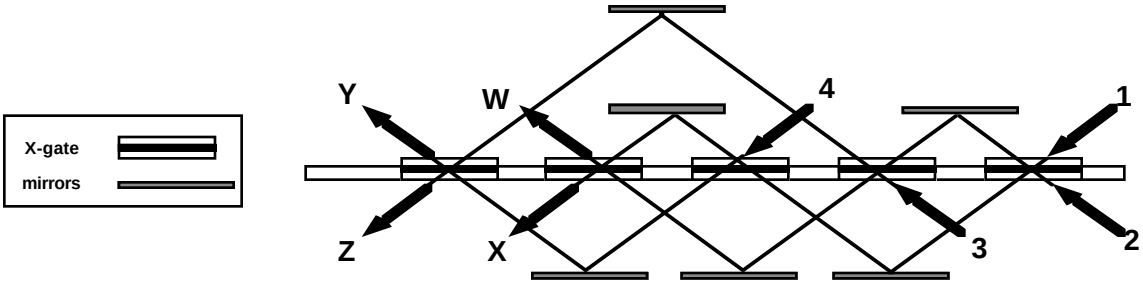

Figure 5-17: Single Wafer plane realization of 5 X-gate 4x4 crossbar switch

systems applications. A 3-D interconnect arrangement using stacked wafers of X-modulator arrays is envisioned to replace previous interconnect technologies because of its fast reconfiguration time, high signal bandwidth, and potentially high data throughput. As a routing device, the X-modulator, whether electrically or optically controlled, is very promising. Regular arrays of X- or R-gates (i.e. 2-D and 3-D stacked structures of quantum well devices) can also be used to realize field programmable gate arrays (FPGA's)[10] and other more complex functions (such as full adders and other logic units). Figure 5-19 shows an optical FPGA implemented using X-gates in a binary lookup table design, which is essentially the triangular crossbar switch above with the devices rotated by 90˚. The conservative and reversible nature of the X- and R-gates can be efficiently utilized in automatic logic synthesis and layout (CAD). The all optical full adder of Figure 5-20 was obtained using a synthesis approach, and is realized with only 5 X-gates (and one for fan-out), which demonstrates another improvement over the full adders described in Chapter 3. This implementation would require optically controlled devices or some optoelectronic conversion between devices.

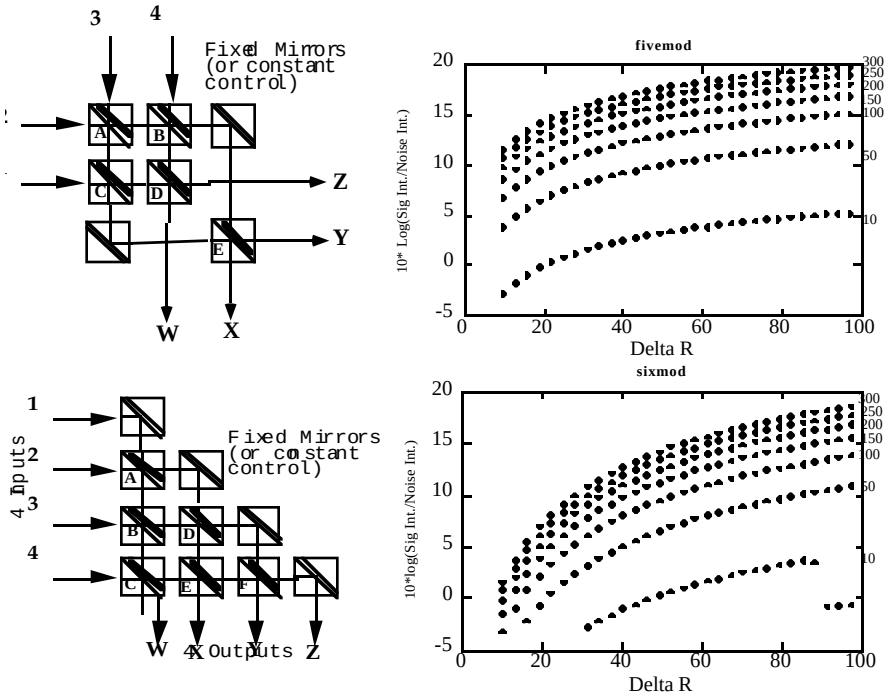

Figure 5-18: Worst case signal to noise ratios for 5 and 6 X-gate 4x4 crossbar switches versus change in reflectivity (ΔR) with contrast ratio as a parameter

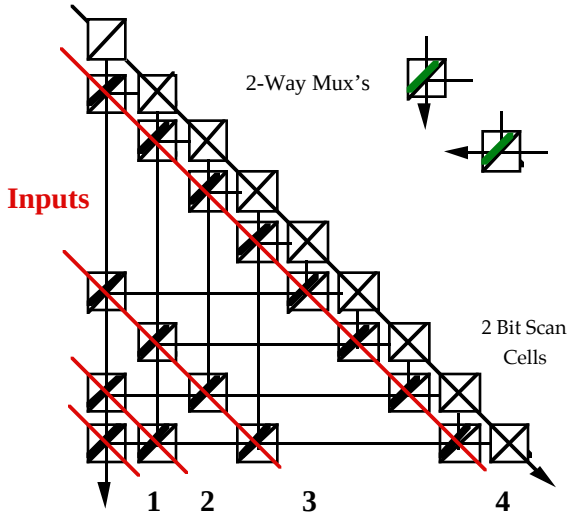

Figure 5-19: Optical implementation of an FPGA using X-gates in a binary lookup table

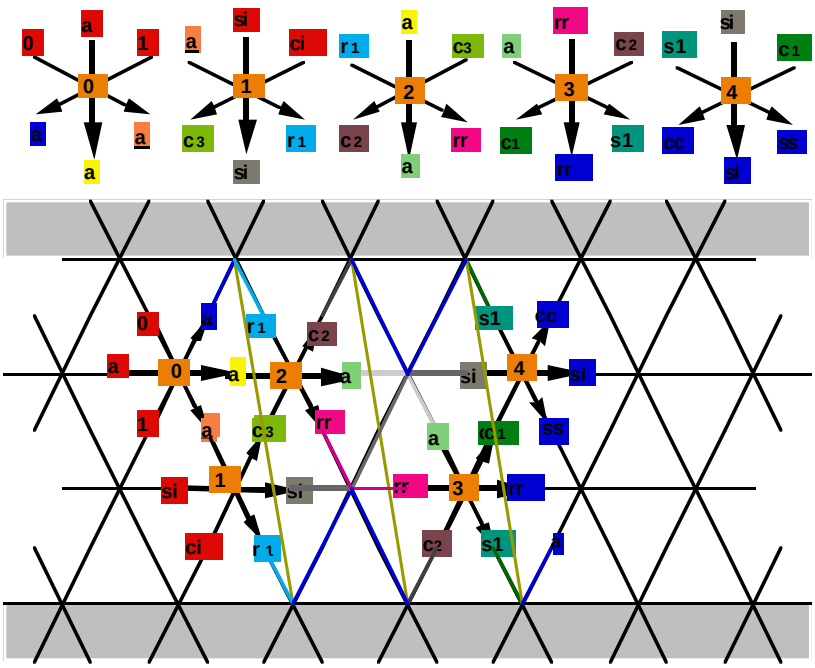

Figure 5-20: All optical full adder implemented with 5 X-gates

Larger crossbar switches can be assembled from smaller 2x2 or in general N by N crossbars in various configurations. For example, we could simply extend our triangular array of devices to an NxN array. However, the number of devices required by this arrangement grows as N^2, which is usually an unacceptable complexity. Numerous other networks have been proposed in the literature, for example that of Figure 5-21[11], which indicates how larger crossbars may be built up recursively from smaller ones. The figure also compares the number of devices needed for a regular triangle implementation to a smarter method. All of these networks may be realized with our X- and R-gates. In most cases, even the implementation shown in the figure is not the minimal realization. For example, Figure 5-22 demonstrates how an 8x8 crossbar can be constructed with only 12 2x2 switches. Some of these proposed networks are more adapted to our technology than others. In general the more regular the architecture of the network, the better suited it is to X-gate implementation.

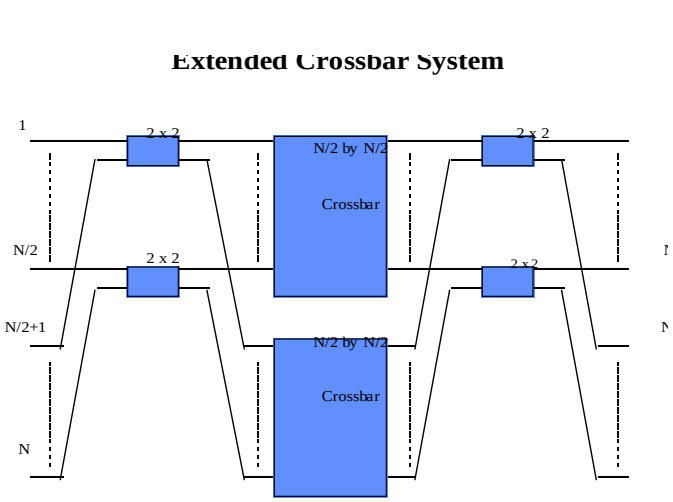

Network Size in terms of

N	regular
4	6
8	28
16	120
32	496
64	2,016
128	8,128
256	32,640
512	130,816
1024	523,776
2048	2,096,128
4096	8,386,560
8192	33,550,336
16384	134,209,536

Figure 5-21: Construction of a larger crossbar switch using smaller crossbars. Comparison of the number of X-gates required for this implementation compared to a regular triangle array.

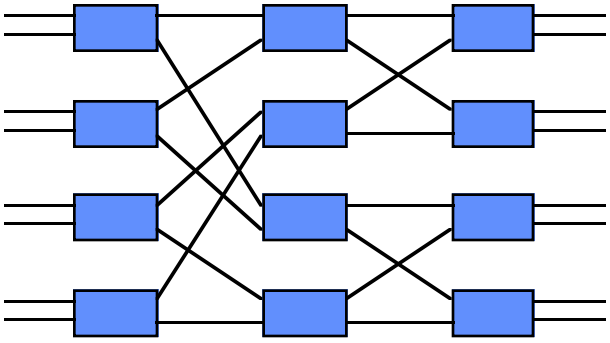

Figure 5-22: 8x8 Crossbar switch

We are in the process of comparing our technology with AT&T's SEED-CMOS technology[12], where GaAs modulator arrays are flip-chip bonded onto silicon CMOS circuitry. This technology will be described in the next chapter. We have implemented a 4x4 crossbar switch with this technology where the crossbar is in silicon and the optical inputs and outputs are GaAs modulators and photodiodes. This design will be compared with our 4x4 crossbar where the data path is all optical, hence the data bandwidth in our design is not limited by electronics (>100 GHz).

So far we have looked at applications of X-gates for building optical routing and switching architectures. A single R-gate can be constructed from 2 X-gates in cascade (Figure 5-23), by having each X-gate exchange 2 different inputs. We also note that this

implementation requires optically controlled X-gates, or at least optoelectronic conversion for the control signals. This fact also indicates that the R-gate is a natural 'all-optical' device (control and data signals are optical). We discuss optical control possibilities in a later section of this chapter. Figure 5-23 also clearly indicates the rotational symmetry of the R- (or L-) gates. An R-gate type router can be obtained by a non-minimal but symmetric arrangement of 3 X-gates (Figure 5-24). R/L gates can also be constructed from the thresholding elements of chapter 3.

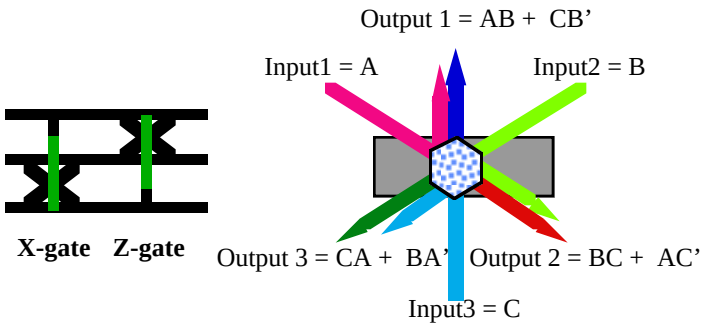

Figure 5-23: Rotationally symmetric representation of R-gate

Controls	Output
1 2 3	1 2 3
R R R	A B C
R R T	A B C
R T R	A B C
R T T	A C B
T R R	A B C
T R T	C B A
T T R	B A C
T T T	B C A

R=Reflective, T=Transmissive

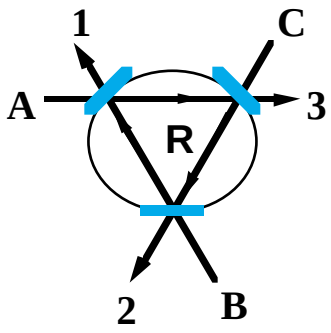

Figure 5-24: R-gate style 3x3 router/switch implemented with 3 X-gates

5.5 Refinements for Optical Switching Systems

It is clear that our proof of concept devices are not ideally suited to systems applications. In this section, we begin to address three specific aspects of the structures which should make them more amenable to use in a systems context. First of all, the voltages at which the initial device operated (40 Volts) is much too large to use in an optoelectronic system or to integrate with electronic systems. A partial solution for this problem was experimentally proven feasible. Second, for many applications, it is necessary to have all three inputs of the device be optical. Thus, it is desirable to somehow replace the electrical control signal of the modulator with an integral optical control, which means that we must depart from the use of the quantum confined Stark effect as our means of absorption modulation. Several potential methods for accomplishing this goal have already been demonstrated by others and will be described here, along with their benefits and shortcomings. Finally, although we term our devices 'power-conserving', the maximum transmission is still only 60-70%, which will lead to problems with fan-out and cascading of devices. One method of increasing this maximum transmission or reflection is described, which involves incorporating forward biased quantum wells into the Fabry-Perot cavity to provide gain in addition to the lossy quantum wells to modulate the absorption.

5.5.1 Voltage Reduction

The high voltage of operation in the original X-modulator is partially due to the use of strained 75Å $In_{0.2}Ga_{0.8}As$ quantum wells. The use of this strained material requires the use of large, 200 Å AlGaAs barrier regions to reduce the overall indium concentration and hence strain in the active region. This reduced strain permits the structure to be below the Matthew's-Blakesly critical thickness[13]. Beyond this limit the crystal relaxes through

formation of dislocations and the exciton resonances are quenched. As a first step towards reducing these voltages, we have used a graded buffer region and strain compensation techniques to reduce the thickness of the barrier regions to 100Å. This reduces the required switching voltage of a similar structure by ~35%. In this technique, the bottom and top mirror layers are varied in composition from 0% indium at the substrate up to about 12% indium at the onset of the quantum well region. This 12% value is chosen so that the alternating barrier and well layers, which are strained in opposite directions (tensilely and compressively), compensate each other and thus result in approximately zero net strain.[14] This graded structure is illustrated in Figure 5-25. The photocurrent data for this structure, both with 200Å barriers and 100Å barriers is shown in Figure 5-26. The thickness of the active region was reduced by 40% and can probably be reduced by about 60% with even thinner barriers. This reduction in active area thickness increases the effectiveness of the applied field. As shown in Figure 5-26, at 5 Volts the exciton shifts by 30 Å in the thick barrier case and 100Å in the thin case, and at 10 Volts, 130Å compared to 320Å. We are currently working on a structure with 50Å barriers, as well as some coupled well structures, which can operate at even lower voltages by using spatial separation of carriers to change the absorption rather than the QCSE. Coupled quantum wells can possibly reduce the voltage of operation even more by providing a large amount of absorption per well. Another possibility for reducing the voltage is the incorporation of phosphorous in the barrier material, which will reduce the strain even more by providing a more closely latticed matched material. As a final note on voltage reduction, one could also potentially form a structure consisting of folded or interleaved thin layers in which each layer has a smaller voltage applied to it. In such a structure the quantum wells would still be optically serial but at the same time be electrically parallel. A waveguide implementation of an X modulator would also reduce the operating voltage at the expense of density of devices on a single chip. Both of these alternate solutions involve many fabrication issues which are not the focus of this work and thus not discussed here.

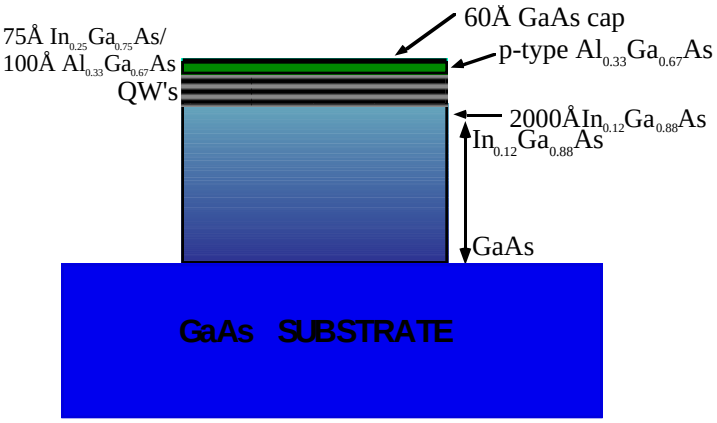

Figure 5-25: Device structure of graded buffer device.

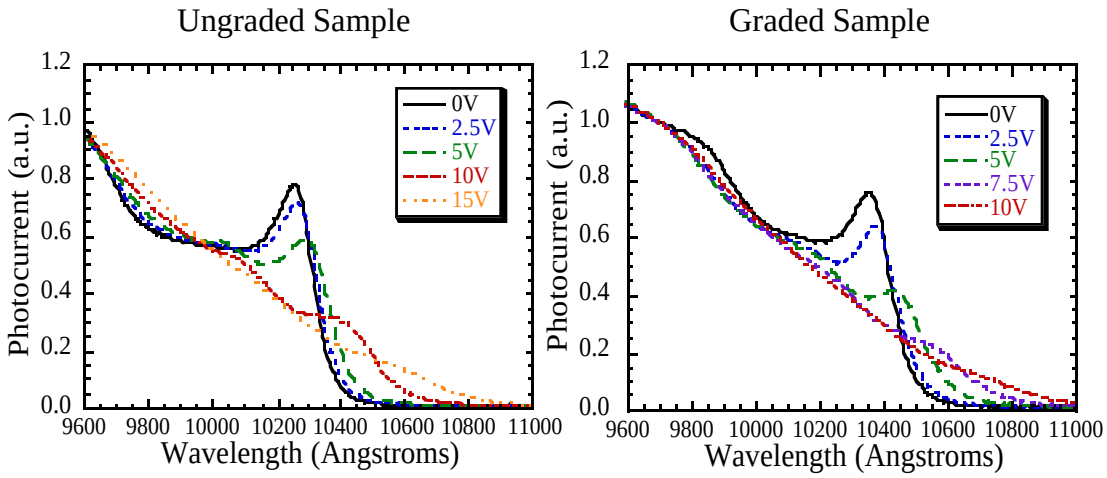

Figure 5-26: Photocurrent data for graded buffer region, showing voltage enhancement.

5.5.2 Optical Control

As mentioned previously in this chapter, it is desirable for many applications to replace the third input of the X-modulator, which is currently a voltage bias, with an optical control signal, thus converting the device to an all optical input gate. Electrically controlled devices will be limited in speed by the RC time constant of the device itself. The charging and discharging time of the device capacitance, which is essentially that of a simple reverse biased p–i–n diode, limits the ultimate switching time of the gate to between 50 and 100 GHz. For electrically switched devices, we are also investigating flip-chip bonded optoelectronic multi-quantum well modulators on silicon CMOS circuitry using a

technology similar to that offered at a recent AT&T workshop.[12] The beginnings of this work will be described in the next chapter.

The underlying excitons involved in these devices are very short lived. The time for electrons and holes to come to thermal equilibrium with a lattice is thought to be in the picosecond range,[15] and the time for electrons and holes to come in to thermal equilibrium with each other is only a fraction of a picosecond. In addition, temperature dependent line width broadening analysis due to LO phonons gives a room temperature lifetime of excitons of 400 femtoseconds for GaAs quantum wells and even less for InGaAs wells. This is clearly much shorter than the RC time constant limitation and points to the need for alternate methods of modulating excitons.

We have investigated all-optical methods of controlling advanced Fabry-Perot devices such as X-modulators. In particular, we are investigating four types of effects. The first approach is shown in Figure 5-27 below and entails the bleaching of QW excitons using control light resonant with the exciton. Intense control light (about 40 kW/cm^2) generates many photo carriers which screen the QW excitons and thus quench the absorption of the excitons. Band filling by the generated carriers also additionally reduce the absorption.

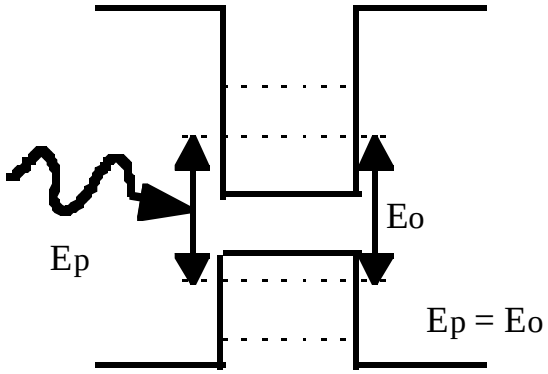

Figure 5-27: Exciton bleaching by generation of carriers, E_p is the photon energy and E_n is the approximate exciton peak

Figure 5-28 demonstrates the difference between this method and the QCSE[16]. Larger $\Delta\alpha$ can be obtained at all λ using this technique. Figure 5-29 shows some experimentally

measured reflectivity spectra taken for 0, 6.6, and 41.2 kW/cm^2 pump intensities.[17] Note that the generated carriers also induce a change in the index of refraction of the material, which shifts the cavity mode towards lower wavelengths. Thus at the operating wavelength, an even larger change in reflectivity is observed than in the case where the mode does not shift. The limitations of this technique are that it requires generation of a large number of carriers, and that for some applications it may be undesirable to have a disparity in the intensities of the three input signals (for example the full adder). The generated carriers must be removed from the device in order for the device to return to its original state. Such techniques have been previously investigated,[18] but this approach might be utilized in Fabry-Perot devices to modulate reflectivity and transmission of incident light. This technique is the easiest of the four described here to implement.

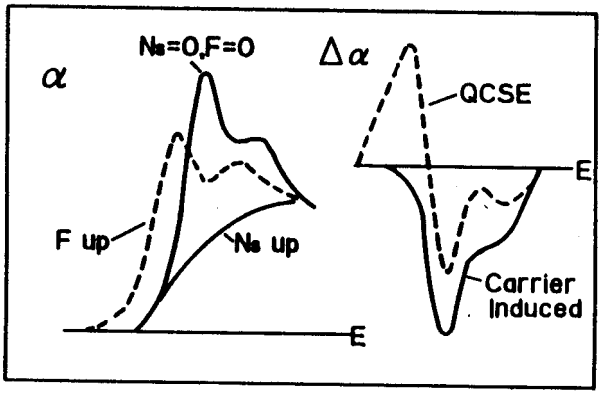

Figure 5-28: Illustration of the difference between QCSE (dotted line) and carrier induced effect (solid line)[16]

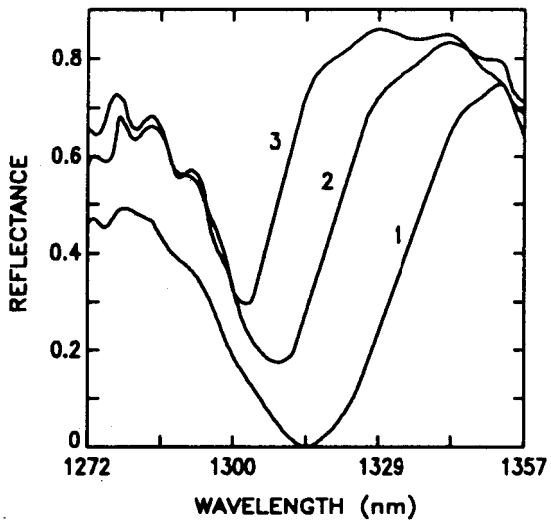

Figure 5-29: Measured reflectivity of a MQW modulator for pump intensities of (1) 0, (2) 6.6, and (3) 41.2 kW/cm^2 [17]

The second technique, shown in Figure 5-30 below, employs what is known as the optical (or a.c.) Stark effect. In this technique, the control light is near, but below the exciton resonance in energy. Thus the control light is not absorbed. Instead, it induces what are called virtual transitions which result in a blue-shift of the exciton resonance (a shift of the absorption to higher energy). Thus absorption is modulated at the energy of the original exciton resonance and refractive index is modulated near and slightly below the band edge. Because the control light does not generate real carriers, the effect lasts only as long as the control beam. From a practical standpoint, if changes in absorption, rather than changes in refractive index are used to perform modulation, the modulated beam generates a very small number of real excitons which decay quickly. The two limitations of this technique are that it requires very intense (a few GW/cm^2) optical beams and that it requires control light at a wavelength other than that of the signals. These two limitations may not be a problem for routing applications, where the intense pulses may be generated locally. Figure 5-31 shows some experimental data illustrating the optical Stark effect in action.[19] In this case, the recovery time of the switching is only 1.2 psec, which makes this technique the most promising in terms of high speed operation.

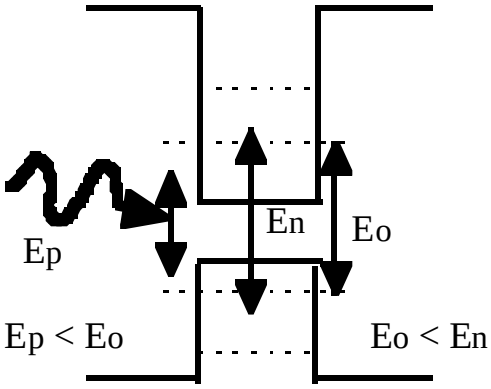

Figure 5-30: Optical Stark Effect: nonresonant light creates virtual transitions and blue-shifts the exciton resonance. E_n is the shifted exciton energy

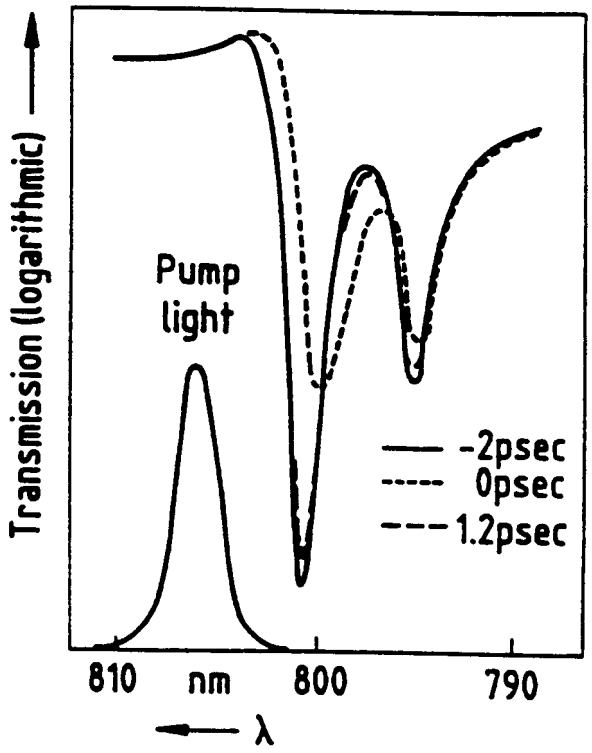

Figure 5-31: Experimentally measured optical Stark effect shown 2 psec before, during, and 1.2 psec after the nonresonant optical excitation of a few GW/cm^2 [19]

The third technique, shown in Figure 5-32, below uses intersubband transitions (those within the valence band) to control interband (between valence and conduction band) absorption. For example, in p-doped quantum wells, normal incidence, intersubband light causes intersubband transitions in the valence band and thus induce changes in the

interband exciton absorption. Here we will discuss both real and virtual intersubband transitions[20] as methods of modulating Fabry-Perot devices. In doped quantum wells, the large exciton absorption resonance is screened by the carriers created by doping. By using control light which is resonant with an intersubband transition (between two states in the valence band, for example). These dopant carriers can be boosted to higher energy levels in the valence band and thus do not contribute to the screening of the lowest level exciton. Thus the absorptive level of the excitons can be controlled. The speed of this technique is limited by the intersubband transition time for the carriers to relax back to the lowest energy band and this time constant could be as short as a few picoseconds. The amount of $\Delta\alpha$ attainable by this technique is not as large as those of the previous two methods.

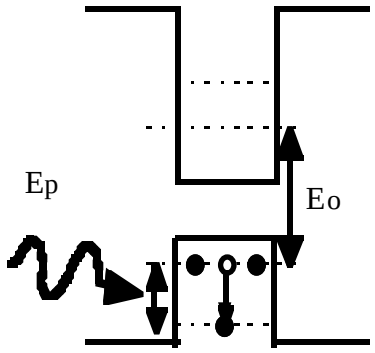

Figure 5-32: Dopant carrier removal through the use of intersubband transitions

Finally, nonresonant intersubband light (where the control light is of slightly less energy than the intersubband transition) may be able to induce virtual transitions between the intersubband states in the doped well as shown in Figure 5-33. In such a case, virtual transitions between the intersubband levels would shift energy levels in that band. This effect would in turn affect the energy of the interband exciton transition. In this case, the movement of energy levels would red-shift the exciton resonance (shift it to lower energy). Since no real carriers move between intersubband levels, the modulation should last only as long as the incident beam. In the investigation of such intersubband light controlling interband absorption, we need to investigate the effects of dopant level and control line

intensity, especially when attempting to employ virtual transitions. The complexity of this effect probably eliminates it as a viable option.

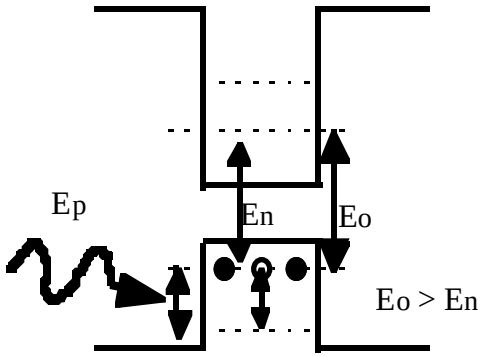

Figure 5-33: Intersubband light used to optically Stark shift instersubband levels, thus red-shifting the excitonic transitions

5.5.3 Dual Zone Structures

As previously mentioned, our test devices as originally designed have a maximum transmission of 60-70% and a minimum transmission of about 6%, hence a contrast ratio of 10. Ideally these percentages should more closely approach 100% and 0%, or possibly even greater than 100% in the maximum transmission case (i.e. amplification) for fan-out purposes. We are attempting to overcome this problem by investigating structures that include two layers, or zones; one that performs the modulation of the light (X-modulator, for example) and one that will amplify the light, in essence restoring the energy that is lost in the modulator.

As an initial design for such a device, we consider two possible configurations. In the first configuration, the gain quantum wells are contained within the same Fabry-Perot cavity as the absorptive wells, as shown in Figure 5-34. In this structure, there are two individually biased regions, so that we end up with a n-i-p-i-n stacking of layers. The gain layers are forward biased to provide a gain of approximately 600 cm^{-1} per well, and the absorptive wells are switched between around 11,000 and 50 cm^{-1} per well loss using the quantum confined Stark effect. It may also be desirable to switch the gain layers between

gain and loss, however the speed of this switching is limited by the amount of time required to sweep the carriers out of the quantum well region. We have simulated the device in the case that only the absorptive wells are switched. The results of this simulation are shown in Figure 5-35. As can be seen in the figure in one state, the device is highly reflective (95% reflection, ~0.3% transmission). Other structures may produce a higher reflectivity than 95%, but are more difficult to correctly grow using MBE. In the transmissive state, the device amplifies the signal transmitted by a factor of ~2 (with ~5% reflection). Thus, we have demonstrated that our devices can incorporate gain layers within the optical cavity to restore some of the light lost to absorption. The optimal reflection and transmission percentages depends upon the architectural configuration of the devices involved. In some cases an asymmetric device such as this may be an acceptable solution or even desirable (for example for use in tapped delay lines or crossbar switches). By simply changing the reflectivity of the front mirror, this device may be transformed into a reflection modulator with gain. The simulated results for this device are shown in Figure 5-36, where the device switches between 110% reflection and reflectivity near zero.

A second possible device structure would consist of two cavities, where the coupling between the modulator cavity and the gain cavity is small to prevent coupled cavity effects. In this case, a large reflectivity mirror is required between the two cavities, which results in a high Q modulator and makes our design difficult to realize. A better solution may involve anti-reflection coating the top of the device so that there is essentially only one cavity present. In this case, the gain layers are only single or double pass depending on the state of the device and thus a larger number of wells would be required. The first configuration is the more promising of the two. The growth and fabrication of these devices would be more complicated than that of a single X-modulator, but similar work has been done at Stanford integrating modulators and LED's.[21]

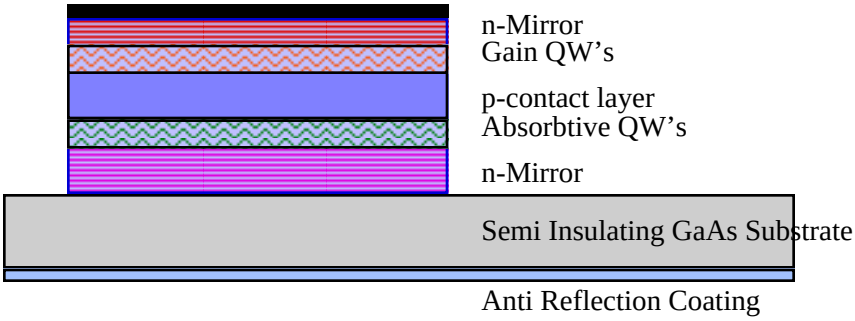

Figure 5-34: X-modulator with gain layer

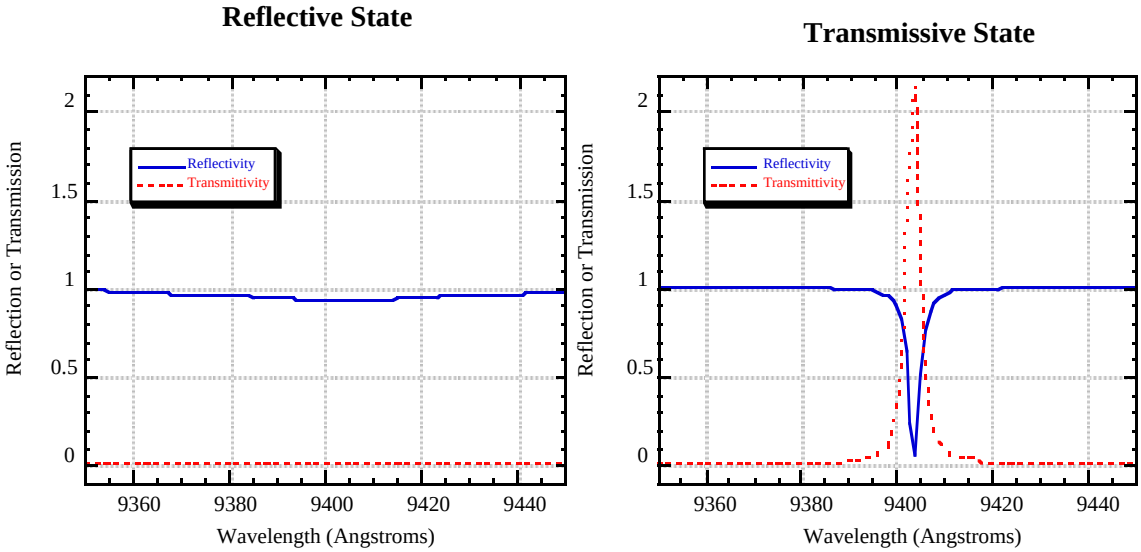

Figure 5-35: Simulation of dual zone reflection/transmission modulator with gain. Contrast ratio asymmetry between the two states

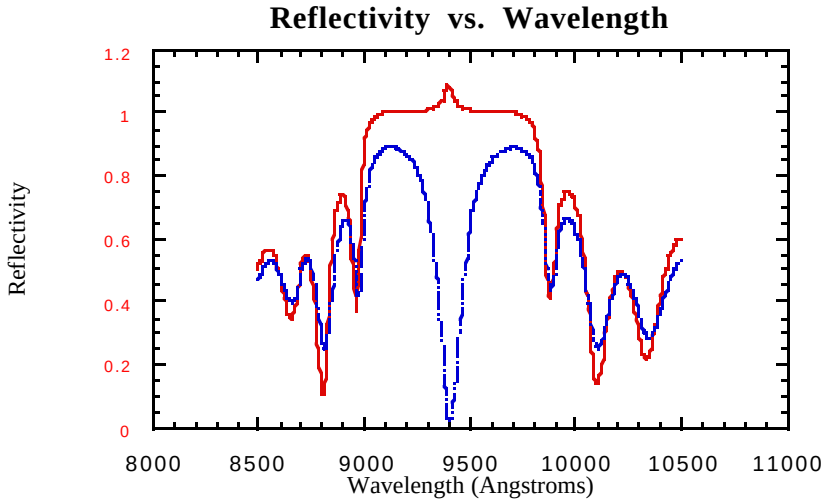

Figure 5-36: Dual zone reflectivity modulator with gain, contrast ratio > 1000

5.5.4 Contrast Enhancing Architecture

As a final note, there are a number of ways to improve contrast ratios and crosstalk by using various arrangements of modulator type devices, and adjusting their parameters where appropriate. Figure 5-37 shows one such arrangement, whereby the contrast ratio is the square of the contrast ratio of the individual devices. Each signal passes through two devices, and some of the undesired crosstalk is filtered out by this arrangement. For our inital devices, this improves the contrast ratio from 10 to 100. This improvement comes at the cost of lowered gain, which could be compensated for by the techniques discussed above, for instance. For modulators with gain for example, contrast ratios can become extremely large. It is also interesting to note that this same switch can timeshare another pair of switching inputs along the anti-diagonal direction, an example that demonstrates that in optics, the same switching space can be reused by more than one set of beams. In addition to the contrast ratio enhancement, several configurations of the individual device states have the effect of symmetrizing the output characteristics, if for example the individual devices were asymmetric from front and back sides, or if they were asymmetric between reflective and transmissive states. Some of the configurations result in essentially an X-modulator from a black box point of view, while others result in various forms of spatial beam shifting and redirection. Some of the possible settings are shown in Figure 5-38.

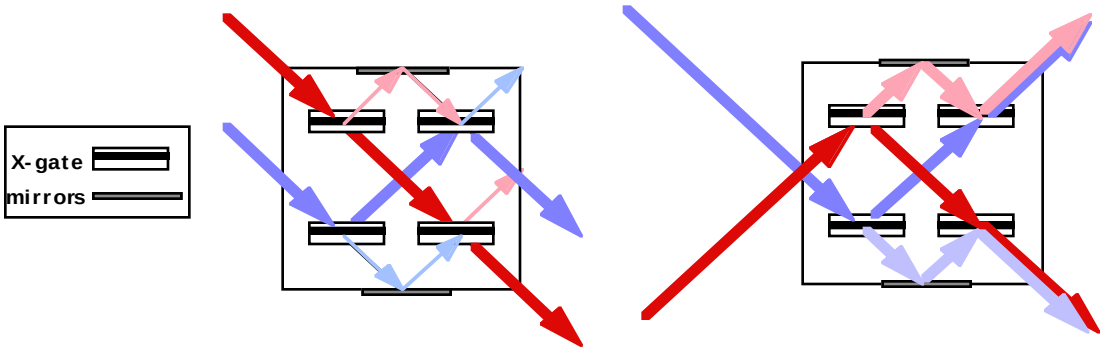

Figure 5-37: Crosstalk improving architecture

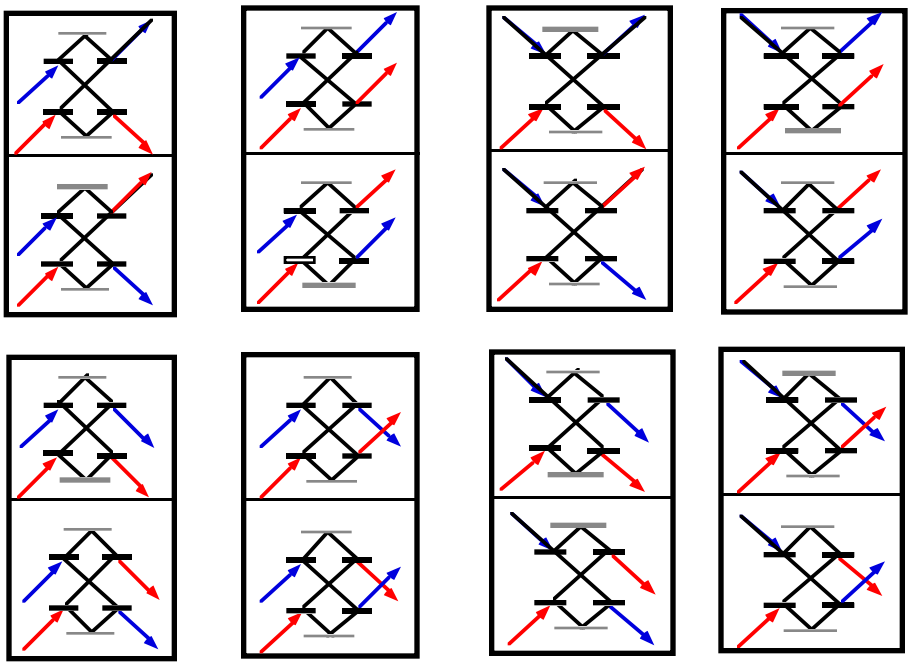

Figure 5-38: Some permutations of the contrast enhancing architecture illustrating the variety of operations that can be performed

5.6 Conclusions

This chapter described the design, fabrication, and testing of vertical cavity X-modulators--structures which allow for conservative invertible switching. Unlike earlier modulator structures which modulate either the amplitude or the phase of light, these modulators act to modulate the direction of the input light without changing the output intensity or phase. We have discussed the use of X- and R-gate devices for switching, routing, and other computations, as well as some aspects of these devices that make them amenable to photonic switching and routing. These devices can potentially be used for both optoelectronic and all-optical implementations. Finally, we have described refinements to the original X-gate design (both current and future efforts) that will make them much more useful for systems applications--voltage reduction, optical control, and level restoration. X-modulators and related devices should have a significant impact on efficient switching, as well as 2-D and 3-D array optical switching, routing, and logic.

Chapter 6--Hybrid SEEDs

6.1 Introduction

In this chapter, a technology pioneered by AT&T Bell Laboratories[1] and Sanders Lockheed Martin[2] which integrates GaAs MQW modulators with state of the art silicon CMOS circuitry will be briefly described. The author of this work attended a workshop describing this hybrid technology and designed a chip using it, which was then fabricated by AT&T. The chip was intended both to explore the AT&T technology and to contrast it to the X-gate technology by implementing 2x2 switches and 4x4 optoelectronic crossbars using it. Both technologies will see broad application in future optical chip-to-chip interconnect and smart pixel systems.

6.2 Description of the Technology

The solder bonding process that has been used very successfully at AT&T/Lucent is illustrated in Fig. 6-1.[3] An array of quantum well modulator/detector diodes is fabricated from GaAs/AlGaAs on a GaAs substrate. Using ion implantation (or using other contacting techniques), the two diode contacts, p and n, are brought to the top surface of each diode. Solder metallization is also deposited on top of these contacts to make the bonding pads. The individual diodes exist as separate mesas on the wafer. The silicon chip that will receive the diodes has a pad layout that matches the diode bonding pads. Additional metallization is also applied to the pads on the silicon chip as required for the solder bonding process. It is important to note that this metallization on the silicon chip can be applied to a fully fabricated silicon chip. The necessary lithography and processing takes place at low temperatures, and is also chemically benign to the silicon chip. Then the

GaAs/AlGaAs modulator array and the silicon chip are placed in a solder bonding machine. The solder bonding machine allows controlled heating of the two chips

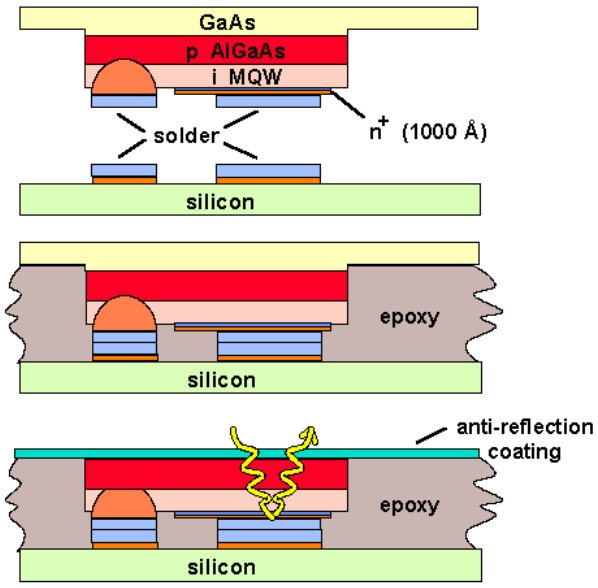

Figure 6-1: Three step hybridization process: 1) Separate fabrication of MQW modulators and silicon CMOS, aligning, and bonding, 2) Flowing epoxy between chips for etch protection, 3) Removal of GaAs substrate and deposition of AR coating [6]

to be bonded, and has optics that allows alignment of the two opposing faces. A relatively standard machine, for example from Research Devices, Inc., can achieve alignment accuracy of about 2 microns, more than adequate for the sizes of the devices for the present project. The heated chips are brought together with controlled pressure in the solder bonding machine, completing the bonding. In the process used at AT&T/Lucent, an epoxy is then flowed in between the two chips by capillary action. This epoxy gives an additional layer of protection to the silicon chip as the final etch is performed to remove the GaAs substrate from the modulator/detector array. The final result is many isolated and separate modulator/detectors bonded onto the silicon chip. The modulators operate in reflection mode, using a metallic mirror layer on the bonded surface of the diode. An antireflection coating can also be applied to the exposed surface of the modulators. This process has been used successfully to bond over 4000 diodes to a 7x7 mm silicon chip by AT&T [4] and over 65,000 spatial light modulators in a 256x256 array by Sanders Lockheed

Martin.[5] A more detailed cross section of the final bonded structure is shown in Figure 6-3 and a top view photograph is shown in Figure 6-2.

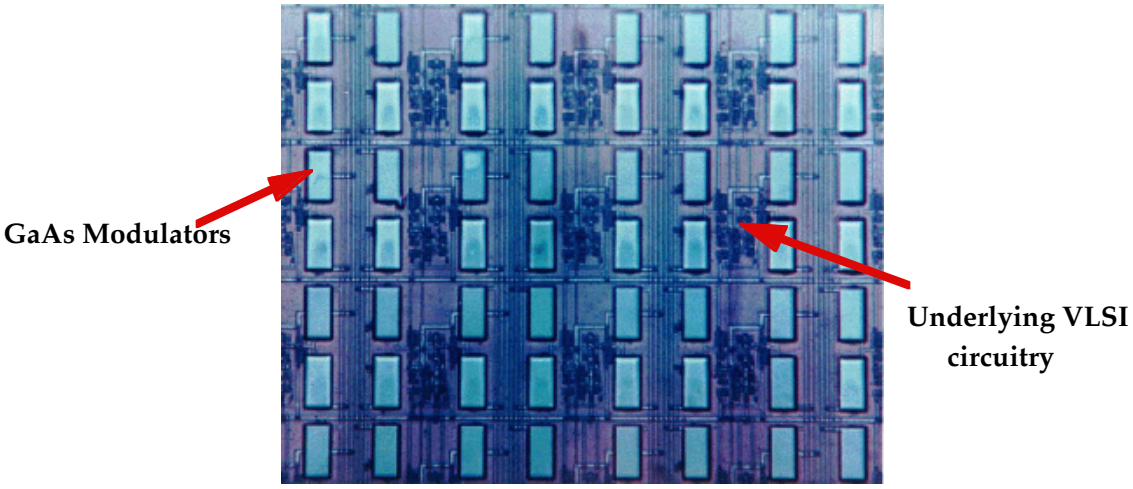

Figure 6-2: Photo of top view of integrated GaAs modulators with underlying CMOS circuitry[6]

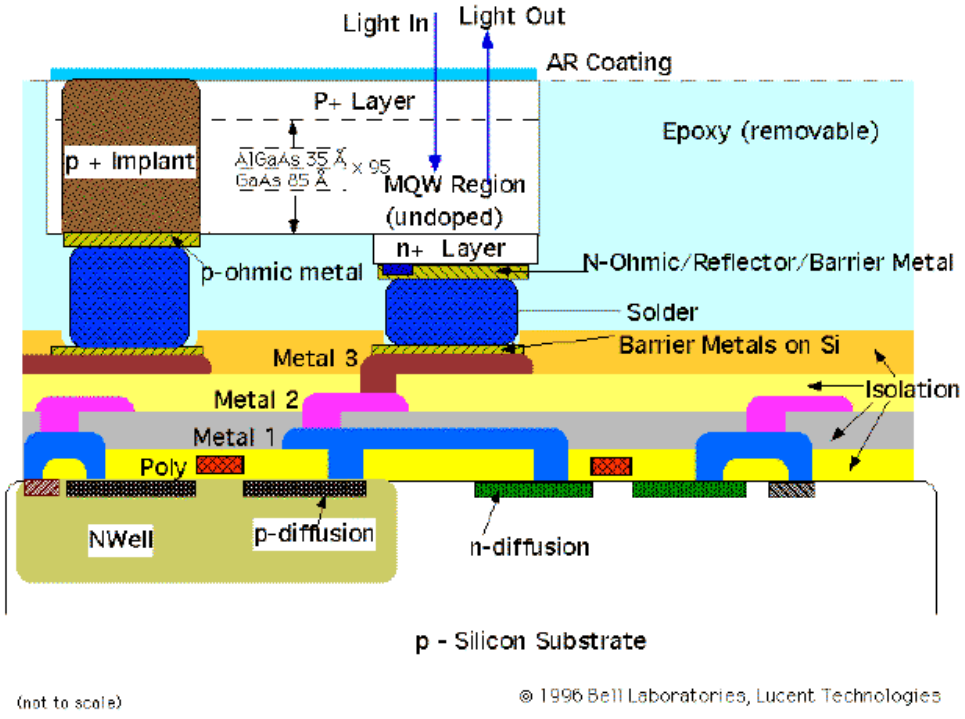

Figure 6-3: Cross sectional view of the finished hybrid SEED devices[6]

6.3 Benefits of this Technology

The main benefit of this technology is that it can provide thousands of optical inputs and outputs to state of the art circuitry capable of sophisticated information processing. Quantum well modulators/detectors hybridized to silicon VLSI chips have demonstrated 1000's of optical inputs or outputs (I/O) on a single chip.[7] Individual I/O circuits have shown speeds of up to 1 Gb/sec. Complex logic circuitry on the chip has been successfully connected to the optical I/O. In addition to the well known physical benefits of optical interconnections, the large number of simple spatial channels in smart pixel arrays has other system advantages for large aggregate interconnect bandwidths, including 1) avoiding any need for complex serialization circuits (multiplexers), and 2) avoiding signal and clock skew. Skew is reduced because the optical input "lines" are all essentially the same length and the receiver and transmitter circuits are simple. Therefore, this technology is very promising for achieving > 1 Tb/s aggregate data rates in 1000's of channels per square centimeter. Some of the factors that limit how many high speed optical I/O's can be implemented in a given chip area are sensitivity, power dissipation, and crosstalk, similar to the limitations for neuron density discussed in Chapter 4. The modulators can function as either photodetectors (in the case of receivers), modulators (in the case of off chip laser as output), or even as LED's (for transmitters), although the devices are not optimally designed for the latter. Smart pixels based upon this technology show immense promise for optoelectronic systems.[8,9,10]

6.4 2x2 Switches and 4x4 Crossbars

The benefits described in the previous section have been demonstrated for 2x2 switching nodes up to 1 GHz operation. These 2x2 switches are clearly quite similar in function to the X-modulator devices of Chapter 5. However, for the hybrid SEED technology, the light must be converted to electrons and holes, then back to light again after

the routing has been performed. This is not the case for the X-modulator implementations of 2x2 switches and 4x4 crossbars, where the data path is all optical. In addition to this, the X-modulators can be switched at least as fast as the 2x2 switches implemented in silicon and potentially operate up to 40 GHz, for they will not have the capacitive delay from the attached silicon CMOS to charge and discharge. The power dissipation of X-modulator based crossbars should be comparable to that of this technology. In the case of crosstalk, the hybrid SEEDs win out until some of the ideas discussed in Chapter 5 (e.g. incorporation of gain) are successfully implemented. To benchmark the X-modulator technology, 2x2 switches and 4x4 crossbars were implemented using the hybrid SEED technology as shown in Figure 6-4. Because of delays in the delivery of the chips from AT&T however, the devices have not yet been tested and will be inherited by another graduate student, as well as the task of bonding some of the devices grown here at Stanford (phase modulators, high contrast modulators, X-modulators, etc.) to silicon circuitry for an even wider variety of applications.

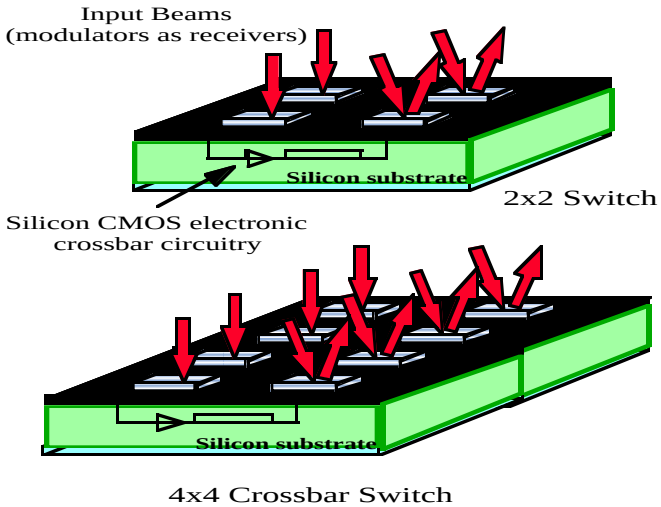

Figure 6-4: 2x2 switches and 4x4 crossbars using hybrid SEED technology

6.5 Conclusions

The technology discussed in this chapter is still quite new and shows much promise for chip to chip interconnection, optical backplanes, and dense array smart pixel

processors. The technology should see widespread use in the near future, as electronic interconnections become bogged down by problems such as clock skew and simple lack of chip area. Some projections for the future of this technology have been made by the Semiconductor Industry Association Roadmap[11] and Professor David A.B. Miller[12] which are summarized in Figures 6-5 and 6-6 and illustrate the future potential of hybridization. Clearly, for pure compuational purposes, silicon will continue to have an edge over optical devices, because of the large density and complexity of circuits. For interconnection however, the benefits of optics push technology towards devices such as optical modulators. A combination of the two worlds garners the advantages of both. For some applications, such as crossbar switches, all optical data path implementations such as that shown for X-modulators will show higher switching speeds and overall better performance. Integrating the variety of modulators designed at Stanford with state of the art silicon CMOS shows vast potential for many array optoelectronic applications.

Year	Feature Size (μm)	Gates	Area (mm2)	On Chip Clock
1995	0.35	800k	400	200 MHz
1998	0.25	2M	600	350 Mhz
2001	0.18	5M	800	500 MHz
2004	0.12	10M	1000	700 MHz
2007	0.10	20M	1250	1 Ghz

Figure 6-5: Projections for CMOS technology [11]

Feature Size (μm)	Bonded Diode Capacitance (fF)	Laser Power (mW)	# Optical Diodes	Optical Loss (dB)
0.70	150	50	1000	12
0.35	67	200	6000	10
0.25	45	400	12000	9
0.18	30	800	24000	8
0.10	13	3200	50000	6

Figure 6-6: Trends in GaAs CMOS-SEED Technology [12]

Chapter 7--Zero Chirp Modulator Using Coupled Quantum Wells

7.0 Introduction

In this chapter, we will depart from the amplitude-only view of the previous chapters and examine a modulator which exhibits zero phase change over a constant voltage swing. This zero-chirp reflection modulator is created by placing coupled quantum wells in the active region of the modulator, instead of the single uncoupled wells that are more commonly used. Unlike single wells which can produce zero chip between two operating voltages[1] these coupled quantum wells can provide large absorption changes with zero refractive index changes over the entire voltage swing; the resultant cavity structure shows reflectivity changes with zero experimental phase change over the same voltage range. The tradeoff in reflectivity change required in order to obtain zero-chirp is described. This tradeoff is a result of the different switching mechanisms used in coupled quantum well vs. single quantum wells.

Reflection modulators based upon large absorption changes in quantum wells have shown high contrast ratios[2] while exhibiting lower parasitic phase modulation than conventional waveguide modulators.[3] While single quantum wells are capable of large absorption changes ($\Delta\alpha$), they can exhibit large refractive index changes (Δn) during the switching cycle.[4] These refractive index changes induce modulation of the reflected phase, ϕ, and thus create unwanted frequency modulation since $\omega=\omega_0\pm d\phi/dt$ where $1/t$ is the desired switching frequency.[5] The ratio of phase shift to absorption is typically reported through the chirp parameter where a low chirp parameter is desirable for low-distortion amplitude modulation. Previously, it has been shown how zero parasitic refractive index changes can be obtained between two voltages, and a Fabry-Perot device which exhibits zero phase change between the on and off states has been demonstrated.[6] Subsequently,

we developed asymmetric coupled quantum wells with varying width and depth to modulate absorption via the spatial separation of carriers[7] (oscillator strength modulation, OSM). This technique produces changes in absorption per change in applied electric field several times larger than that of single wells with zero refractive index change over the entire switching cycle. In this chapter, we utilize coupled quantum wells in a Fabry-Perot modulator yielding a pure amplitude reflection modulator with a true zero chirp parameter. At the operating wavelength, the device exhibits an amplitude reflectivity change with zero phase change over all voltage points. In addition, we describe the limitations on reflectivity changes induced by the use of the OSM technique. We note that this device also applies to eliminating chirp in waveguide modulators which rely upon OSM.

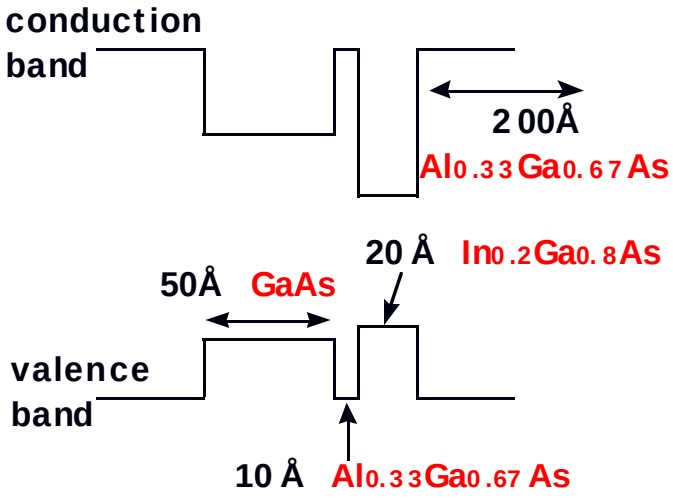

Figure 7-1: Coupled quantum well band structure

7.1 Device Theory and Design

While we previously obtained zero phase change absorption modulation from both coupled GaAs/InGaAs quantum wells and coupled $In_xGa_{1-x}As/In_yGa_{1-y}As$ quantum wells, in order to minimize the effects of strain, we used GaAs/InGaAs coupled quantum wells. Specifically, the coupled well system consisted of a 50Å GaAs well and a 20Å $In_{0.2}Ga_{0.8}As$ quantum well separated from each other by a 10Å $Al_{0.33}Ga_{0.67}As$ barrier. Coupled well

systems were separated from one another by 200Å $Al_{0.33}Ga_{0.67}As$ barriers. This structure is shown in Figure 7-1. The absorption and zero refractive index change behavior as a function of electric field are shown in Figure 7-2, where they are compared with the behavior of a single quantum well system. In single wells, the QCSE dominates the absorptive properties as the exciton peak shifts, and $\Delta n = 0$ only between two specific points of operation. For coupled wells, however, at low bias at 8175 Å, we see a reduction in absorption, but no shift in the peak wavelength, resulting in $\Delta n=0$ until the QCSE begins to dominate above 5 volts.

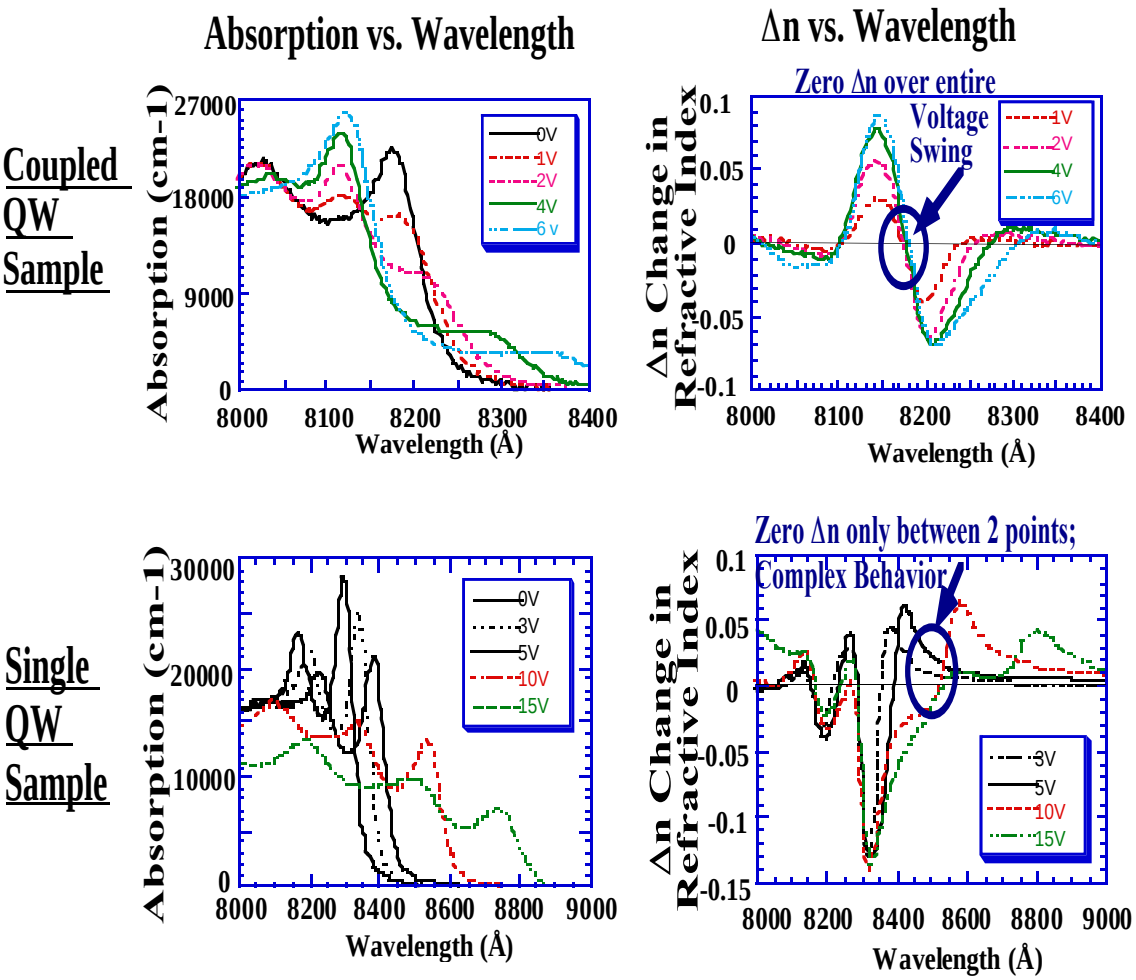

Figure 7-2: Comparison of absorption and refractive index change modulation for double and single quantum well systems.

For this coupled quantum well system, typical absorption changes are from α_{max}=22000 cm^{-3} to α_{min}=3500 cm^{-3} with zero change in refractive index using an applied electric field of 90 kV/cm. We note that exact values of the absorption coefficient depend quite sensitively upon material quality, although small or zero change in refractive index is always obtained. Coupled quantum wells can provide a greater range of absorption change at lower bias than single wells. The zero change in refractive index is a result of the aspect of the Kramers-Kronig relation discussed in Chapter 2, whereby if there is a local maximum in the absorption spectrum that is broad enough, zero refractive index change will result. The reason that a local maximum is maintained at low voltages in coupled quantum well systems is a result of the method of modulation employed, which is due to bias induced changes in the spatial separation of the electron and hole wavefunctions. Figure 7-3 illustrates this separation of carriers into the two wells at low bias. The theory behind coupled well oscillator strength modulation is described in detail by John Trezza in his Ph.D. thesis, from which these illustrative figures have been borrowed.[8] As shown in Figure 7-3, at zero bias, the electron is mostly in the GaAs well, the first heavy hole is in the GaAs well, and the second heavy hole is in the InGaAs well. As the voltage is increased, the first heavy hole is switched to the InGaAs well, thus decreasing its overlap integral (which determines absorption) with the electron wavefunction--the carriers become spatially separated, but the electron-heavy hole 1 exciton peak remains at 8175 Å and is reduced in magnitude. Conversely, the second heavy hole is switched into the GaAs well, increasing its overlap integral with the electron and enhancing the absorption peak at 8125 Å. At higher voltages, the quantum confined Stark effect dominates the absorptive properties and we see the same behavior as described in Chapter 2 and the zero chirp is lost.

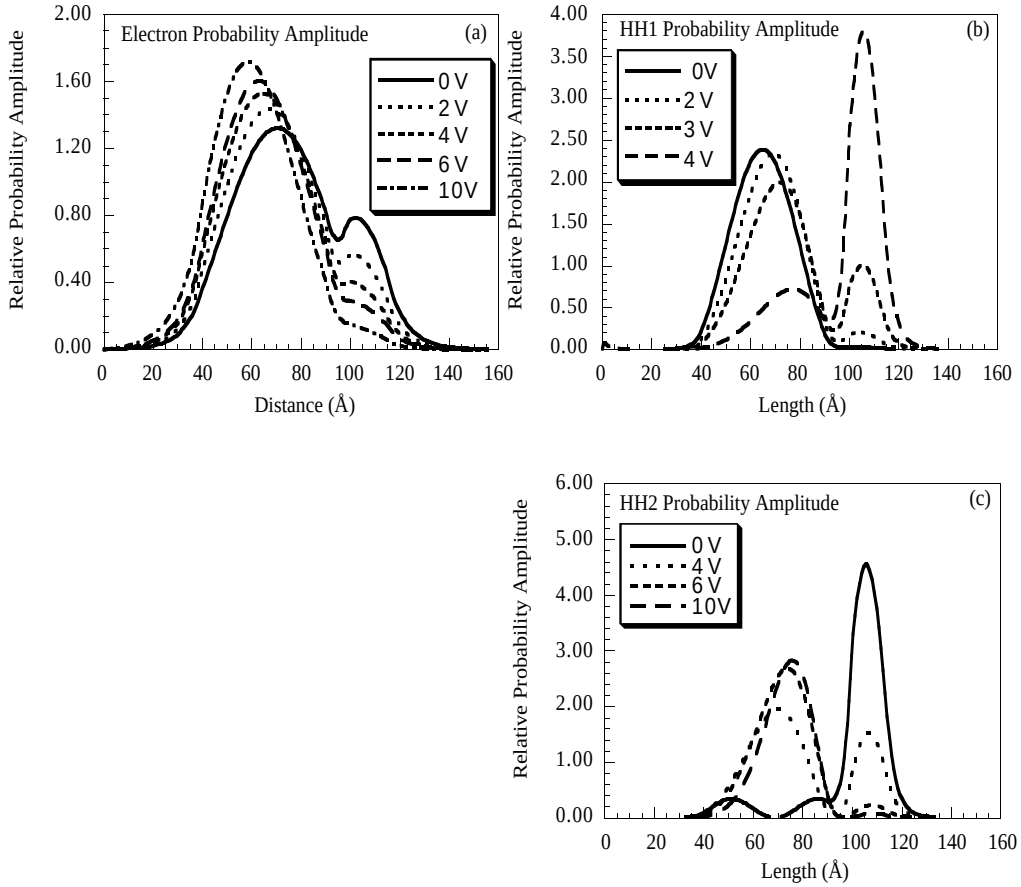

Figure 7-3: Probability amplitude ($\psi^*\psi$) for the (a) electron, (b) highest and (c) second highest hole states in the experimental structure as a function of applied bias. The separation of wavefunctions with applied bias can be seen.

7.2 Device Structure

The devices were grown by molecular beam epitaxy on N+ GaAs substrates. An asymmetric Fabry-Perot structure with 10 coupled quantum wells with the aforementioned dimensions was used. The wells were placed between a bottom quarter wave stack of 24 periods n-doped AlAs/$Al_{.33}Ga_{0.67}As$ and a top mirror consisting of 6 periods of p-doped AlAs/$Al_{.33}Ga_{0.67}As$. This structure formed a p-i-n diode which was reverse biased to apply an electric field across the active region. Because the absorptive switching in coupled quantum wells occurs at such a low electric field, it is important to account for the built-in electric field of the diode. Failure to account for this internal field can result in a coupled quantum well sample which is already 'switched' with zero externally applied electric field.

Our thin-film program and in-situ measurement technique[9] were used to ensure that the Fabry-Perot reflectivity minima occurred at the maximum $\Delta\alpha$ of the quantum well's zero Δn wavelength. In this sample, this wavelength was 8180 Å. Once growth was completed, mesas were etched to isolate devices, a Au/Ge/Ni/Au diffused contact was placed on the back of the wafer for n-type contact and a Ti/Au ring was placed around the top of the mesa to provide a p-type contact and optical access.

7.3 Experimental Results

Experimental results of the total reflectivity versus wavelength are shown in Figure 7-4(a). The device was designed to operate before the matching condition where decreasing cavity absorption increases device reflectivity. As can be seen, at a wavelength of 8180Å, the reflectivity of this device changes from ~40% to ~70% reflectivity with an applied bias of 5 volts. The optical bandwidth of this experimental device is 100Å.

To extract information about the reflected phase of the device (and hence the chirping characteristics), two techniques were used. First, a direct phase versus voltage measurement was made at 8180Å using a modified Michelson interferometer setup.[10] In this setup, one of the arms of the interferometer impinges on the device while the other reflects from a mirror on a piezoelectric mount. As the piezoelectric mirror is scanned, a sinusoidal curve is traced. By varying the voltage on the device and tracing several sinusoidal curves, a direct phase measurement can be made with an accuracy of ~2 degrees. The inset of Figure 7-4(b) shows reflectivity and phase versus bias at 8180 Å. The reflected phase is unchanging with applied electric field (within our measurement error) up to an applied bias of 5.5 Volts. Hence, over the voltage range depicted in Figure 7-4(b), the reflection modulator operates with zero chirp. At low biases, in coupled quantum well samples, modulation occurs through OSM. However, at higher electric fields, individual exciton peaks begin to red-shift due to the quantum confined Stark effect. At applied biases

above 5.5V, the reflected phase increases due to this Stark effect red-shifting of the exciton peaks. However, as the maximum absorptive change occurs at biases below this transition, zero chirp amplitude modulation is possible. The second phase analysis technique relies on the Kramers-Kronig relation between the logarithm of reflected amplitude and reflected phase. Thus, a broad spectra phase picture can be obtained quickly from the experimental reflectivity data. Figure 7-4(b) shows the reflected phase versus wavelength for the sample as determined from the Kramers-Kronig transformation of the reflectivity data over a wide wavelength range (of which Figure 7-4(a) shows a portion). Again at 8180Å, there is no change in reflected phase over the switching cycle.

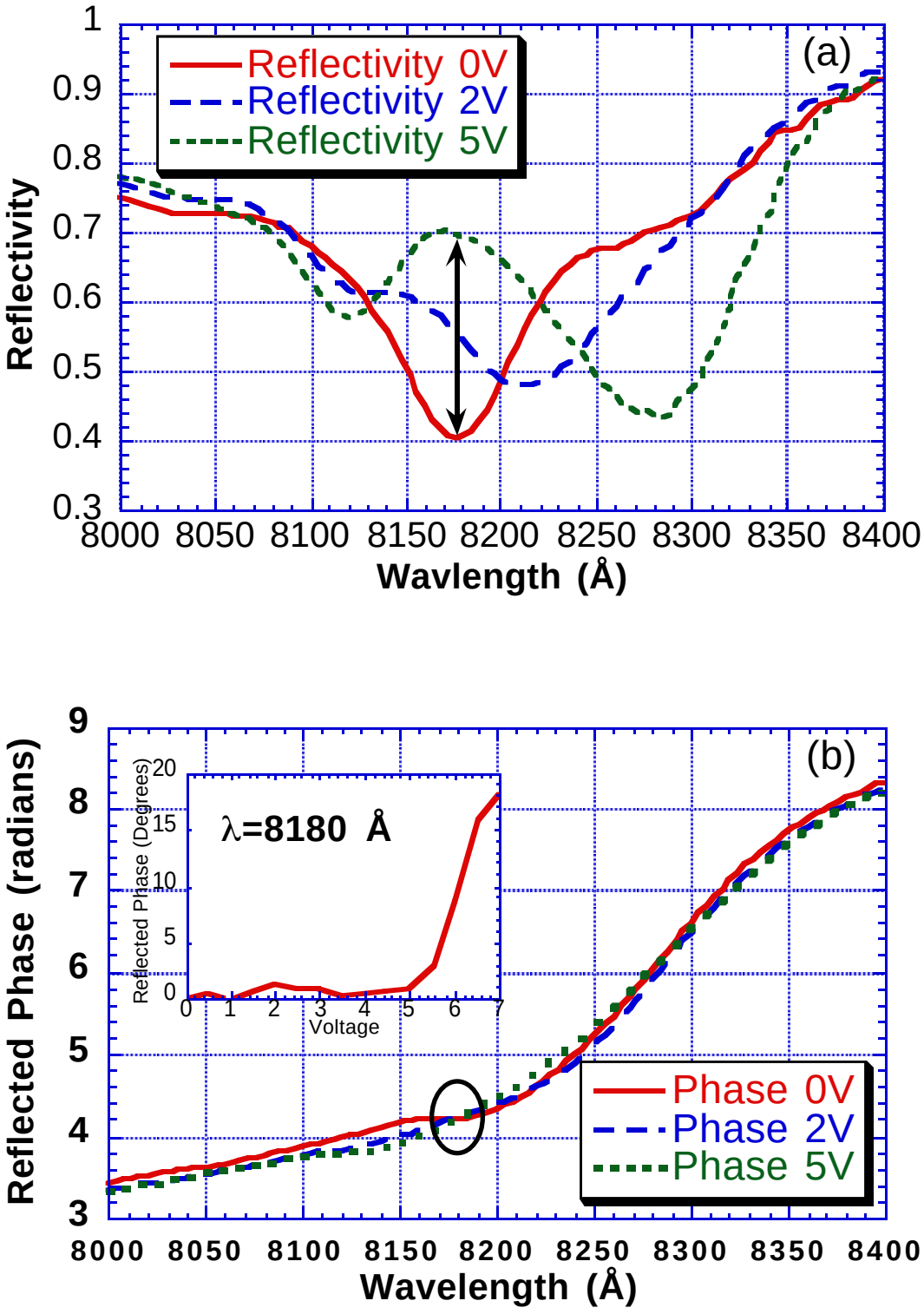

Figure 7-4: Experimental (a) reflectivity and (b) phase vs. wavelength for zero-chirp modulator for several applied biases

7.4 Parameter Space: Single, Double, and Triple Wells

It was noted above that the typical coupled quantum well sample had a minimum absorption, α_{min}, of 3500 cm^{-1}. In contrast, devices using single quantum wells and employing the quantum confined Stark effect have α_{min} at least an order of magnitude lower. Fabry-Perot cavities can translate changes in absorption to changes in amplitude[11], phase[12], or direction[13]. However, limited absorption ratios translate directly into limitations in device performance. For example the maximum change in reflectivity of an optimal Fabry-Perot cavity is limited by the quantum well absorption ratio (α_{max} / α_{min}).[14] On the other hand, coupled quantum wells permit much larger total changes in absorption (α_{max} − α_{min}) and also larger changes in absorption per unit applied bias than are typically possible in devices using single quantum wells. This translates into lower operational voltages and the need for lower finesse optical cavities--which results in wider optical bandwidths. Figures 7-5, 7-6, and 7-7 depict the theoretical design parameter space for amplitude reflection modulators optimized to provide the maximum change in reflectivity. For reflection modulators using coupled quantum wells, the maximum reflectivity change obtainable is between 57% and 64%, depending upon the number of quantum wells. Optimizing for maximum ΔR results in contrast ratios between 8 and 10. We note that incorporation of gain in the active region could increase contrast ratios at the possible risk of reintroducing chirp.

Fabry-Perot cavities with bottom mirrors having higher reflectivity than top mirrors modulate light by decreasing overall reflectivity with increasing cavity absorption. Such devices are said to operate “before the matching condition”. This was the type of experimental device described in this chapter. Conversely, cavities which have top mirrors

more reflective than bottom mirrors *increase* reflectivity with increasing cavity absorption.[14] Such devices operate "beyond the matching condition." In order to get large reflectivity change in devices operating beyond the matching condition, high Q cavities are needed; resulting in much smaller optical bandwidth than for devices operating before the matching condition. Quantum well characterisitics determine which cavity type can produce larger changes in reflectivity. From looking at the optical bandwidth in Figure 7-5, it is clear that for a small number of coupled quantum wells (fewer than 40), maximum changes in reflectivity are found for devices operating before the matching condition. However, for modulators with a large number of coupled quantum wells, high reflectivity changes require high finesse cavities and operation beyond the matching condition. Figure 7-6 shows the contrast ratio and optical bandwidth for single quantum wells. In the single quantum well case, the larger absorptive ratio allows maximum changes in reflectivity of over 90% and contrast ratios over 100. However, optical bandwidths are a bit lower than for coupled quantum wells due to the lower allowed change in absorption. In addition, maximum changes in reflectivity always occur for devices operated before the matching condition. Furthermore, the QCSE used in single quantum wells requires a higher electric field than the OSM in coupled quantum wells, thus the required voltages are higher in single wells. There is thus a tradeoff between maximum allowable ΔR in single QWs vs. zero chirp and low voltage operation in coupled QWs. One compromise coupled well structure is the triple quantum well structure[15] which operates via OSM, but allows greater separation of the carriers after switching. Thus lower α_{min}'s are realizable. Figure 7-7 shows that these structures, when optimized, can produce maximum $\Delta R \sim 80$ with contrast ratios of 35 and operation before the matching condition for devices with fewer than 60 quantum wells. The optimization of triple quantum wells for zero chirp operation can be performed, although it requires very precise control of growth processes.

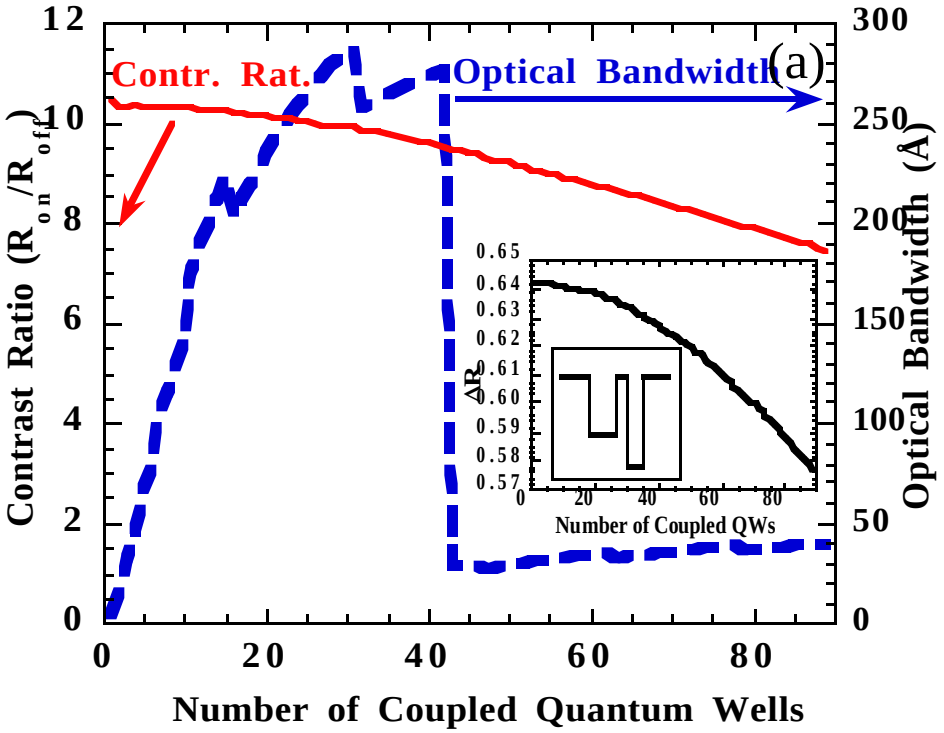

Figure 7-5: Parameter space for contrast ratio, optical bandwidth, and change in reflectivity vs. number of double quantum wells

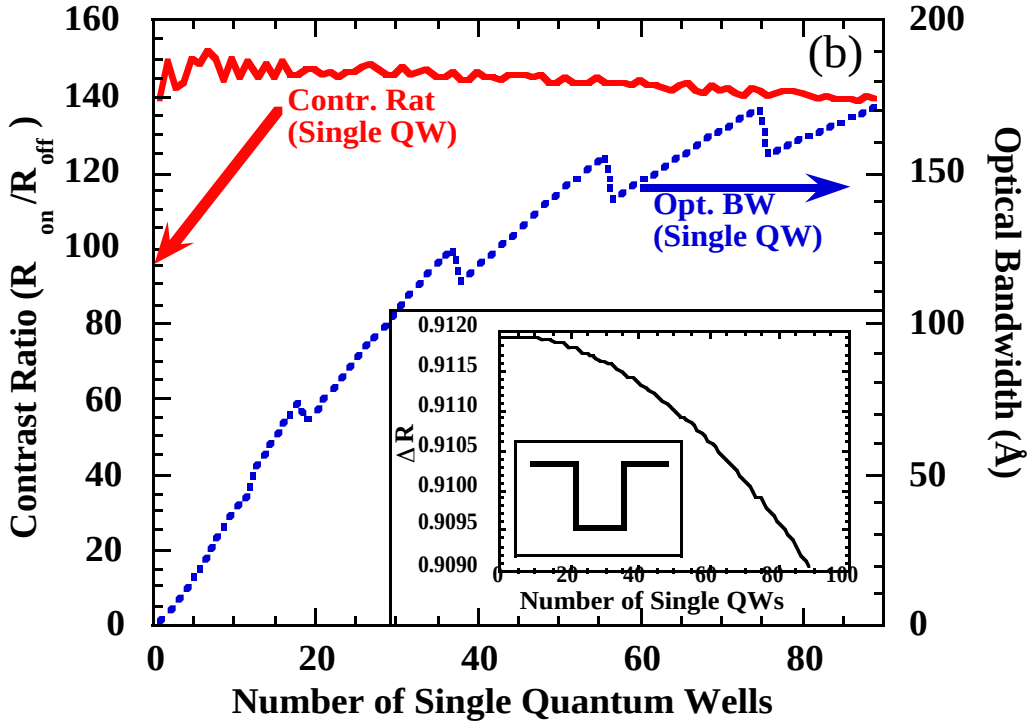

Figure 7-6: Parameter space for contrast ratio, optical bandwidth, and change in reflectivity vs. number of single quantum wells.

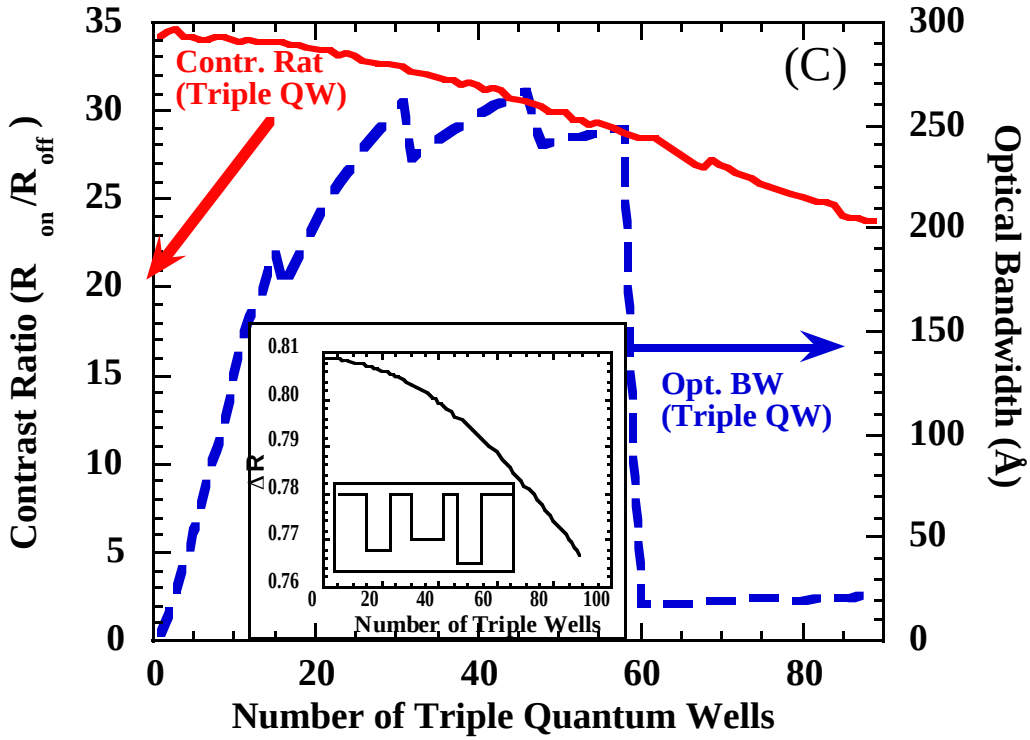

Figure 7-7: Parameter space for contrast ratio, optical bandwidth, and change in reflectivity vs. number of triple quantum wells.

7.5 Conclusions

In this chapter, zero-chirp reflection modulators were demonstrated which incorporated coupled double (GaAs-AlGaAs-InGaAs) quantum wells to provide changes in absorption with zero refractive index changes through oscillator strength modulation. These devices displayed zero measured phase change over the entire voltage swing (5V). In addition, the parameter space of reflection modulators employing single, coupled (double), and triple quantum wells was analyzed for devices optimized for maximum change in reflectivity. The performance tradeoffs required to achieve zero chirp behavior were described and demonstrated in coupled quantum well modulators.

Chapter 8--Summary and Suggestions for for Future Work

8.0 Summary

In this work, we have explored several systems applications of vertical cavity optoelectronic modulators which demonstrate their broad applications in the areas of optical computing, neural networks, interconnection, and routing. We have explored both the aspects of modulators as stand-alone devices well as their integration with GaAs and silicon electronics. We have approached the devices both from a device physics and a systems level point of view. The goal of this two-sided approach is creating devices beneficial for a variety of systems applications.

In Chapter 2, we introduced the background necessary for understanding the physics of modulators including quantum well excitonic absorption, Fabry-Perot cavities, and the Kramers-Kronig relation (important for phase devices). We discussed how the devices are grown using molecular beam epitaxy as well as the design methodology used to produce devices with certain desired characteristics. Some of these characteristics include high contrast ratio, large optical bandwidth, and change in reflectivity.

In Chapter 3, a particular configuration of quantum well modulators known as a SEED (self electro-optic effect device) was explored, with optical logic and computing as an intended application. We discussed their uses for Boolean logic and for threshold logic, and experimentally demonstrated S-SEED devices performing threshold logic. A full adder may be constructed using such thresholding elements, which has fewer switching elements than an adder using only Boolean logic. A model of the switching speed of SEED devices was discussed and compared to experimentally measured data. The speed of these devices is limited not by the devices themselves, but by the capacitances of the driving circuitry. and bonding pads.

Realizing that the simple threshold element of Chapter 3 can also serve as the basic neuron element in an optical neural network, Chapter 4 explored aspects of modulators relevant to optical neural network applications. Modulators integrated with electronics (either GaAs or silicon) turn out to be a effective implementation of an optoelectronic neuron. In such a neuron, the modulator acts simply as an output device, and the electronics performs the summation and thresholding of the input signals.

In Chapter 5 we turned our attention to a modulator which switches between reflective and transmissive modes and can have inputs from the top and bottom of the device. Such a device turns out to be the optical implementation of a Fredkin gate, which can be used to construct any logic function. We discussed conservative invertible logic and showed how a full adder with even fewer switching elements can be constructed. The device theory and design were explained and several systems in which they may be used were discussed. These X-gate type modulators, although capable of performing optical computing, will have greater uses in routing and interconnection. Several refinements to the initial device were explored, including reduction of the operating voltage, optical control, and incorporation of gain. A simple architecture using 4 X-gates was also demonstrated, which has the effect of improving the contrast ratio of the individual device and in some cases correcting for any asymmetries between switching states.

The very promising hybrid integration of GaAs modulators on silicon VLSI was discussed in Chapter 6. A hybrid chip was designed and produced which implemented 2x2 switches and 4x4 crossbars. This chip will be used to compare X-gate crossbars with this hybrid technology. X-gate based switches should prove superior in terms of switching speed, however, until several fabrication issues are resolved, integration of modulators with electronics will be the more fruitful approach. Dense arrays of modulators integrated with VLSI has vast potential for optical backplanes, board to board interconnections, smart pixels, optical neural networks, optical correlation, and addressing holographic memory.

In Chapter 7, we discussed modulators in terms of their phase characteristics, whereas in previous chapters we had focused on their amplitude modulating properties. In particular we described how oscillator strength modulation may be employed as a means of changing the quantum well absorption instead of the quantum confined Stark effect used in earlier chapters. Using OSM with coupled quantum wells we are able to design and produce devices with zero refractive index change over a five volt swing. Refractive index change results in phase change and thus unwanted frequency modulation. We performed simulations to explore the parameter space of these devices using single, double, and triple quantum wells in the absorptive region. This allowed us to optimize for maximum change in reflectivity, while maintaining zero phase change. The optical bandwidth and contrast ratio tradeoffs of these devices were also predicted.

8.1 Contributions

The contributions of this thesis encompass both device physics and systems level aspects of vertical cavity multi quantum well optoelectonic modulators. In this section, we will simply list these contributions in brief form.

8.1.1 Device physics aspects

Reflection and reflection/transmission modulators were designed and optimized for particular systems applications in terms of contrast ratio, optical bandwidth, change in reflectivity, and other parameters. Dual zone structures were simulated which should provide a more flexible device design space. Incorporation of gain into X-modulators and its implications were simulated. Several methods of optical control of modulators were investigated. These techniques may also be used for standard reflection only modulators. Strain compensation techniques were used to reduce the operating voltages of X-modulators (or any modulators in general). Coupled quantum wells were employed to produce zero chirp devices over an entire voltage swing.

8.1.2 Systems level aspects

We have designed, grown, fabricated, and tested MQW modulators for a wide variety of optical computing applications, including optical logic, neural networks, interconnection, and routing. Threshold logic using SEEDs was simulated and demonstrated experimentally We have investigated several systems applications of X-modulators including crossbar switches, optical logic, and FPGAs. 2x2 and 4x4 optical crossbar switches were implemented using AT&T's hybrid SEED technology, whereby modulators are integrated with silicon VLSI electronics.

8.2 Suggestions for Future Work

As is the case for many research projects, this one has created more problems than it has solved and generated many avenues of future investigation that may be explored. Logic other than Boolean logic, such as threshold logic or CI logic, can decrease the size of many circuits (either electronic or optical). Tools should be developed to take advantage of alternative logic forms, particularly CI logic implemented with X-gates. The probable usefulness of X-gates will be in the area of crossbar switches however, and thus more work should be done towards producing an X-gate in a packaged form easily connectable to other components.

Further reduction of operating voltages of modulators is still desirable to keep them compatible and competitive with silicon electronics. Much experimentation can still be done in the area of optical control of modulators by the effects discussed in this work. Dual zone structures incorporating gain or adding additional amplitude or phase modulation to a structure can provide much of the design flexibility that is currently lacking in the modulator parameter space. At present, a device can be designed to fit the parameters of a given system application to some extent, but there are tradeoffs involved. Many of these

tradeoffs can be alleviated by going to dual zone structures. More complicated quantum well system design (coupled, triple, or more wells) may also be beneficial.

For much of what modulators have to offer to be useful, many packaging, fabrication, and integration issues must be explored. A method to easily connect an array of modulators to an array of fibers should be devised. Tunable devices should also be designed, as well as devices with either large or narrow bandwidth for WDM applications. Integration of modulators with VLSI electronics is a rapidly growing field and will be the focus of much research in the near future. The possibilities of this hybrid approach have only just begun to be explored.

8.3 Conclusions

Apart from the conclusions offered in the summary and at the end of each chapter, this section will discuss some overall conclusions on the state of optoelectronic modulators and their expected future role.

Although there are several interesting applications of modulators for optical logic and computing, their uses in these areas will be limited by the difficulty of interconnecting individual devices. The small size and high density of today's electronic circuits will continue to provide cheaper, more reliable computation power than any purely optical computer. On the other hand modulators will be increasingly used for routing and interconnections in board to board interconnects, local area networks, and long distance communications because of their very high speeds of operation.

At this point in time, the most promising applications of modulators lies in their integration with GaAs or silicon VLSI electronics. This hybrid solution takes advantage of the strengths of the electronic and the optical solutions to many problems. Large arrays of modulators simply driven by electronics or acting as part of smart pixel elements will prove to be the optimum solution in many applications, including optical memory addressing,

neural networks, correlation, beam steering and shaping, and many others which have yet to be imagined.

[1] K. W. Goossen, J. A. Walker, L. A. D'Asaro, S. P. Hui, B. Tseng, R. Leibenguth, D. Kossives, D. D. Bacon, D. Dahringer, L. M. F. Chirovsky, A. L. Lentine, and D. A. B. Miller, "GaAs MQW Modulators Integrated with Silicon CMOS", *IEEE Photonics Tech. Lett.* **7**, 360-362 (1995).

[2] A. L. Lentine, R. A. Novotny, D. J. Reiley, R. L. Morrison, J. M. Sasian, M. G. Beckman, D. B. Buchholz, S. J. Hinterlong, T. J. Cloonan, G. W. Richards, and F. B. McCormick, "Demonstration of an experimental single chip optoelectronic switching system", Postdeadline paper PD2.5, IEEE LEOS Annual Meeting, San Francisco, November 1995.

[3] A. L. Lentine, K. W. Goossen, J. A. Walker, L. M. F. Chirovsky, L. A. D'Asaro, S. P. Hui, B. T. Tseng, R. E. Leibenguth, D. P. Kossives, D. W. Dahringer, D. D. Bacon, T. K. Woodward, and D. A. B. Miller, "Arrays of Optoelectronic Switching Nodes Comprised of Flip-Chip- Bonded MQW Modulators and Detectors on Silicon CMOS Circuitry", *IEEE Photonics Tech. Lett*. **8**, 221-223 (1996).

[4] T. K. Woodward, A. V. Krishnamoorthy, A. L. Lentine, K. W. Goossen, J. A. Walker, J. E. Cunningham, W. Y. Jan, L. A. D'Asaro, L. M. F. Chirovsky, S. P. Hui, B. Tseng, D. Kossives, D. Dahringer, and R. Leibenguth, "1-Gb/s Two-Beam Transimpedance Smart-Pixel Optical Receivers Made from Hybrid GaAs MQW Modulators Bonded to 0.8 micron Silicon CMOS", *IEEE Photonics Tech. Lett* 8, 422 - 424 (1996).

[5] A. Krishnamoorthy, A. L. Lentine, K. W. Goossen, J. A. Walker, T. K. Woodward, J. E. Ford, G. F. Aplin, L. A. D'Asaro, S. P. Hui, B. Tseng, R. Leibenguth, D. D. Kossives, D. Dahringer, L. M. F. Chirovsky, and D. A. B. Miller, "3-D Integration of MQW Modulators Over Active Submicron CMOS Circuits: 375 Mb/s Transimpedance Receiver-Transmitter Circuit", *IEEE Photonics Tech. Lett* **7**, 1288-90 (1995).

[6] E. A. De Souza, M. C. Nuss, W. H. Knox, and D. A. B. Miller, "Wavelength-division multiplexing with femtosecond pulses", *Optics Letters* **20**, 1166-1168 (1995).

[7] H. S. Hinton, T. J. Cloonan, F. B. McCormick, A. L. Lentine, and F. A. P. Tooley, "Free- space digital optical systems", Proc. IEEE 82, 1632-1649 (1994) [8] F. B. McCormick, T. J. Cloonan, A. L. Lentine, J. M. Sasian, R. L. Morrison, M. G. Beckman, S. L. Walker, M. J. Wojcik, S. J. Hinterlong, R. J. Crisci, R. A. Novotny, and H. S. Hinton, "Five-stage free-space optical switching network with field-effect transistor self-electrooptic- effect-device smart-pixel arrays", *Appl. Opt*. **33**, 1601- 1618 (1994).

[9] G. D. Boyd, G. Livescu, L. M. F. Chirovsky, and A. L. Lentine, "Mode-locked pulse operation of GaAs/AlGaAs field effect transistor self-electro-optic effect device smart pixels and saturation considerations", *Appl. Phys. Lett*. **65**, 3108-3110 (1994).

[10] G. Livescu, G. D. Boyd, L. M. F. Chirovsky, R. A. Morgan, and T. Mullally, "Picosecond switching of GaAs/AlGaAs smart pixels" *Optics Lett*. **19**, 2122-2124 (1994).

[11] T. K. Woodward, A. L. Lentine, and L. M. F. Chirovsky, "Experimental sensitivity studies of diode-clamped FET- SEED smart-pixel optical receivers", *IEEE J. Quantum Electron*. **30**, 2319-2324 (1994).

[12] A. L. Lentine, L. M. F. Chirovsky, and T. K. Woodward, "Optical energy considerations for diode-clamped smart pixel optical receivers", *IEEE J. Quantum Electron*. **30**, 1167-1171 (1994).

[13] L. A. D'Asaro, L. M. F. Chirovsky, E. J. Laskowski, S. S. Pei, T. K. Woodward, A. L. Lentine, R. E. Leibenguth, M. W. Focht, J. M. Freund, G. G. Guth, and L. E. Smith, "Batch fabrication and operation of GaAs-AlGaAs field- effect transistor-self-electrooptic effect device (FET- SEED) smart pixel arrays", *IEEE J. Quantum Electron*. **29**, 670-677 (1993).

[14] D. A. B. Miller, M. D. Feuer, T. Y. Chang, S. C. Shunk, J. E. Henry, D. J. Burrows, and D. S. Chemla, "Field-effect transistor self-electrooptic effect device: integrated photodiode, quantum well modulator and transistor", *IEEE Phot. Tech. Lett*. **1**, 61-64 (1989).

[15] N.M. Jokerst, M.A. Brooke, O. Vendier, S. Wilkinson, S. Fike, M. Lee, E. Twyford, J. Cross, B. Buchanan, and S. Wills, "Thin-film multimaterial optoelectronic integrated circuits", *IEEE Trans.Comp. Pack. Manufact. Tech.* **B.19**, 97-106 (1996).

[16] D. J. McKnight, K. M. Johnson, and R. A. Serati, "256x256 liquid-crystal-on-silicon spatial light modulator", *Appl. Optics* **33**, 2775-2784 (1994).

[17] S. Matsuo, T. Nakahara, Y. Kohama, Y. Ohiso, S. Fukushima, and T. Kurokawa, "Monolithic integrated photonic switching device using an MSM PD, MESFET's, and a VCSEL", *IEEE Photonics Tech. Lett*. **7**, 1165-1167 (1995).

[18] S. Matsuo, T. Nakahara, and T. Kurokawa, "Smart pixels using vertical-cavity surface-emitting lasers", Paper JWA2, 1996 Topical Meeting on Optical Computing, Sendai, Japan, (Japan Society of Applied Physics, 1996).

[19] S. Chandrasekhar, L. D. Barrett, L. M. Lunardi, A. G. Dentai, D. A. Burrus, and E. C. Burrows, "Investigation of crosstalk performance of eight-channel p-i-n/HBT OEIC photoreceiver array modules", *IEEE Photonics Tech. Lett*. **8**, 682 - 684 (1996).

[20] K. Takahata, Y. Muramoto, Y. Akatsu, Y. Akahori, A. Kozen, and Y. Itaya, "10-Gb/s two-channel monolithic photoreciever array using waveguide p-i-n PD's and HEMT's", *IEEE Photonics Tech. Lett*. **8**, 563 - 565 (1996).

[21] S. Tsuda, W. H. Knox, E. A. de Souza, W. Y. Jan, and J. E. Cunningham, "Low-loss intracavity AlAs/AlGaAs saturable Bragg reflector for femtosecond mode locking in solid-state lasers" *Optics Lett*. **20**, 1406-1408 (1995).

[22] D. Kopf, G. Zhang, R. Fluck, M. Moser, and U. Keller, "All-in-one dispersion-compensating saturable absorber mirror for compact femtosecond laser sources", *Optics Lett*. **21**, 486-488 (1996).

[23] S. D. Personick, "Receiver design for optical fiber systems", Proc. IEEE, 65, 1670 (1977).

[24] L. E. Eng, K. Bacher, W. Yuen, J. S. Harris, Jr., and C. G. Chang-Hasnain, "Multiple Wavelength Vertical Cavity Laser Arrays on Patterned Substrates", IEEE J. Selected Topics in Quantum Electron., 1, 624 - 628 (1995).

[25] L. E. Eng, K. Toh, C. J. Chang-Hasnain, K. Bacher, and J. S. Harris, Jr., "Periodically Induced Mode Shift in Vertical Cavity Fabry-Perot Etalons Grown by Molecular Beam Epitaxy", to be published, IEEE Phot. Tech. Lett, March 1996.

[26] L. E. Eng, K. Bacher, W. Yuen, M. Larson, G. Ding, J. S. Harris, Jr., and C. J. Chang-Hasnain, "Wavelength Shift in Vertical Cavity Laser Arrays on a Patterned Substrate", Electr. Lett., 31, 562-563 (1995).

[27] A. M. Fox, D. A. B. Miller, G. Livescu, J. E. Cunningham, W. Y. Jan, "Quantum well carrier sweep out: relation to electroabsorption and exciton saturation" IEEE J. of Quantum Electronics, 27, 2281-2295, (1991).

[28] K. W. Goossen, J. E. Cunningham, W. Y. Jan, D. A. B. Miller "Interleaved-contact electroabsorption modulator using doping-selective electrodes with 250 C to 950 C operating range" IEEE Photo. Tech. Lett. 5, 181-183 (1993).

[29] J. A. Trezza, B. Pezeshki, M. C. Larson, S. M. Lord and J. S. Harris, Jr., "High Contrast Asymmetric Fabry-Perot," Appl. Phys. Lett. 74, pp.452-454, August 1993.

[30] C. Dragone, C. A. Edwards, and R. C. Kistler "Integrated Optics NxN Multiplexer on Silicon" IEEE Phot. Tech. Lett. 3, 896-899 (1991).

[31] D. A. B. Miller, D. S. Chemla, T. C. Damen, A. C. Gossard, W. Wiegmann, T. H. Wood and C. A. Burrus, "Electric Field Dependence of Optical Absorption near the Bandgap of Quantum Well Structures", Phys. Rev. B32, 1043-1060 (1985).

[32] K. Bacher, B. Pezeshki, S. M. Lord and J. S. Harris, Jr., "Molecular Beam Epitaxy Growth of Vertical Cavity Optical Devices with In Situ Corrections," Appl. Phy. Lett. 61 pp. 1387-1889, September 1992.

[33] L.A. Eyres, C.B. Ebert, J. S. Harris, Jr., H.C. Chui, and M.M. Fejer, “Fabrication of GaAs orientation template substrates for quasi-phasematched guided-wave nonlinear optics,” Proceedings of O.S.A. Conference on Nonlinear Guided Waves and Their Applications, Dana Point, California, Feb. 23-25, 1995, pp. 156-158.

[34] B. Pezeshki, S. M. Lord, T. B. Boykin, B. L. Shoop, and J. S. Harris, Jr., "AlGaAs/AlAs QW Modulator for 6328 Å Operation", Elect. Letts., 27, pp. 1971-1973, October 1991.

[35] S. M. Lord, J. A. Trezza, M. C. Larson, B. Pezeshki, and J. S. Harris, Jr., "1.3 μm Electroabsorption Reflection Modulators on GaAs," Appl. Phys. Lett. 63 pp. 806-808, August 1993.

[36] S.-D. Kim, J. A. Trezza, and J. S. Harris, Jr., "Observation of 1.5 μm Quantum Confined Stark Effect in InGaAs/AlGaAs Multiple Quantum Wells on GaAs Substrates," Submitted to Journal of Vacuum Science and Technology. 1994.

[37] E.D. Palik, ed. *Handbook of Optical Constants of Solids*, Academic Press, Orlando, Florida, 1985.

[38] L. E. Eng, K. Bacher, W. Yuen, J. S. Harris, Jr., and C. J. Chang-Hasnain, "Multiple Wavelength Vertical Cavity Laser Arrays on Patterned Substrates, "Journal of Quantum Electronics, XX (Y) PP. 100-103, Oct. 1994.

[39] S. Schmitt-Rink, D. S. Chemla, and D. A. B. Miller, "Linear and nonlinear optical properties of semiconductor quantum wells", Adv. Phys., 38, 89-188, (1989).

[40] D. A. B. Miller, J. E. Henry, A. C. Gossard and J. H. English, "Integrated Quantum Well Self-Electro-Optic Effect Device: 2x2 Array of Optically Bistable Switches", Appl. Phys. Lett. 49, 821-823 (1986).

[41] A. L. Lentine, H. S. Hinton, D. A. B. Miller, J. E. Henry, J. E. Cunningham, and L. M. F. Chirovsky, "Symmetric self-electro-optic effect device: Optical set-reset latch", Appl. Phys. Lett., 52, 1419-1421, (1988).

[42] A. L. Lentine, H. S. Hinton, D. A. B. Miller, J. E. Henry, J. E. Cunningham, and L. M. F. Chirovsky, "Symmetric Self-Electrooptic Effect Device: Optical Set-Reset Latch, Differential Logic Gate, and Differential Modulator/Detector", IEEE J. of Quantum Electronics, 25, 1928-1936, (1989).

[43] A. L. Lentine, F. A. P. Tooley, S. L. Walker, F. B. McCormick, R. L. Morrison, L. M. F. Chirovsky, M. W. Focht, J. M. Freund, G. D. Guth, R. E. Leibenguth, G. J. Przybyled, L. E. Smith, L. A. D'Asaro, D. A. B. Miller "Logic self-electrooptic effect devices: quantum-well optoelectronic multiplexers, and shift registers," IEEE J. of Quantum Electronics, 28, 1539-1553 (1992).

[44] D. A. B. Miller "Quantum-well self-electro-optic effect devices", Optical and Quantum Electronics, 22, S61-S98, (1990).

[45] A. L. Lentine, D. A. B. Miller "Evolution of the SEED technology: bistable logic gates to optoelectronic smart pixels" IEEE J. of Quantum Electronics, 29, 655-669 (1993).

[46] D. A. B. Miller, M. D. Feuer, T. Y. Chang, S. C. Shunk, J. E. Henry, D. J. Burrows, D. S. Chemla, "Field-effect transistor self-electrooptic effect device: integrated photodiode, quantum well modulator and transistor", IEEE Photonics Tech. Lett., 1, 61-64, (1989).

[47] D. A. B. Miller, "Optics for low-energy communication inside digital processors: quantum detectors, sources, and modulators as efficient impedance converters", Optics Letters, 14, 146-148, (1989).

[48] U. Keller, D. A. B. Miller, G. D. Boyd, T. H. Chiu, J. F. Ferguson, and M. T. Asom "Solid-state low-loss intracavity saturable absorber for Nd:YLF lasers: an antiresonant semiconductor Fabry-Perot saturable absorber" Optics Letters, 17, 505-507 (1992).

[49] A. V. Krishnamoorthy, T. K. Woodward, R. A. Novotny, K. W. Goossen, J. A. Walker, A. L. Lentine, L. A. D'Asaro, S. P. Hui, B. Tseng, R. Leibenguth, D. Kossives, D. Dahringer, L. M. F. Chirovsky, G. F. Aplin, R. G. Rozier, F. E. Kiamilev, D. A. B. Miller,"Ring oscillators with optical and electrical readout based

on hybrid GaAs MQW modulators bonded to 0.8 μm silicon VLSI circuits" Electronics Letters, 31, 1917-1918.

[50] G. W. Yoffe, D. G. Schlom and J. S. Harris, Jr., "Modulation of Light by Electrically Tunable Multi-Layer Interference Filter," Appl. Phys. Lett. 51 (23), 1876-1878, 7 December 1987.

[51] G. W. Yoffe, D. G. Schlom and J. S. Harris, Jr., "Summary Abstract: MBE Growth of Tunable Multi-Layer Interference Optical Modulators," J. Vac. Sci. Technol. B. 6 (2), 688, Mar/Apr 1988.

[52] J. D. Morse, M. D. Pocha, R. W. Dutton, G. D. Anderson, and J. W. Adkisson, "Picosecond Pulsing and Sampling by GaAs Photodetectors Fabricated on Silicon Substrates," Proceedings of SPIE Conference on Optoelectronics/Fiber Optics and Lasers, Boston, MA, August 1988.

[53] G. N. Nasserbakht, J. W. Adkisson, T. I. Kamins, B. A. Wooley, and J. S. Harris, Jr., "Monolithically Integrated Fiber-Optic Front-End Receiver in GaAs on Si Technology", Proceedings of VLSI Circuits Dig. Tech. Symposium, pp. 83, May 1989.

[54] S. Munnix, R. K. Bauer, D. Bimberg, J. S. Harris Jr., R. Köhrbrück, E. C. Larkins, Ch. Maierhofer, D. E. Mars and J. N. Miller, "Growth Kinetics, Impurity Incorporation, Defect Generation, and Interface Quality of MBE-grown AlGaAs/GaAs Quantum Wells: Role of group III and group V Fluxes," J. Vac. Sci. Technol., B7, (4) pp. 704-709, Jul/ Aug 1989.

[55] B. Pezeshki, D. Thomas, and J. S. Harris, Jr., "Optimization of Modulation Ratio and Insertion Loss in Reflective Electroabsorption Modulators", Appl. Phys. Lett. 57, (15), pp. 1491-1492, October 1990.

[56] B. Pezeshki, D. Thomas, and J. S. Harris, Jr., "Optimization of Reflection Electro-Absorption Modulators", Proceedings of Physical Concepts of Materials for Novel Optoelectronics Device Applications II: Device Physics and Applications, (1990), SPIE 1362, pp. 559-563, October 1990.

[57] J. S. Harris, Jr., and M. M. Fejer "Quantum Wells and Artificially Structured Materials for Non-Linear Optics," Proceedings of Physical Concepts of Materials for Novel Optoelectronics Device Applications II: Device Physics and Applications, (1990) SPIE 1361, pp. 262-273, October 1990.

[58] B. Pezeshki, D. Thomas, and J. S. Harris, Jr., "Large Reflectivity Modulation Using InGaAs-GaAs," IEEE Photonics Technology Lett., 2, pp. 807-809, November 1990.

[59] B. Pezeshki, D. Thomas, and J. S. Harris, Jr., "Wannier-Stark Localization in a Strained InGaAs/GaAs Superlattice", Appl. Phys. Lett. 57, (20), pp. 2116-2117, November 12, 1990.

[60] B. Pezeshki, D. Thomas, and J. S. Harris, Jr., "Novel Cavity Design for High Reflectivity Changes in a Normally Off Electroabsorption Modulator," Appl. Phys. Lett. 58, pp. 813-815, February 1991.

[61] B. Pezeshki, R. Apte, S. M. Lord, and J. S. Harris, Jr., "Dynamic Optical Grating for Laser Beam Steering Applications", OSA Proceedings on Photonic Switching, Salt Lake City, UT, March 1991.

[62] D. Thomas, B. Pezeshki, and J. S. Harris, Jr., "Reflection Electro-Absorption Modulator with High Reflectivity Change in a Novel Normally-Off Configuration", Proceedings from Quantum Optoelectronics, pp. 30-33, Salt Lake City, UT, March 1991.

[63] B. Pezeshki, S. M. Lord and J. S. Harris, Jr., "Electroabsorptive Modulators in InGaAs/AlGaAs", Appl Phys. Lett., 59 pp. 888-890, August 1991.

[64] B. Pezeshki, R. B. Apte. S. M. Lord, and J. S. Harris, "Quantum Well Modulators for Optical Beam Steering Applications", IEEE Phot. Tech. Lett., 3, pp.790-792, 9/91.

[65] B. Pezeshki, S. M. Lord, J. S. Harris, Jr., "Electro-Absorption in InGaAs/AlGaAs Quantum Wells", Proceedings of the 18th International Symposium on GaAs and Related Compounds, September 1991, Seattle, WA.

[66] B. L. Shoop, B. Pezeshki, J. W. Goodman, and J. S. Harris, Jr., "Noninterferometric Optical Subtraction using Reflection-Electroabsorption Modulators," Optics Letters, 17, pp.58-60, January 1992.

[67] S. Takigawa, K. Bacher, L. B. Aronson, and J. S. Harris, Jr., "Low Threshold Current Grating-Coupled Surface-Emitting Strained-InGaAs Single Quantum Well Laser with GaAs Optical Confinement Structure", Appl. Phys. Lett., 60, pp. 265-267, January 1992.

[68] B. L. Shoop, B. Pezeshki, J. W. Goodman, and J. S. Harris, Jr., "Laser-Power Stabilization Using a Quantum-Well Modulator," IEEE Photonics Tech. Lett., February 1992.

[69] B. Pezeshki, G. A. Williams, and J. S. Harris, Jr. "Optical Phase Modulator Utilizing Electroabsorption in a Fabry-Perot Cavity," Appl. Phys. Lett. 60, pp. 1061-1063, March 1992.

[70] G. N. Nasserbakht, J. W. Adkisson, B. A. Wooley, J. S. Harris, Jr., T. I. Kamins, and S. S. Wong, "Monolithic Integration GaAs and Si Bipolar Devices for Optical Interconnect Systems", to be published in the IEEE/ISCC proceedings International Solid State Circits Conference, San Francisco, 1992.

[71] S. M. Lord, G. Roos, B. Pezeshki and J. S. Harris, Jr., "Hydrogen Passivation of Defects in InGaAs/AlxGa1-xAs Quantum Wells," Proceedings from MRS Spring Meeting, 262, pp. 881-886, April/May 1992.

[72] S. M. Lord, G. Roos, B. Pezeshki, J. S. Harris, Jr., and N. M. Johnson, "Enhancement of Photoluminescence Intensity in InGaAs/Al(x)Ga(1-x)As Quantum Wells by Hydrogenation," Appl. Phys. Lett. 60, pp. 2276-2278, May 1992

[73] N. Yamada and J. S. Harris, Jr., "Strained InGaAs/GaAs Single Quantum Well Lasers with Saturable Absorbers Fabricated by Quantum Well Intermixing," Appl. Phys. Lett. 60, pp. 2463-2465, May 1992.

[74] B. Pezeshki, S. M. Lord, T. B. Boykin and J. S. Harris, Jr., "GaAs/AlAs Quantum Wells for Electroabsorption Modulators," Appl. Phys. Lett.,60, pp. 2779-2781, 6/92.

[75] B. Pezeshki, D. Liu, S. M. Lord and J. S. Harris, Jr. "Visible Wavelength Fabry-Perot Reflection Modulator Using Indirect-Gap AlGaAs/As," Elect. Lett. 28, pp. 1170-1171, June 1992.

[76] S. M. Lord, B. Pezeshki and J. S. Harris, Jr., "Investigation of High In Content InGaAs Quantum Wells Grown on GaAs by Molecular Beam Epitaxy," Elect. Lett. 28, pp. 1193-1195, 1992.

[77] T. B. Boykin, B. Pezeshki and J. S. Harris, Jr., "Anti-Resonances in the Transmission of a Simple Two-State Model," Phys. Rev. B, pp. , 1992.

[78] S. M. Lord, B. Pezeshki, S. D. Kim and J. S. Harris, "1.3 μm Exciton Resonances in InGaAs Quantum Wells Grown by Molecular Beam Epitaxy Using a Slowly Graded Buffer Layer," Jrnl. Crys. Grwth. pp. 759-764, 1992.

[79] S. M. Lord, B. Pezeshki, A. F. Marshall, J. S. Harris, Jr., R. Fernandez and A. Harwit, "Graded Buffer Layers for Molecular Beam Epitaxial Growth of High In Content InGaAs on GaAs for Optoelectronics," Proceedings MRS Fall Meeting, 1992.

[80] S. M. Lord, B. Pezeshki, S. D. Kim and J. S. Harris, Jr., "1.3 μm Exciton Resonances in InGaAs Quantum Wells Grown by Molecular Beam Epitaxy Using a Slowly Graded Buffer Layer," proceedings from the Seventh International Conference on Molecular Beam Epitaxy, Schwabish Gmund, Germany, pp. 759-764, 1993.

[81] D. Liu, B. Pezeshki, S. M. Lord and J. S. Harris, Jr., "Phase Characteristics of Reflection Electro-Absorption Modulators," Appl. Phys. Letts. 62, pp. 2158-2160, May 1993.

[82] J. A. Trezza, M. C. Larson, S. M. Lord and J. S. Harris, Jr., "Large, Low-Voltage Absorption Changes and Absorption Bistability in GaAs/AlGaAs/InGaAs Asymmetric Quantum Wells," J. Appl. Phys. 74, pp. 1972-1978, August 1993.

[83] J. A. Trezza, M. C. Larson, S. M. Lord and J. S. Harris, "Low Voltage, Low Chirp, Absorptively Bistable Transmission Modulators Using Type IIA and Type IIB In0.3Ga0.7As/Al0.33Ga0.67As/In0.15Ga0.85As Asymmetric Coupled Quantum Wells," J. Appl. Phys. 74, p. 6495, December 1, 1993.

[84] S. M. Lord, B. Pezeshki, A. F. Marshall, J. S. Harris, Jr., R. Fernandez and A. Harwit, "Graded Buffer Layers for Molecular Beam Epitaxial Growth of High In Content InGaAs On GaAs for Optoelectronics," Mat. Res. Soc. Symp. Proc. 281, pp. 221-225, 1993.

[85] J. A. Trezza, M. C. Larson, and J. S. Harris, Jr., "Zero Chirp Quantum Well Asymmetric Fabry-Perot Reflection Modulators Operating Beyond the Matching Condition," J. Appl. Phys. 74(12), p. 7061-7066, December 15, 1993.

[86] J. S. Trezza, B. Pezeshki, M. C. Larson, S. M. Lord and J. S. Harris, Jr., "High Contrast Reflection Electro-absorption Modulators with Zero Phase Change," J. Appl. Phys. Lett., 63, 452.

[87] S. M. Lord, B. Pezeshki, J. S. Harris, Jr., "Electroabsorption Modulators Operating at 1.3 μm on GaAs substrates," Optical and Quantum Electronics, 25 (1993), P. S953-S964.

[88] J. A. Trezza, J. S. Harris, Jr., "Creation and Optimization of vertical Cavity Phase Flip Modulators," Journal of Applied Physics, 75 (10), May 15, 1994.

[89] K. Bacher, J. S. Harris, Jr., "Wet Selective Etch for Intracavity Contacts in Vertical Cavity Surface Emitting Lasers," Submitted to Journal of the Electrochemical Society, 11/94.

[90] L. E. Eng, K. Bacher, W. Yuen, M. Larson, G. Ding, J. S. Harris, Jr., and C. J. Chang-Hasnain, "Wavelength Shift in Vertical Cavity Laser Arrays on a Patterned Substrate," Submitted to Electronics Letters, Dec. 1994.

[91] J. A. Trezza and J. S. Harris, Jr., "Coupled Quantum Wells for Optical Modulation," to be published in Confined Electron and Photon Systems, 1994.

[92] M. C. Larson, B. Pezeshki, and J. S. Harris, Jr., "Vertical coupled-cavity microinterferometer on GaAs with deformable-membrane top mirror," IEEE Photonics Technology Letters,7 (4) 382-384, April 1995.

[93] J. A. Trezza, M. Morf, and J. S. Harris, Jr., "Creation and Optimization of Vertical Cavity X-Modulators," Submitted to J. Quantum Electronics.

[94] J. A. Trezza and J. S. Harris, Jr., "Advanced Quantum Well Structures for Optimized Optoelectronic Devices," submitted to Photonics Technology Letters.

[95] M. C. Larson and J. S. Harris, Jr., “Broadly -Tunable Resonant-Cavity Light-emitting Diode,” IEEE Photon. Techn. Lett. 7, 1267, (1995).

[96] M. C. Larson, A. R. Massengale, J. S. Harris, Jr., “Continuously-tunable micromachined vertical-cavity surface-emitting laser with 18 nm range,” Electronics Letters 32, 330 (1996).

[97] M. C. Larson and J. S. Harris, Jr., “Broadly Tunable Resonant-cavity Light Emission,” Appl. Phys. Lett. 67, 590 (1995).

[98] B. Sung, H. C. Chui, E. L. Martinet and J. S. Harris, Jr., “Control of Quasi-Bound States by Electron Bragg Mirrors in GaAs/Al0.3Ga0.7As Quantum Wells”, Appl. Phys. Lett. 68, 2720 (1996).

References

Chapter 1

1. B. Pezeshki, D. Thomas, and J. S. Harris, Jr., *Appl. Phys. Lett.*, **57**, 1491-1492, (1990).

2. B. Pezeshki, D. Thomas, and J. S. Harris, Jr., "Large Reflectivity Modulation Using InGaAs-GaAs," IEEE Photonics Technology Lett., 2, pp. 807-809, November 1990.

3. B. Pezeshki, D. Thomas, and J. S. Harris, Jr., "Novel Cavity Design for High Reflectivity Changes in a Normally Off Electroabsorption Modulator," Appl. Phys. Lett. 58, pp. 813-815, February 1991.

4. B. Pezeshki, R. Apte, S. M. Lord, and J. S. Harris, Jr., "Dynamic Optical Grating for Laser Beam Steering Applications", OSA Proceedings on Photonic Switching, Salt Lake City, UT, March 1991.

5. B. Pezeshki, R. B. Apte. S. M. Lord, and J. S. Harris, "Quantum Well Modulators for Optical Beam Steering Applications", IEEE Phot. Tech. Lett., 3, pp.790-792, 9/91.

6. B. Pezeshki, G. A. Williams, and J. S. Harris, Jr. "Optical Phase Modulator Utilizing Electroabsorption in a Fabry-Perot Cavity," Appl. Phys. Lett. 60, pp. 1061-1063, March 1992.

7. J. A. Trezza, B. Pezeshki, M. C. Larson, S. M. Lord and J. S. Harris, Jr., "High Contrast Asymmetric Fabry-Perot," Appl. Phys. Lett. 74, pp.452-454, August 1993.

8. J. A. Trezza, M. C. Larson, S. M. Lord and J. S. Harris, "Low Voltage, Low Chirp, Absorptively Bistable Transmission Modulators Using Type IIA and Type IIB In0.3Ga0.7As/Al0.33Ga0.67As/In0.15Ga0.85As Asymmetric Coupled Quantum Wells," J. Appl. Phys. 74, p. 6495, December 1, 1993.

9. J. A. Trezza, M. C. Larson, and J. S. Harris, Jr., "Zero Chirp Quantum Well Asymmetric Fabry-Perot Reflection Modulators Operating Beyond the Matching Condition," J. Appl. Phys. 74(12), p. 7061-7066, December 15, 1993.

10. J. S. Trezza, B. Pezeshki, M. C. Larson, S. M. Lord and J. S. Harris, Jr., "High Contrast Reflection Electro-absorption Modulators with Zero Phase Change," J. Appl. Phys. Lett., 63, 452.

11. J. A. Trezza, J. S. Harris, Jr., "Creation and Optimization of vertical Cavity Phase Flip Modulators," Journal of Applied Physics, 75 (10), May 15, 1994.

12. J. A. Trezza and J. S. Harris, Jr., "Coupled Quantum Wells for Optical Modulation," to be published in Confined Electron and Photon Systems, 1994.

13. J. A. Trezza, M. Morf, and J. S. Harris, Jr., "Creation and Optimization of Vertical Cavity X-Modulators," Submitted to J. Quantum Electronics.

14. Psaltis, D. et al. "Optical image correlation with a binary spatial light modulator" OPTICAL ENGINEERING Nov.-Dec. 1984. vol.23, no.6, p. 698-704

15. U. Keller, G. Hooft, W.H. Knox, and T.K. Woodward, Proc. OSA Quantum Optoelectronics Top. Meet., Salt Lake City, UT, 1991, paper WB2.

16. Takizawa, K. et al. "Analog-to-digital converter: a new type using an electrooptic light modulator" APPLIED OPTICS 15 Sept. 1979. vol.18, no.18, p. 3148-51 (Journal Paper - English)

17. Song, Q.W. et al. "Holographic associative memory system using a thresholding microchannel spatial light modulator" OPTICAL ENGINEERING May 1989. vol.28, no.5, p. 533-6 (Journal Paper - English)

18. Bar-Tana, I. et al. "Smart-pixel spatial light modulator for incorporation in an optoelectronic neural network" OPTICS LETTERS 1 Feb. 1995. vol.20, no.3, p. 303-5 (Journal Paper - English)

19. McArdle, N. et al. "A smart-pixel parallel optoelectronic computing system with free-space dynamic interconnections" Proceedings of Massively Parallel Processing Using Optical Interconnections. Held: Maui, HI, USA 27-29 Oct. 1996. Proceedings of the Third International Conference on Massively Parallel Processing Using Optical Interconnections (Cat. No.96TB100092) (1996) p. 146-57 (Conference Paper)

Chapter 2

1. Weisbuch, C. (Claude), 1945-
TITLE: Quantum semiconductor structures : fundamentals and applications / Claude Weisbuch, Borge Vinter.
IMPRINT: Boston : Academic Press, c1991.
xii, 252 p. : ill. ; 23 cm.

2. . S. Chuang, *Physics of Optoelectronic Devices*,, John Wiley and Sons, 1995.

3. N. Peyghambarian, S. Koch, A. Mysrowicz, *Introduction to Semiconductor Optics*, Prentice Hall, 1993.

4. Miller, D.A.B. et al. "Electric field dependence of optical absorption near the band gap of quantum-well structures" PHYSICAL REVIEW B (CONDENSED MATTER) 15 July 1985. vol.32, no.2, p. 1043-60 (Journal Paper - English)

5. Miller, D.A.B. et al. "Band-edge electroabsorption in quantum well structures: the quantum-confined Stark effect" PHYSICAL REVIEW LETTERS 26 Nov. 1984. vol.53, no.22, p. 2173-6 (Journal Paper - English)

6. B. Pezeshki, personal communication.

7. Haug, Hartmut.
TITLE: Quantum theory of the optical and electronic properties of semiconductors / Hartmut Haug, Stephan W. Koch.
IMPRINT: 3rd ed. Singapore : World Scientific, 1994.
xv, 473 p. : ill. ; 23 cm.

8. Bhattacharya, Pallab.
TITLE: Semiconductor optoelectronic devices / Pallab Bhattacharya.
IMPRINT: 2nd ed. Upper Saddle River, NJ : Prentice Hall, c1997.
xxv, 613 p. : ill. ; 24 cm.

9. Harwit, A. et al. "Calculated quasi-eigenstates and quasi-eigenenergies of quantum well superlattices in an applied electric field" JOURNAL OF APPLIED PHYSICS 1 Nov. 1986. vol.60, no.9, p. 3211-13 (Journal Paper - English)

10. B. Pezeshki, S. M. Lord, T. B. Boykin, B. L. Shoop, and J. S. Harris, Jr., "AlGaAs/AlAs QW Modulator for 6328 Å Operation", Elect. Letts., 27, pp. 1971-1973, October 1991.

11. S. M. Lord, J. A. Trezza, M. C. Larson, B. Pezeshki, and J. S. Harris, Jr., "1.3 μm Electroabsorption Reflection Modulators on GaAs," Appl. Phys. Lett. 63 pp. 806-808, August 1993.

12. S.-D. Kim, J. A. Trezza, and J. S. Harris, Jr., "Observation of 1.5 μm Quantum Confined Stark Effect in InGaAs/AlGaAs Multiple Quantum Wells on GaAs Substrates," Submitted to Journal of Vacuum Science and Technology. 1994.

13. E.D. Palik, ed. *Handbook of Optical Constants of Solids*, Academic Press, Orlando, Florida, 1985.

14. B. Pezeshki, D. Thomas, and J. S. Harris, Jr., "Optimization of Reflection Electro-Absorption Modulators", Proceedings of Physical Concepts of Materials for Novel Optoelectronics Device Applications II: Device Physics and Applications, (1990), SPIE 1362, pp. 559-563, October 1990.

15. Macleod, H. A. (Hugh Angus)
TITLE: Thin-film optical filters / H A Macleod.
IMPRINT: 2nd ed. N.Y. : Macmillan Pub. Co., c1986.
xxii, 519 p. : ill. ; 24 cm.

16. K. Bacher, B. Pezeshki, S. M. Lord and J. S. Harris, Jr., "Molecular Beam Epitaxy Growth of Vertical Cavity Optical Devices with In Situ Corrections," Appl. Phy. Lett. 61 pp. 1387-1889, September 1992.

17. B. Pezeshki, PhD Thesis

18. J. Trezza, PhD Thesis

19. Weber, S. et al. "Thermal carrier emission from a semiconductor quantum

well" PHYSICAL REVIEW B (CONDENSED MATTER) APS through AIP, 15 Nov. 1995. vol.52, no.20, p. 14739-47 (Journal Paper - English)

20. Miller, A. et al. "Optical switching and transient carrier transport phenomena in MQW structures" Nonlinear Optics III. Held: Los Angeles, CA, USA 20-22 Jan. 1992. Proc. SPIE - Int. Soc. Opt. Eng. (USA), Proceedings of the SPIE - The International Society for Optical Engineering (1992) vol.1626 p. 179-91 (Conference Paper; Journal Paper)

21. Herman, Marian A.
TITLE: Molecular beam epitaxy : fundamentals and current status / M. A. Herman, H. Sitter.
IMPRINT: Berlin ; New York : Springer-Verlag, c1989.
xii 382 p. : ill. (some col.) ; 24 cm.

22. The Technology and physics of molecular beam epitaxy / edited by E.H.C. Parker.
IMPRINT: New York : Plenum Press, c1985.
xx, 686 p. : ill. ; 26 cm.

Chapter 3

1. D. A. B. Miller "Quantum-well self-electro-optic effect devices", Optical and Quantum Electronics, 22, S61-S98, (1990).

2. A. L. Lentine, H. S. Hinton, D. A. B. Miller, J. E. Henry, J. E. Cunningham, and L. M. F. Chirovsky, "Symmetric Self-Electrooptic Effect Device: Optical Set-Reset Latch, Differential Logic Gate, and Differential Modulator/Detector", IEEE J. of Quantum Electronics, 25, 1928-1936, (1989).

3. Sohmer, A. et al. "Twofold increase in sensitivity with a dual-beam illumination arrangement for electronic speckle pattern interferometry" OPTICAL ENGINEERING SPIE, July 1996. vol.35, no.7, p. 1943-8 (Journal Paper - English)

4. Weste, Neil H. E.
TITLE: Principles of CMOS VLSI design : a systems perspective / Neil H.E. Weste, Kamran Eshraghian.
IMPRINT: 2nd ed. Reading, Mass. : Addison-Wesley Pub. Co., c1993.
xxii, 713 p., [16] p. of plates : ill. (some col.) ; 24 cm.

5. Dertouzos, Michael L. THRESHOLD LOGIC (Cambridge, M.I.T. Press [1965])

6. An approach similar to that of
Park, Byung Gook. VERTICALLY INTEGRATED RESONANT TUNNELING DIODES (1990)

7. Lentine, A.L. et al. "Circuit model of a multiple-quantum-well diode" APPLIED OPTICS 10 March 1994. vol.33, no.8, p. 1376-9 (Journal Paper - English)

8. Singh, J. et al. "Implementation of neural networks using quantum well based excitonic devices-device requirement studies" Held: San Diego, CA, USA 24-27 July 1988. IEEE International Conference on Neural Networks (IEEE Cat. No.88CH2632-8) (1988) p. 411-19 vol.2 (Conference Paper) Singh, J. et al. "Quantum confined Stark effect of excitonic transitions in GaAs/AlGaAs MQW structures for implementation of neural networks: basic device requirements" APPLIED OPTICS 1 Nov. 1988. vol.27, no.21, p. 4554-61 (Journal Paper - English)

9. Bigo, S. et al. "20 GHz all-optical clock recovery based on fibre laser mode-locking with a fibre nonlinear loop mirror as variable intensity/phase modulator" Proceedings of 21st European Conference on Optical Communications. Held: Brussels, Belgium 17-21 Sept. 1995. 21st European Conference on Optical Communication, ECOC'95, including Symposium on Photonic versus Electronic Technologies in Switching and Interconnection. Symposium on Broadband Networks for Video and Multimedia Services (IEEE Cat. No.95TH8127) (1995) p. 945-8 vol.2 (Conference Paper)

10. Goodwill, D.J. et al. "Optical interconnect module extensible to 10,000 parallel channels for a smart-pixel optical backplane" Digest IEEE/Leos 1996 Summer Topical Meeting. Advanced Applications of Lasers in Materials and Processing. Held: Keystone, CO, USA 5-9 Aug. 1996. Digest. IEEE/LEOS 1996 Summer Topical Meetings. Advanced Applications of Lasers in Materials Processing; Broadband Optical Networks - Enabling Technologies and Applications; Smart Pixels; Optical MEMs and their Applications (Cat. No.96TH8164) (1996) p. 61-2 (Conference Paper)

11. Dickinson, A. et al. "A programmable optical computer architecture" Optics in Complex Systems. Held: Garmisch-Partenkirchen, West Germany 5-10 Aug. 1990. Proc. SPIE - Int. Soc. Opt. Eng. (USA), Proceedings of the SPIE - The International Society for Optical Engineering (1990) vol.1319 p. 177-8 (Conference Paper; Journal Paper)

Chapter 4

1. Miller, Richard Kendall. NEURAL NETWORKS: implementing associative memory models in neurocomputers (Lilburn, GA : Fairmont Press ; c1990)

2. Schalkoff, Robert J. PATTERN RECOGNITION (New York : J. Wiley, c1992) LOCATION: Math & Comp Sci Q327.S27 1992

3. McVey, Eugene S. ARTIFICIAL NEURAL NETWORK IMPLEMENTATION OF A NEAR-IDEAL ERROR PREDICTION CONTROLLER [MICROFORM] (Charlottesville, Va. : Dept. of Electrical Engineering, School of Engineering and Applied Science, University of Virginia ; 1992])

4. McCulloch, W.S. and Pitts, W. A Logical Calculus of Ideas Imminent in Nervous Activity. Bulletin of Mathematical Biophysics Vol. 5,115-133, 1943.

5. Principles of neural science / edited by Eric R. Kandel, James H. Schwartz, Thomas M. Jessell.PRINCIPLES OF NEURAL SCIENCE. 3rd ed. (New York : Elsevier, c1991)

6. Hertz, John A. INTRODUCTION TO THE THEORY OF NEURAL COMPUTATION (Redwood City, Calif. : Addison-Wesley Pub. Co., 1991)
LOCATION: Math & Comp Sci QA76.5.H475 1991 (Library has c.1)
Engineering QA76.5.H475 1991 (Library has c.2)

7. Hsin-Yu Sidney Li et al. "Optical network for real-time face recognition" APPLIED OPTICS 10 Sept. 1993. vol.32, no.26, p. 5026-35 (Journal Paper - English)

8. S.H. Lin, Optoelectronic Integrated Circuits for Optical Neural Network Applications, PhD thesis, California Institute of Technology, Pasadena, CA 91125, 1991.

9. Psaltis, D. and Farhat, N.H., "Optical information processing based on an associative-memory model of neural nets with thresholding and feedback," Optics Letters 10, 98-100 (1985).

10. Anderson, D.Z., and Linninger, D.M., "Dynamic optical interconnects: volume holograms as optical two-port operators," Applied Optics 26, 5031-5038 (1987).

11. Psaltis, D. Brady, D. and Wagner, K. "Adaptive optical networks using photorefractive crystals," Applied Optics 27, 1752-1759, (1988).

12.Singh, J. et al. "Implementation of neural networks using quantum well based excitonic devices-device requirement studies" Held: San Diego, CA, USA 24-27 July 1988. IEEE International Conference on Neural Networks (IEEE Cat. No.88CH2632-8) (1988) p. 411-19 vol.2 (Conference Paper)
Singh, J. et al. "Quantum confined Stark effect of excitonic transitions in GaAs/AlGaAs MQW structures for implementation of neural networks: basic device requirements" APPLIED OPTICS 1 Nov. 1988. vol.27, no.21, p. 4554-61 (Journal Paper - English)

13. Kim, J.H. et al. "Monolithically integrated two-dimensional arrays of optoelectronic threshold devices for neural network applications" Laser Diode Technology and Applications. Held: Los Angeles, CA, USA 18-20 Jan. 1989. Proc. SPIE - Int. Soc. Opt. Eng. (USA), Proceedings of the SPIE - The International Society for Optical Engineering (1989) vol.1043 p. 44-52 (Conference Paper; Journal Paper)

14. D. A. B. Miller, M. D. Feuer, T. Y. Chang, S. C. Shunk, J. E. Henry, D. J. Burrows, and D. S. Chemla, "Field-effect transistor self-electrooptic effect device: integrated photodiode, quantum well modulator and transistor", *IEEE Phot. Tech. Lett*. **1**, 61-64 (1989).

15. Luo, J. et al. "Optical FET receivers for neural network applications"

Optoelectronic Interconnects III. Held: San Jose, CA, USA 8-9 Feb. 1995. Proc. SPIE - Int. Soc. Opt. Eng. (USA), Proceedings of the SPIE - The International Society for Optical Engineering (1995) vol.2400 p. 355-62 (Conference Paper; Journal Paper)

16. Waddle, A.J. et al. "A smart-pixel optical neural network design using customised error propagation" Proceedings of International Conference on Optical Computing. Held: Edinburgh, UK 22-25 Aug. 1994. Optical Computing. Proceedings of the International Conference (1995) p. 511-14 (Conference Paper)

17. McCormick, F.B. et al. "Cascaded operation of two 128-Pixel FET-SEED Smart pixel arrays" Held: Palm Springs, CA, USA 16-19 March 1993. Optical Computing. Summaries of Papers Presented at the Optical Computing Topical Meeting. 1993 Technical Digest Vol.7. Postconference Edition (1993) p. 222-5 (Conference Paper)

18. Plant, D.V. et al. "Design, modeling, and characterization of FET-SEED smart pixel transceiver arrays for optical backplanes" IEEE JOURNAL OF QUANTUM ELECTRONICS IEEE, Aug. 1996. vol.32, no.8, p. 1391-8 (Journal Paper - English)

Chapter 5

1. Trezza, J.A. et al. "Creation and optimization of vertical-cavity X-modulators" IEEE JOURNAL OF QUANTUM ELECTRONICS IEEE, Jan. 1996. vol.32, no.1, p. 53-60 (Journal Paper - English)

2. T. Toffoli. "Reversible Computing," *Lecture Notes in Computer Science* , G. Goos and J. Hartmanis, ed., vol. 85, Springer–Verlag, Berlin, 1980.

3. E. Fredkin, T. Toffoli, "Conservative Logic", *International Journal of Theoretical Physics*, vol. 21, pp. 219-253, 1982.

4. Martin Morf and Fung Lee personal communication.

5. Shamir, J. et al. "Optical computing and the Fredkin gates" APPLIED OPTICS 15 May 1986. vol.25, no.10, p. 1604-7 (Journal Paper - English)

6. C.L. Chang and C.S. Tsai, Technical Digest, Topical Meeting on Integrated and Guided Wave Optics (Optical Society of America, Washington DC, 1982) paper ThD2.

7. R.A. Forber and E. Marom, Technical Digest, Conference on Lasers and Electro-Optics (Optical Society of America, Washington DC, 1985) paper FL2.

8. J. Trezza, PhD thesis.

9. **J. Trezza, J. Powell, M. Morf, and J.S. Harris, Jr., “Vertical Cavity X-Modulators” ** get this from John!**

10. Oldfield, John V., 1933-

TITLE: Field-programmable gate arrays : reconfigurable logic for rapid prototyping and implementation of digital systems / John V. Oldfield, Richard C. Dorf.
IMPRINT: New York : John Wiley & Sons, Inc., c1995.
xxxii, 327 p. : ill. ; 25 cm.

11. McAulay, Alastair D. OPTICAL COMPUTER ARCHITECTURES (New York : Wiley, c1991)

12. K. W. Goossen, J. A. Walker, L. A. D'Asaro, S. P. Hui, B. Tseng, R. Leibenguth, D. Kossives, D. D. Bacon, D. Dahringer, L. M. F. Chirovsky, A. L. Lentine, and D. A. B. Miller, "GaAs MQW Modulators Integrated with Silicon CMOS", *IEEE Photonics Tech. Lett.* **7**, 360-362 (1995).

13. ***find this! Matthews-Blakeslee***

14. S. M. Lord, B. Pezeshki, A. F. Marshall, J. S. Harris, Jr., R. Fernandez and A. Harwit, "Graded Buffer Layers for Molecular Beam Epitaxial Growth of High In Content InGaAs on GaAs for Optoelectronics," Proceedings MRS Fall Meeting, 1992.

15. Introduction to exciton physics
AUTHOR: Knox, R.S.; Dept. of Phys. & Astron., Univ. of Rochester, Rochester, NY, USA
CONFERENCE: Erice, Italy 15-29 June 1981
PUBLICATION: Collective Excitations in Solids. Proceedings of the NATO Advanced Study Institute, p. 183-245
EDITOR: Di Bartolo, B.
Danko, J.
New York, NY, USA Plenum 1983
xxii+716 p.
171 Refs.

16. Yoshimura, H. et al. "Carrier induced change in refractive index of modulation doped n-AlGaAs/GaAs quantum wells and its application" Held: Tokyo, Japan 25-27 Aug. 1987. Extended Abstracts of the 19th Conference on Solid State Devices and Materials (1987) p. 371-4 (Conference Paper)

17. N. Peyghambarian, S. Koch, A. Mysrowicz, *Introduction to Semiconductor Optics*, Prentice Hall, 1993.

18. Sakaki, H. et al. "Carrier concentration dependent absorption spectra of modulation doped n-AlGaAs/GaAs quantum wells and performance analysis of optical modulators and switches using carrier induced bleaching (CIB) and refractive index change (CIRIC)" JAPANESE JOURNAL OF APPLIED PHYSICS, PART 2 (LETTERS) July 1987. vol.26, no.7, p. L1104-6 (Journal Paper - English)

19. Ebeling, Karl Joachim. [INTEGRIERTE OPTOELEKTRONIK. ENGLISH] INTEGRATED

OPTOELECTRONICS (Berlin ; Springer-Verlag, c1993)
LOCATION: Physics TA1750.E2413 1993.

20. Yamanishi, M. et al. "Field-induced optical nonlinearity due to virtual transitions in semiconductor quantum-well structures" PHYSICAL REVIEW LETTERS 31 Aug. 1987. vol.59, no.9, p. 1014-17 (Journal Paper - English)

21. Daxin Liu, personal communication.

22. Powell, J.S. et al. "Vertical cavity X-modulators for reconfigurable optical interconnection and routing" Proceedings of Massively Parallel Processing Using Optical Interconnections. Held: Maui, HI, USA 27-29 Oct. 1996. Proceedings of the Third International Conference on Massively Parallel Processing Using Optical Interconnections (Cat. No.96TB100092) (1996) p. 352-9 (Conference Paper)

Chapter 6

1. K. W. Goossen, J. A. Walker, L. A. D'Asaro, S. P. Hui, B. Tseng, R. Leibenguth, D. Kossives, D. D. Bacon, D. Dahringer, L. M. F. Chirovsky, A. L. Lentine, and D. A. B. Miller, "GaAs MQW Modulators Integrated with Silicon CMOS", *IEEE Photonics Tech. Lett.* **7**, 360-362 (1995).

2 Worchesky, T.L. et al. "Large arrays of spatial light modulators hybridized to silicon integrated circuits" APPLIED OPTICS Opt. Soc. America, 10 March 1996. vol.35, no.8, p. 1180-6 (Journal Paper - English)

3. D.A.B. Miller, personal communication.

4. A. L. Lentine, K. W. Goossen, J. A. Walker, L. M. F. Chirovsky, L. A. D'Asaro, S. P. Hui, B. T. Tseng, R. E. Leibenguth, D. P. Kossives, D. W. Dahringer, D. D. Bacon, T. K. Woodward, and D. A. B. Miller, "Arrays of Optoelectronic Switching Nodes Comprised of Flip-Chip- Bonded MQW Modulators and Detectors on Silicon CMOS Circuitry*", IEEE Photonics Tech. Lett*. **8**, 221-223 (1996).

5. J. Trezza, K. Kang, etc. talk at Salt Lake City....get this from John*****

6. AT&T Hybrid SEED Workshop notes, held George Mason University, July, 1995.

7. Goodwill, D.J. et al. "Optical interconnect module extensible to 10,000 parallel channels for a smart-pixel optical backplane" Digest IEEE/Leos 1996 Summer Topical Meeting. Advanced Applications of Lasers in Materials and Processing. Held: Keystone, CO, USA 5-9 Aug. 1996. Digest. IEEE/LEOS 1996 Summer Topical Meetings. Advanced Applications of Lasers in Materials Processing; Broadband Optical Networks - Enabling Technologies and Applications; Smart Pixels; Optical MEMs and their Applications (Cat. No.96TH8164) (1996) p. 61-2 (Conference Paper)

8. McArdle, N. et al. "A smart-pixel parallel optoelectronic computing system with free-space dynamic interconnections" Proceedings of Massively

Parallel Processing Using Optical Interconnections. Held: Maui, HI, USA 27-29 Oct. 1996. Proceedings of the Third International Conference on Massively Parallel Processing Using Optical Interconnections (Cat. No.96TB100092) (1996) p. 146-57 (Conference Paper)

9. H. S. Hinton, T. J. Cloonan, F. B. McCormick, A. L. Lentine, and F. A. P. Tooley, "Free- space digital optical systems", Proc. IEEE 82, 1632-1649 (1994) [8] F. B. McCormick, T. J. Cloonan, A. L. Lentine, J. M. Sasian, R. L. Morrison, M. G. Beckman, S. L. Walker, M. J. Wojcik, S. J. Hinterlong, R. J. Crisci, R. A. Novotny, and H. S. Hinton, "Five-stage free-space optical switching network with field-effect transistor self-electrooptic- effect-device smart-pixel arrays", *Appl. Opt*. **33**, 1601- 1618 (1994).

10. Pinkston, T.M. et al. "An asynchronous optical token smart-pixel design based on hybrid CMOS-SEED integration" Digest IEEE/Leos 1996 Summer Topical Meeting. Advanced Applications of Lasers in Materials and Processing. Held: Keystone, CO, USA 5-9 Aug. 1996. Digest. IEEE/LEOS 1996 Summer Topical Meetings. Advanced Applications of Lasers in Materials Processing; Broadband Optical Networks - Enabling Technologies and Applications; Smart Pixels; Optical MEMs and their Applications (Cat. No.96TH8164) (1996) p. 40-1 (Conference Paper)

Chapter 7

1. J. A. Trezza, M. C. Larson, and J. S. Harris, Jr., "Zero Chirp Quantum Well Asymmetric Fabry-Perot Reflection Modulators Operating Beyond the Matching Condition," J. Appl. Phys. 74(12), p. 7061-7066, December 15, 1993.

2. Whitehead, M. et al. "Low-voltage multiple quantum well reflection modulator with on:off ratio >100:1" ELECTRONICS LETTERS 20 July 1989. vol.25, no.15, p. 984-5 (Journal Paper - English)

3. Pezeshki, B. et al. "Optical phase modulator utilizing electroabsorption in a Fabry-Perot cavity" APPLIED PHYSICS LETTERS 2 March 1992. vol.60, no.9, p. 1061-3 (Journal Paper - English)

4. Leeson, M.S. IEE Colloquium 'Towards Terabit Transmission' (Digest.1995/110). London, UK: IEE, 1995. p. 5/1-6 of 107 pp

5. Zucker, J.E. et al. "Electro-optic phase modulation in GaAs/AlGaAs quantum well waveguides" APPLIED PHYSICS LETTERS 21 March 1988. vol.52, no.12, p. 945-7 (Journal Paper - English)

6. Trezza, J.A. et al. "Large, low-voltage absorption changes and absorption bistability in GaAs/AlGaAs/InGaAs asymmetric quantum wells" JOURNAL OF APPLIED PHYSICS 1 Aug. 1993. vol.74, no.3, p. 1972-8 (Journal Paper - English)

7. Trezza, J.A. et al. "Low-voltage, low-chirp, absorptively bistable

transmission modulators using type-IIA and type-IIB In/sub 0.3/Ga/sub 0.7/As/Al/sub 0.33/Ga/sub 0.67/As/In/sub 0.15/Ga /sub 0.85/As asymmetric coupled quantum wells" JOURNAL OF APPLIED PHYSICS 1 Dec. 1993. vol.74, no.11, p. 6495-502 (Journal Paper - English)

8. John Trezza PhD thesis.

9. Bacher, K. et al. "Molecular beam epitaxy growth of vertical cavity optical devices with in situ corrections" APPLIED PHYSICS LETTERS 21 Sept. 1992. vol.61, no.12, p. 1387-9 (Journal Paper - English)

10. D. Liu, S. M. Lord, M. Larson, J. A. Trezza, J. S. Harris, Jr. (OSA Spatial Light Modulators Conference, Palm Springs, 1993). OR
Daxin Liu et al. "Phase characteristics of reflection electroabsorption modulators" APPLIED PHYSICS LETTERS 3 May 1993. vol.62, no.18, p. 2158-60 (Journal Paper - English)

11. T.L. Worchesky, K.J. Ritter, (OSA Conference on Spatial Light Modulators and Applications, Salt Lake City, March, 1995).

12. Trezza, J.A. et al. "Creation and optimization of vertical cavity phase flip modulators" JOURNAL OF APPLIED PHYSICS 15 May 1994. vol.75, no.10, pt.1, p. 4878-84 (Journal Paper - English)

13. Trezza, J.A. et al. "Creation and optimization of vertical-cavity X-modulators" IEEE JOURNAL OF QUANTUM ELECTRONICS IEEE, Jan. 1996. vol.32, no.1, p. 53-60 (Journal Paper - English)

14. Pezeshki, B. et al. "Optimization of modulation ratio and insertion loss in reflective electroabsorption modulators" APPLIED PHYSICS LETTERS 8 Oct. 1990. vol.57, no.15, p. 1491-2 (Journal Paper - English)

15. J.A. Trezza, J.S. Harris, Jr.(in Nato Advanced Study Institute on Confined Electrons and Photons 1995, C. Weisbuch, E. Burnstein eds., p.701)

References

Chapter 1

Chapter 2

Chapter 3

Chapter 4

1. Miller, Richard Kendall. NEURAL NETWORKS: implementing associative memory models in neurocomputers (Lilburn, GA : Fairmont Press ;
c1990)

2. Schalkoff, Robert J. PATTERN RECOGNITION (New York : J. Wiley, c1992)
LOCATION: Math & Comp Sci Q327.S27 1992

3. McVey, Eugene S. ARTIFICIAL NEURAL NETWORK IMPLEMENTATION OF A NEAR-IDEAL
ERROR PREDICTION CONTROLLER [MICROFORM] (Charlottesville, Va. : Dept. of
Electrical Engineering, School of Engineering and Applied Science,
University of Virginia ; 1992])

4. McCulloch, W.S. and Pitts, W. A Logical Calculus of Ideas Imminent in Nervous Activity. Bulletin of Mathematical Biophysics Vol. 5,115-133, 1943.

5. Principles of neural science / edited by Eric R. Kandel, James H.
Schwartz, Thomas M. Jessell.PRINCIPLES OF NEURAL SCIENCE. 3rd ed. (New York : Elsevier, c1991)

6. Hsin-Yu Sidney Li et al. "Optical network for real-time face recognition"
APPLIED OPTICS 10 Sept. 1993. vol.32, no.26, p. 5026-35 (Journal Paper - English)

7. Hertz, John A. INTRODUCTION TO THE THEORY OF NEURAL COMPUTATION (Redwood
City, Calif. : Addison-Wesley Pub. Co., 1991)
LOCATION: Math & Comp Sci QA76.5.H475 1991 (Library has c.1)
Engineering QA76.5.H475 1991 (Library has c.2)

8.S.H. Lin, Optoelectronic Integrated Circuits for Optical Neural Network Applications, PhD thesis, California Institute of Technology, Pasadena, CA 91125, 1991.

9. Psaltis, D. and Farhat, N.H., “Optical information processing based on an axxociative-memory model of neural nets with thresholding and feedback,” Optics Letters 10, 98-100 (1985).

10. Anderson, D.Z., and Linninger, D.M., “Dynamic optical interconnects: volume holograms as optical two-port operators,” Applied Optics 26, 5031-5038 (1987).

11. Psaltis, D. Brady, D. and Wagner, K. “Adaptive optical networks using photorefractive crystals,” Applied Optics 27, 1752-1759, (1988).

12.Singh, J. et al. "Implementation of neural networks using quantum well based excitonic devices-device requirement studies" Held: San Diego, CA, USA 24-27 July 1988. IEEE International Conference on Neural Networks (IEEE Cat. No.88CH2632-8) (1988) p. 411-19 vol.2 (Conference Paper) Singh, J. et al. "Quantum confined Stark effect of excitonic transitions in GaAs/AlGaAs MQW structures for implementation of neural networks: basic device requirements" APPLIED OPTICS 1 Nov. 1988. vol.27, no.21, p. 4554-61 (Journal Paper - English)

Lin, S. et al. "GaAs optoelectronic neuron arrays" APPLIED OPTICS 10 March 1993. vol.32, no.8, p. 1275-89 (Journal Paper - English)

Lin, S.H. et al. "Integration of high-gain double heterojunction GaAs bipolar transistors with a LED for optical neural network application" Held: Ithaca, NY, USA 7-9 Aug. 1989. Proceedings. IEEE/Cornell Conference on Advanced Concepts in High Speed Semiconductor Devices and Circuits (Cat. No.89CH2790-4) (1989) p. 344-52 (Conference Paper)

Kim, J.H. et al. "Monolithically integrated two-dimensional arrays of optoelectronic threshold devices for neural network applications" Laser Diode Technology and Applications. Held: Los Angeles, CA, USA 18-20 Jan. 1989. Proc. SPIE - Int. Soc. Opt. Eng. (USA), Proceedings of the SPIE - The International Society for Optical Engineering (1989) vol.1043 p. 44-52 (Conference Paper; Journal Paper)

Psaltis, D. et al. "Optoelectronic implementations of neural networks" IEEE COMMUNICATIONS MAGAZINE Nov. 1989. vol.27, no.11, p. 37-40, 71 (Journal Paper - English)

Mead, Carver. ANALOG VLSI AND NEURAL SYSTEMS (Reading, Mass. : Addison-Wesley, c1989)

Chapter 5

1.

2.

3.

Chapter 6

1. AT&T

2. Worchesky, Martin Marietta

3. Goossen

4. more AT&T

5. Worchesky, T.L. et al. "Large arrays of spatial light modulators hybridized to silicon integrated circuits" APPLIED OPTICS Opt. Soc. America, 10 March 1996. vol.35, no.8, p. 1180-6 (Journal Paper - English)

6. AT&T Workshop notes Hybrid SEED workshop

7. 1000's of I/O on a single chip

8. Smart Pixel Ref. 1

9. Smart Pixel Ref 2

10. Smart Pixel Ref 3

Chapter 7

1. J. A. Trezza, M. C. Larson, and J. S. Harris, Jr., "Zero Chirp Quantum Well Asymmetric Fabry-Perot Reflection Modulators Operating Beyond the Matching Condition," J. Appl. Phys. 74(12), p. 7061-7066, December 15, 1993.
2. Whitehead, M. et al. "Low-voltage multiple quantum well reflection modulator with on:off ratio >100:1" ELECTRONICS LETTERS 20 July 1989. vol.25, no.15, p. 984-5 (Journal Paper - English)
3. 1) Pezeshki, B. et al. "Optical phase modulator utilizing electroabsorption in a Fabry-Perot cavity" APPLIED PHYSICS LETTERS 2 March 1992. vol.60, no.9, p. 1061-3 (Journal Paper - English)
4. 5.Leeson, M.S. IEE Colloquium 'Towards Terabit Transmission' (Digest.1995/110). London, UK: IEE, 1995. p. 5/1-6 of 107 pp

5. Zucker, J.E. et al. "Electro-optic phase modulation in GaAs/AlGaAs quantum well waveguides" APPLIED PHYSICS LETTERS 21 March 1988. vol.52, no.12, p. 945-7 (Journal Paper - English)

6. Trezza, J.A. et al. "Large, low-voltage absorption changes and absorption bistability in GaAs/AlGaAs/InGaAs asymmetric quantum wells" JOURNAL OF APPLIED PHYSICS 1 Aug. 1993. vol.74, no.3, p. 1972-8 (Journal Paper - English)

7. Trezza, J.A. et al. "Low-voltage, low-chirp, absorptively bistable transmission modulators using type-IIA and type-IIB In/sub 0.3/Ga/sub 0.7/As/Al/sub 0.33/Ga/sub 0.67/As/In/sub 0.15/Ga /sub 0.85/As asymmetric coupled quantum wells" JOURNAL OF APPLIED PHYSICS 1 Dec. 1993. vol.74, no.11, p. 6495-502 (Journal Paper - English)

8. John Trezza PhD thesis.

9. Bacher, K. et al. "Molecular beam epitaxy growth of vertical cavity optical

devices with in situ corrections" APPLIED PHYSICS LETTERS 21 Sept. 1992. vol.61, no.12, p. 1387-9 (Journal Paper - English)

10. 10 D. Liu, S. M. Lord, M. Larson, J. A. Trezza, J. S. Harris, Jr. (OSA Spatial Light Modulators Conference, Palm Springs, 1993). OR
Daxin Liu et al. "Phase characteristics of reflection electroabsorption modulators" APPLIED PHYSICS LETTERS 3 May 1993. vol.62, no.18, p. 2158-60 (Journal Paper - English)

11. Worchesky? Amplitude modulators ? ?
T.L. Worchesky, K.J. Ritter, (OSA Conference on Spatial Light Modulators and Applications, Salt Lake City, March, 1995).

12. Trezza, J.A. et al. "Creation and optimization of vertical cavity phase flip modulators" JOURNAL OF APPLIED PHYSICS 15 May 1994. vol.75, no.10, pt.1, p. 4878-84 (Journal Paper - English)

13. Trezza, J.A. et al. "Creation and optimization of vertical-cavity X-modulators" IEEE JOURNAL OF QUANTUM ELECTRONICS IEEE, Jan. 1996. vol.32, no.1, p. 53-60 (Journal Paper - English)

14. Pezeshki, B. et al. "Optimization of modulation ratio and insertion loss in reflective electroabsorption modulators" APPLIED PHYSICS LETTERS 8 Oct. 1990. vol.57, no.15, p. 1491-2 (Journal Paper - English)

15. J.A. Trezza, J.S. Harris, Jr.(in Nato Advanced Study Institute on Confined Electrons and Photons 1995, C. Weisbuch, E. Burnstein eds., p.701)

1. T. Toffoli. "Reversible Computing," *Lecture Notes in Computer Science* , G. Goos and J. Hartmanis, ed., vol. 85, Springer–Verlag, Berlin, 1980.

2. E. Fredkin, T. Toffoli, "Conservative Logic", *International Journal of Theoretical Physics*, vol. 21, pp. 219-253, 1982.

3. K. Bacher, B. Pezeshki, S.M. Lord, and J.S. Harris, Jr., "Molecular beam eptiaxy growth of vertical cavity optical devices with in-situ corrections," *Applied Physics Letters*, vol. 61, pp.1387-1389, 1992.

4. J.A. Trezza, B. Pezeshki, M.C. Larson, S.M. Lord, and J. S. Harris, Jr., "High contrast asymmetric Fabry-Perot electro-absorption modulator with zero phase change," *Applied Physics Letters*, vol. 63, pp. 452-454, 1993.

5. J.A. Trezza, M. Morf, and J. S. Harris, Jr., "Creation and Optimization of Vertical Cavity X-Modulators," *IEEE Journal of Quantum Electronics*, forthcoming, January 1996.

6. A.L. Lentine, et. al., "700 Mb/s operation of optoelectronic switching nodes comprised of flip-chip bonded GaAs/AlGaAs MQW modulators and detectors on silicon CMOS circuitry," Conference on Lasers and Optoelectronics postdeadline paper CPD11 (1995).

References

1. Peyghambarian
2. Haug/Koch
3. Hunsperger
4. Fredkin
5. Toffoli
6. Fung Fung Lee Notes
7. Trezza thesis
8. Bardia Thesis
9. Harwit article
10. MacLeod text
11. In Situ paper
12. X-Mod paper
13. MPPOI paper
14. Zero Chirp paper
15. Dertouzos Thresh. Logic text
16. Psaltis article
17. McAuley Text
18. DABM Self Linearized SEED paper
19. DABM FET-SEED stuff
20. DABM Survey paper on SEEDs
21. Worchesky article
22. QCSE paper (DABM)
23. Optical Fredkin gate paper
24. Picton paper
25. Bhattacharya Text